Università degli Studi di Napoli "Parthenope"

Dipartimento di Scienze e Tecnologie

Corso di Dottorato in Scienze Applicate al Mare, Ambiente e Territorio

Curriculum "Geomatica, Geodesia e Navigazione"

Ciclo XXIX

Fuzzy techniques applied to GNSS for quality assessment and reliability testing in difficult signal scenarios

June 2017

Autore: Anna Innac

Tutor: Prof. Salvatore Gaglione

Co-Tutor: Prof. Heidi Kuusniemi

Coordinatore: Prof. Enrico Zambianchi

ABSTRACT

Thanks to the rapid development of several Global Navigation Satellite Systems (GNSS) occurring in the last years, multiple constellations are available to enhance navigation performance and safety. Due to the growing number of satellite, great levels of availability and integrity can be expected for GNSS navigation even if, on the other hand, a challenge will be to deal with the differences among systems.

GNSS navigation is critical in “hostile” scenarios where the solution can be degraded by errors such as multipath reflections and weak geometries, caused by obstacles surrounding the user. In some conditions, it is possible to reduce the effect of the errors, using weights inversely related to the quality of the received signals, once a proper quality measure for each signal is defined. In this research, a quality index, derived from the fuzzy integration of various information related to the quality of the received signals, is defined; the index is used to effectively weight each measure in a Weighted Least Square (WLS) estimation process. The design of the proposed fuzzy controller is presented in detail and its performance in the position domain is compared with the most common weighting strategies in literature.

Furthermore, in these scenarios, appropriate reliability monitoring algorithms are necessary to detect and exclude the blunders influencing the measurements set. Through successful Fault Detection and Exclusion (FDE) techniques, navigation accuracy and reliability can be improved even in signal-degraded scenario. In this thesis, an agreement between the two approaches, blunder exclusion or mitigation through de-weighting, is analyzed and provided.

To validate the proposed approach, GNSS real data have been collected through a High Sensitivity GNSS receiver placed in typical urban canyon environments, and processed in Single Point Positioning. Experimental results show significant improvements obtained using fuzzy controller with respect to the other weighting strategies. Thanks to the use of the fuzzy logic for the computation of the GNSS weights, the performance of the used FDE algorithm are also enhanced.

ACKNOWLEDGEMENTS

This Ph.D has been a life-changing experience for me and it would not have been possible to do without the support and guidance that I received from many people.

Firstly, I would like to express my sincere gratitude to my advisor Prof. Salvatore Gaglione for the continuous support of my Ph.D study and related research, for his patience, motivation, and immense knowledge. His supervision helped me in all the time of research and writing of this thesis. He believed in myself from the first time we met until today and I could not have imagine having a better advisor and mentor for my Ph.D study.

I would like to express my deep appreciation to Dr. Antonio Angrisano for his help during my Ph.D study and for "patiently" reviewing the manuscript.

I sincerely thank my co-supervisor, Prof. Heidi Kuusniemi, for her support and guidance throughout my visit at Finnish Geospatial Research Institute and after I returned in Italy; she gave me the possibility to work in her great team. She provide me all possible research facilities to improve my research and she patiently reviewed my thesis with her precious suggestions. I am also grateful for her appreciations about my research giving me a great personal satisfaction.

I would acknowledge Prof. Antonio Maratea for bringing the research idea about the application of Fuzzy Logic in GNSS context and for his guidance during the study of the basic concepts.

I would also like to thank to the referees of my thesis, Prof. Donatella Dominici, Prof. Jon Glenn Gjevestad, Prof. Anna B.O. Jensen, for reading the manuscript. I also want to thank them for letting my defense be a possible event, and for their comments and suggestions.

I would also to thank my lab-mates and colleagues with whom I had the pleasure of working both in "Parthenope" University of Naples and Finnish Geospatial Research Institute: Halyna Klymenko, Umberto Papa, Silvio del Pizzo, Vincenzo Piscopo, Franco Rossi, Prof. Salvatore Troisi, Gaetano Castaldo, Silvia Pennino, Pia Isojärvi, Stefan Söderholm, Zahidul Bhuiyan, Salomon Honkala, Martti Kirkko-Jaakkola, Simo Gröhn, and all the rest of people that I met during my journey towards the PhD experience.

A special thanks to my friends that I met in Helsinki, Maria and Marit, with whom I was able to survive to the cold Finnish winter spending nice free time together and for any support I received from them.

Finally, I would like to thank my family: my parents, Antonio and Carla, and my sister, Paola, for supporting me spiritually during my whole studying career and my life in general with their love and encouragement.

Last but not the least, I would express my sincere thankfulness to my love, Vincenzo, who was always my support when there was no one to answer my questions. He provided me the best advice I would have wanted to receive. Without him, this part of my life would have been much more difficult.

Contents

LIST OF PUBLICATIONS

Some ideas presented in this thesis have already been published in international conferences. The following articles represent the basis of the author's research:

[P1] Gaglione, S., Angrisano, A., Gioia, C., Innac, A., & Troisi, S. (2015). NeQuick Galileo version model: Assessment of a proposed version in operational scenario. Paper presented at the International Geoscience and Remote Sensing Symposium (IGARSS), 2015-November, 3611-3614. doi:10.1109/IGARSS.2015.7326603

[P2] Gaglione, S., Angrisano, A., Castaldo, G., Freda, P., Gioia, C., Innac, A., Troisi, S.,Del Core, G. (2015). The first galileo FOC satellites: From useless to essential. Paper presented at the International Geoscience and Remote Sensing Symposium (IGARSS), 2015-November 3667-3670. doi:10.1109/IGARSS.2015.7326618

[P3] Gaglione, S., Angrisano, A., Freda, P., Innac, A., Vultaggio, M., & Crocetto, N. (2015). Benefit of GNSS multi-constellation in position and velocity domain. Paper presented at the 2nd IEEE International Workshop on Metrology for Aerospace, MetroAeroSpace 2015 - Proceedings, 9-14. doi:10.1109/MetroAeroSpace.2015.7180618

[P4] Gaglione, S., Angrisano, A., Castaldo, G., Gioia, C., Innac, A., Perrotta, L., Del Core, G., Troisi, S. (2015). GPS/Barometer augmented navigation system: Integration and integrity monitoring. Paper presented at the 2nd IEEE International Workshop on Metrology for Aerospace, MetroAeroSpace 2015 - Proceedings, 166-171. doi:10.1109/MetroAeroSpace.2015.7180647

[P5] Innac, A., Bhuiyan, M.Z.H., Söderholm, S., Kuusniemi, H., Gaglione, S., (2016) Reliability testing for multiple GNSS measurement outlier detection. In: Proceedings of European Navigation Conference (ENC) 2016, 30th May-2nd June 2016, IEEE Xplore, doi: 10.1109/EURONAV.2016.7530540

LIST OF ABBREVIATIONS

ABAS	Aircraft Based Augmentation Systems
BDS	BeiDou
BDT	BeiDou Time
BGTO	BeiDou to GPS Time Offset
BIH	Bureau International de l Heure
BOC	Binary Offset Carrier
BPSK-R	Binary Phase Shift Keying with Rectangular spreading symbols
C/A	Coarse-Acquisition
CDMA	Code Division Multiple Access
CGCS2000	China Geodetic Coordinate System 2000
C/N_0	Carrier-to-Noise density power ratio
CQI	Channel Quality Index
CS	Central Synchronizer
DoD	Department of Defense
DoF	Degrees of Freedom
DOP	Dilution Of Precision
ECI	Earth-Centered-Inertial
ECEF	Earth-centered Earth-fixed
EDOP	East Dilution Of Precision
EGNOS	European Geostationary Navigation Overlay System
ENU	East North Up
EU	European Union
FDE	Fault Detection and Exclusion
FDMA	Frequency Division Multiple Access
FOC	Full Operational Capability
GA	Ground Antenna
GBAS	Ground Based Augmentation System
GCS	Ground Control Segment
GDOP	Geometric Dilution Of Precision

GGTO	Galileo to GPS Time Offset
GLONASS	GLObal Navigation Satellite System
GMS	Ground Mission Segment
GNSS	Global Navigation Satellites Systems
GPS	Global Positioning System
GPST	Global Positioning System Time
GSS	Galileo Sensor Stations
GST	Galileo System Time
GT	Global Test
GTRF	Galileo Terrestrial Reference Frame
HDOP	Horizontal Dilution Of Precision
HMI	Hazardously Misleading Information
HPL	Horizontal Protection Level
HPE	Horizontal Position Error
HRE	Horizontal Radial Error
HS	High-Sensitivity
ICA	Ionospheric Correction Algorithms
IERS	International Earth Rotation and Reference Systems Service
IOV	In-Orbit Validation
ITRF	International Terrestrial Reference Frame
LBS	Location-Based Services
LOS	Line Of Sight
LS	Least Squares
LT	Linguistic Term
LV	Linguistic Variable
MDB	Minimum Detectable Blunder
MCS	Master Control Station
MF	Membership Function
MI	Misleading Information
MS	Monitor Station
NDOP	North Dilution Of Precision
NNSS	Navy Navigation Satellite System

OS	Open Service
P(Y)	Precision code
PDOP	Position Dilution Of Precision
PHMI	Probability of Hazardously Misleading Information
PL	Protection Level
PPL	Position Protection Level
PPS	Precise Positioning Service
PRN	Pseudo-Random-Noise
PRS	Public Regulated Service
PVT	Position Velocity Time
PZ90.02	Parametrop Zemp 1990 version 2
QZSS	Quasi-Zenith Satellite System
RAIM	Receiver Autonomous Integrity Monitoring
RNP	Required Navigation Performance
SAR	Search and Rescue Service
SARPs	Standards and Recommended Practices
SBAS	Satellite Based Augmentation System
SLR	Laser Ranging Stations
SNR	Signal-to-Noise Ratio
SoL	Safety-of-Life
SOW	Seconds Of Week
SPS	Standard Positioning Service
SPP	Single Point Positioning
SS	Space Segment
SU	Soviet Union
TDOP	Time Dilution Of Precision
TFS	Time and Frequency System
TOA	Time Of Arrival
TTA	Time To Alert
TT&C	Telemetry, Tracking and Command centers
ULS	Up-Link Stations
US	User Segment

UTC	Universal Time Coordinated
USNO	United States Naval Observatory
VDOP	Vertical Dilution Of Precision
VPL	Vertical Protection Level
WAAS	Wide Area Augmentation System
WGS84	World Geodetic System 1984
WLS	Weighted Least Squares

LIST OF FIGURES

LIST OF TABLES

1. Introduction

This chapter provides an overview about the background and motivation for this research, starting from the significance and limitations of satellite navigation, especially in urban environment, the development of the several Global Navigation Satellites Systems (GNSS) and the advanced methods necessary to mitigate the effects related to a urban signal scenario. Then the main objectives of this dissertation and the author's contribution are described and finally the outline of the thesis concludes the chapter.

1.1. Motivations and Background

GNSS are developed to provide, with global coverage and in all weather conditions, three-dimensional position, velocity and time synchronization for users equipped with a suitable receiver/processor (Hoffmann-Wellenhof et al, 1992).

GNSS was initially born to assist and improve military operations and subsequently it has gradually expanded its use into several fields such as surveying, automotive, agriculture, aviation, etc. Various systems and services use position information provided by the GNSS; in fact, GNSS receivers are embedded in many of the devices used in daily lives. Applications range from the provision of a reference time source for synchronizing computer networks to guidance of robotic vehicles (Kaplan, 2005; Groves, 2013).

The aviation community has propelled the use of GNSS and various augmentations to make available the guidance for the en-route through precision approach phases of flight. The continuous global coverage capability of GNSS allows aircraft to fly directly from one location to another, if some factors such as obstacle clearance and required procedures are known by the users.

GNSS also enables various functions for spacecraft applications such as attitude determination (i.e., heading, pitch and roll), time synchronization, orbit determination and absolute and relative position determination.

Commercial and recreational maritime communities take advantage of GNSS enhancing the navigation of all bodies of waters, from oceanic travel to riverways, especially in inclement weather (Kaplan, 2005).

The majority of GNSS users are land-based. Applications range from leisure hiking to fleet vehicle management (Kaplan, 2005). The decreasing price of GNSS receiver components

has led to the development of a variety of location-based services (LBS). An example of LBS is the ability of the user to request emergency assistance via forwarding his or her location to an emergency response dispatcher. An expanding worldwide market is the deployment of automatic vehicle location systems for fleet and emergency vehicle management.

In the last years, GNSS have played a significant role in the development of Urban Navigation applications and related services. Indeed, for example, thanks to equipping smartphones with GNSS, users are able to plan and carry out their activities, e.g., to calculate routes (used as a navigation system), to share their location on social networks, or to geo-localize images.

A major concern of the constant growth of GNSS-based urban applications is related to the GNSS Standard Positioning Service (SPS) deficiency to match the required navigation performance (RNP), defined in terms of:

- Accuracy, defined as the difference between the estimated position and the real one. The accuracy must be referred to both in the horizontal plane and along the vertical dimension. Considering that the errors of satellite systems are a function of satellites' geometry, the probability that the position error does not exceed an assigned value must be at least 95%.
- Integrity, defined as the ability of the system to recognize and point out any system dysfunctions that can compromise the required performance for the operation that you are carrying out. The integrity is defined by the probability to point out such dysfunction and the Time To Alert (TTA) indicates the time between the instance of the dysfunction and the sign of such an event to the user.
- Availability, defined as the percentage in time within which the system is able to function providing the performance required by the operation. Such a parameter is a function of the features of the measurement environment and receiver technology.
- Continuity, defined as the ability of a system to allow completion of an undertaken operation without any break in the service caused by anomalies that can compromise the safety. Such a parameter is defined by the probability that a system is available throughout the operation if it was available at the beginning.

In a signal-degraded scenario, such as in city centers, dense vegetation, or mountains areas, the positioning system is not able to guarantee a continuous and accurate solution (Innac et al., 2016), as obstructions block many GNSS signals, reducing satellite availability (Ackermann et al., 2014), weakening observation geometry, and in the extreme case

compromising the navigation solution computation. Obstructions can also reflect the signals causing the multipath phenomenon and the greatest measurement errors (blunders). These effects severely influence the pseudo-range and Doppler measurements, used by a GNSS receiver for the position, velocity and time computation. Therefore, advanced methods are necessary to mitigate the undesired effects deriving from the urban environment and to improve the accuracy of the navigation solution. Indeed, in these operational scenarios a single GNSS is not able to satisfy all the RNP due to the poor satellite geometry, lower availability of measurements or the presence of blunders influencing the measurements set. A possible way to overcome this problem is to use multi-constellation GNSS that enhances the measurement redundancy (Shytermeja et al, 2014).

The recent improvement of the existing GNSSs, such as the Global Positioning System (GPS) and the GLObal NAvigation Satellite System (GLONASS), and the development of new GNSSs, such as Galileo and BeiDou, suggests the use of the combined GNSS in order to increase the satellite navigation performance in these critical signal environments. Several authors (Gaglione et al, 2016; Gioia, 2015; Angrisano et al, 2013a) showed that the benefits of the multi-constellation system are the increased availability and integrity while the enhancement in terms of accuracy is subject to the operational scenario; indeed the use of the multi-constellation approach might increase the probability of obtaining accurate positioning but still it does not guarantee a measure of trust of the positioning solution even in environments difficult for satellite navigation (Shytermeja et al, 2014).

Furthermore, in the last years, low-cost high-sensitivity (HS) GNSS receivers are being used by the geodetic community also for high-precision static positioning (Schwieger, 2008); they offer more availability than conventional receivers, being able to track weak signals in difficult environments, such as urban canyons and even some indoors, providing in average more measurements (Wieser et al, 2005). As a side effect, in presence of many multipath reflections, echo-only signals and low-power signals, HS GNSS measurements are biased and noisy, and multiple blunders can occur in the same measurements set. Possible approaches to mitigate the effects of biases or gross errors should be used such as:

- excluding the erroneous measurements through an integrity monitoring approach;
- modifying the stochastic model assigning weights inversely related to the quality of the received signal.

There are two important aspects for the optimal processing of GNSS observations: the definition of the functional relationship between the GNSS observations and the unknown parameters, and the corresponding stochastic model referring to the statistics of the GNSS

observations (Leick et al, 2015). While the functional model is well understood and a multitude of papers and textbook cover the topic, the stochastic model of GNSS observations is more diversified. There is a lack of simple and applicable formulas provided by experiences or by device manufacturers. This may indicate that the stochastics of GNSS observations are not simple (Wieser, 2002). Many authors have focused their research on the choice of the correct stochastic model, especially for high-accuracy applications (Brunner et al, 1999; Han, 1997; Barnes et al, 1998; Wang et al, 1998), identifying it as a critical factor to be improved. To this purpose, scientific literature describes essentially two variables as measurement indicators of quality: satellite elevation and Signal-to-Noise Ratio (SNR). A combination of the aforesaid indicators is considered too (Satirapod 2004; Realini and Reguzzoni, 2013).

Furthermore, the concept of integrity is well-known from civil aviation, being a Safety-of-Life (SoL) application, where very stringent performance requirements should be satisfied with the provision of timely warnings when the system should not be trusted to provide an accurate and continuous position solution. Several studies have addressed the problematics of integrity monitoring in urban environments (Kuusniemi, 2005; Liu et al, 2010; Angrisano et al, 2013a; Salvatori et al, 2014). An integrity monitoring algorithm for a navigation system is essential to guarantee that the navigation solution is within tolerable limits. Ideal integrity monitoring involves the detection, isolation and the removal of faulty measurement sources from the navigation solution.

Two different approaches exist to provide integrity. The first employs a network of ground stations to monitor GNSS signals and the integrity information is transmitted to the users by a data link; typical examples of this mode are GBAS (Ground Based Augmentation System) and SBAS (Satellite Based Augmentation System) systems. The second approach is the Receiver Autonomous Integrity Monitoring (RAIM) technique, where the integrity of GNSS navigation signals is monitored without the use of external systems, but only analyzing the navigation signals themselves (Angrisano et al, 2013a). The common principle of the RAIM algorithms is mainly based on the consistency check of redundant measurements through a statistical hypothesis test of the Least Squares (LS) residuals. Several RAIM schemes have been studied and are present in the literature. Gao (1993) studied a GPS integrity test procedure with reliability assurance to offer real-time precision and reliability checks on navigation solutions. Walter and Enge (1995) presented a weighted form of RAIM where measurement sources are weighted based on a priori information or broadcast weighting information. Sang and Kubik (1997) proposed a probabilistic approach for the determination

of geometrical criteria in order to assess of GPS RAIM availability. Romay et al. (2001) examined the availability of RAIM computed for GPS, Galileo and combined GPS/Galileo constellations through simulations.

Since the classical RAIM algorithms were developed mainly for the safety-critical aviation applications, there is the necessity to modify and improve them in order to extend their use for urban applications, since multiple simultaneously faults are more likely to occur in these areas influencing the accuracy of the navigation solution. In urban areas, an important task is to analyze, localize and exclude any blunders present in the measurements set and caused by signal obscuration and software or hardware failures, in order to guarantee the desired level of performance. Furthermore, with the challenge in GNSS navigation leading to a future of higher satellite availability, the single outlier assumption will be unrealistic. In literature, there are several publications about the development of RAIM - Fault Detection and Exclusion (FDE) algorithm extended to the multiple outliers situation (Atkinson and Riani, 1997; Kuusniemi, 2005; Hewitson and Wang, 2006b; Angrisano et al, 2013a).

For these reasons, there is a growing necessity to adopt RAIM procedures aimed to FDE in view of the future GNSS scenario and focused on navigation applications in degraded signal environments.

However, rejection of observations affected by signal distortion helps to avoid the bias, but often compromise the strength of the solution. If there is clear evidence that a measurement is worthless, it should be rejected, otherwise, it may be better to reduce only the degree of their influence on the results (Wieser, 2002). In conclusion, an agreement between the two approaches, blunder exclusion or mitigation, should be examined and considered.

1.2. Research Objectives

In signal-degraded environments, the GNSS solution is affected by errors such as multipath reflections and signal obstructions, compromising the accuracy of the positioning system solution. By weighting GNSS measurements, it is possible to reduce the effect of the errors, once a proper quality measure for each signal is considered.

Moreover, obtaining an estimate about the reliability of the solution may be useful: some applications depend on the latest reliable user position solution and certainty information. FDE procedures also provide to the user information about the possible effects of undetected blunders.

In signal-degraded scenarios, appropriate reliability monitoring algorithms are necessary to detect and exclude the blunders. Through successful FDE techniques, navigation accuracy and reliability can be improved even in "hostile" environments. An important condition for an effective FDE is the selection of a proper variance modeling for the navigation measurements (Kuusniemi, 2005).
FDE capability is quite limited in some conditions, and thus its performance should be improved and an alternative approach should be considered.

This dissertation investigates the performance of fuzzy logic for the integration of various information related to the quality of the received signals, allowing to effectively weight each measure in a Weighted Least Square (WLS) estimation process and in the computation of the test statistic used in the RAIM algorithm.
Fuzzy logic is a generalization of the Boolean logic where an object can belong to more than one set with a given degree and where the truth has values in the interval [0,1]. Most notably it allows to translate a linguistic expression (e.g. "low elevation") into a numerical value and vice-versa. Thanks to this generalization, linguistic variables and quantifiers can be defined in order to mimic the human imprecise way of representing information, and inference based on them can be performed (Zadeh et al., 1996).
The potential benefit of fuzzy theory for geodetic data analysis has been recognized and there are several papers addressed to this topic. Kutterer (2001b) provided an outline of different types of uncertainty which need to be taken into account for geodetic data analysis. Keller and Gnägi (2001), and Shyllon (2001) defined the potential application of fuzzy set based methods in the analysis of geo-data. Kutterer (2001a) and Leinen (2001) applied fuzzy theory to GPS carrier phase ambiguity fixing. The former suggested the potential use of fuzzy set theory to assess the degree of membership of a candidate set of integers to the search space. Leinen used a fuzzy decision making approach to replace the crisp failed/passed decision of a statistical testing by "local" fuzzy rating of how well a certain test is passed. Wieser (2002) used fuzzy methods for several problems in GPS data processing such as: satellite selection, modelling the variance of GPS phase observation and quality assessment of GPS processing results.

Based on this topic, the main objectives of this dissertation are:

- To propose a method based on fuzzy logic to set the weighting matrix used in WLS estimation. In order to improve the accuracy of positioning, the most common quality

measures of the received signals are fuzzified and integrated. Then, a rule base is used to obtain an aggregated fuzzy weight, finally defuzzified in a numerical value.

- To analyze the performance of the proposed fuzzy weighting schema, called FWLS, comparing it with classical weighting methods that adopts the same quality indicators – satellite elevation and SNR – performing the accuracy analysis in the position domain.
- To assess the performance of the proposed method FWLS using a multi-constellation scenario in order to weight pseudorange ranging from different GNSSs
- To apply the RAIM algorithm using the different weighting scheme and verify the enhancement obtained thanks to the use of FWLS in terms of RAIM performance.
- To evaluate the performance of the proposed approach in difficult signal environments.
- To investigate the performance of the FWLS used in WLS estimation process and RAIM algorithm in static and vehicular tests carried out in the considered operational environments.

1.3. Author's Contribution

In [P1] the author considered two Ionospheric Correction Algorithms (ICA): Klobuchar model used by the U.S. Global Positioning System (GPS) and NeQuick-G model adopted by the European Galileo system. These models are used to compute the ionospheric delay starting from a model and using parameters broadcast in the navigation message. The main goal of the paper was to analyze the performance of a modified approach for NeQuick-G (defined NeQuick VP) by comparing its performance, in position domain, with respect to the standard NeQuick-G algorithm and to the Klobuchar one. NeQuick VP is a methodology proposed to reduce the complexity characterizing NeQuick-G model. The performance was evaluated using real data collected by an open-sky station.

In August 2014, the European Global Navigation Satellite System Galileo successfully completes its In-Orbit Validation phase and the first two Full Operational Capability (FOC) satellites were launched. Since in February 2015 Galileo consisted of four IOV satellites and two FOC ones (but only three IOVs and one FOC were working correctly), the author in [P2] investigated the potential improvements on constellation geometry provided by the inclusion of the FOCs and analyzed Galileo single-point positioning performance.

In [P3] the author analyzed the performance of multi-GNSS (GPS, GLONASS, Galileo) in position and velocity domain. In order to improve the accuracy of the considered multi-GNSS, which not always overcomes the GPS-only case, a smoothing filter on measurements was considered. A Position, Velocity, Time (PVT) algorithm based on the Carrier Smoothing Code observables was implemented and the performance of this method was compared with classical Single Point Positioning technique.

GNSS-based navigation is not sufficient to support air navigation in specific applications; so it is necessary to introduce Augmentation Systems. The performance of an Aircraft Based Augmentation Systems (ABAS) was investigated by the author in [P4] based on the integration of GPS and a barometer sensor, and the performance is evaluated in terms of position accuracy and system integrity, key Required Navigation Parameters (RNP) of an air navigation system.

Finally, in order to improve the detection capability of classic RAIM to work properly when multiple outliers occurs, a scheme based on a w-test used in (Hewitson and Wang, 2006b) was adopted and modified by the author in [P5] to enhance the compromise between efficiency and effectiveness when multiple faults detection is carried out. Its performance was compared with respect to the Observation Subset Testing in the position domain. Furthermore, a Channel Quality Index (CQI) parameter proposed as a satellite selection method for an improved multi-GNSS positioning performance in (Bhuiyan et al, 2015) was used in [P5] by the author to give information about the measurement quality through the weighting matrix. The experiment to demonstrate the performance of the compared methods was performed using a multi-GNSS signal simulator with GPS, Galileo and BeiDou signals. For the experimental analysis and comparison, a software-defined multi-frequency multi-GNSS receiver developed at the Finnish Geospatial Research Institute (FGI) was used.

1.4. Thesis Outline

Chapter 2 provides an overview on the four GNSSs such as: GPS, GLONASS, Galileo and Beidou. The main features of these systems are described in terms of Space, Ground Control and User Segment. The principles of satellite navigation are presented and GNSS observables with the main error sources are illustrated.

Chapter 3 discusses the estimation theory used in this research for user position, velocity and time computation, providing mathematical details. In particular, WLS method is used and described in the chapter; several weighting methods existing in literature are described.

In chapter 4, an overview about the benefit obtained using the multi-constellation approach is provided and the differences between the analyzed GNSS constellations are described. Finally, the PVT algorithm for the combination of the four GNSSs existing is illustrated.

In chapter 5, reliability monitoring is discussed with an introduction to the concept of integrity and reliability. Furthermore, theory of reliability – including general hypothesis and statistical reliability testing based on residuals analysis – is presented. Details about FDE are provided and the implemented RAIM-FDE algorithm is described.

Chapter 6 describes the concept of fuzzy logic, including an introduction to fuzzy sets, logical operators applied to the fuzzy sets, fuzzy rules and the defuzzification method. Finally, the fuzzy controller design adopted in the PVT algorithm is described.

In chapter 7, the tests carried out are presented with details about the adopted equipment and the operational environment. Results of the several GNSS configurations are analyzed; the tests, both static and kinematic, performed with a High Sensitivity receiver, are evaluated.

Finally, the Chapter 8 concludes the thesis.

2. GNSS Overview

GNSSs are designed to provide three-dimensional position, velocity and time synchronization to Universal Time Coordinated (UTC) scale (Hoffmann-Wellenhof et al, 1992; Kaplan, 2005).

Before satellite navigation development, for navigation terrestrial long wave radio transmitters were used instead of satellites. These positioning systems broadcasted a radio pulse from a known master location, followed by repeated pulses from a number of slave stations. The delay between the reception of the master signal and the slave signals made possible the computation of the distances between the receiver and the stations, providing a position estimate.

In 1957 with the launch of Sputnik, scientists confirmed that Doppler distortion could be used to calculate ephemerides, and if a satellite's position was known, the position of a receiver on Earth could be determined.

Within two years of the Sputnik launch, the first of five low-altitude "Transit", formally known as Navy Navigation Satellite System (NNSS), satellites for global navigation was launched (Sentman, 1987). Transit was the first satellite navigation system and provided continuous service from 1964 to 1996. With the Transit development started the satellite navigation era.

In the 80s, while GPS was under development by U.S. Department of Defense, the Soviet Union started to develop a similar system called GLONASS (Jones, 1987).

Currently the U.S. GPS and the Russian GLONASS are fully operational, while new GNSSs such as Galileo and BeiDou are either nearing completion or deployment. Other regional systems are the European EGNOS (European Geostationary Navigation Overlay System), the U.S. WAAS (Wide Area Augmentation System), the Japanese QZSS (Quasi-Zenith Satellite System) and the Indian Gagan.

In this research GPS, GLONASS, Galileo and BeiDou constellations are described. They are characterized by a similar structure but with several significant differences described in the following sections.

This chapter provides an overview about GNSS structure, operational principle, GNSS observables and error sources.

2.1. GNSS structure

The architecture of GNSS is organized in three segments: the Space Segment (SS), the Ground Control Segment (GCS) and the User Segment (US) (Parkinson et al, 1996; Kaplan, 2005).
The SS consists of an artificial satellite constellation. Satellites broadcast signals necessary to positioning and each GNSS has its own constellation, characterized by different orbital parameters.
The US is made up of all the system users, equipped with a GNSS receiver/processor able to receive and decode the GNSS signal to obtain position/velocity/time information.
The GCS consists of a master control station (MCS), worldwide monitor stations (MS) and ground control antennas (GA). The MSs obtain ranging measurements from the satellites and send these to the MCS. The MSs are placed at known surveyed locations and have synchronized clocks, enabling their ranging measurements to be used to compute the satellite orbits and calibrate the satellite clocks. The MCS calculates the navigation data message for each satellite and decides whether any maneuvers must be performed; this information is then transmitted to the SS by the GA. Most satellite maneuvers are small and infrequent corrections, known as station keeping, which are used to maintain the satellites in their correct orbits. However, major relocations are performed in the event of satellite failure (Groves, 2013). GPS, GLONASS, BeiDou and Galileo have an independent control segment, detailed later in this chapter.

In the next sections, the structure of the considered GNSSs is described including the architecture and the features of GNSS signals.

2.1.1. GPS

Created and realized by the U.S. Department of Defense (DoD), GPS constellation is composed of 31 healthy GPS satellites transmitting signals evenly spread across six orbital planes (Navcen.uscg.gov, 2016). This is more than the designed 24 satellites, in order to provide redundant measurements to the receiver and guarantee global coverage in case of outages. With a designed orbital inclination angle of 55^{o} and orbital altitude of approximately 20200 km, the GPS satellites have an orbital period of approximately 11

hours 58 minutes and a satellite configuration that recurs identically each sidereal day (DoD Positioning Navigation and Timing Executive Committee, 2008).

The current GPS operational control segment includes a master control station, an alternate master control station, 12 command and control antennas and 16 monitoring sites. The locations of these facilities are shown in Figure 2.1.

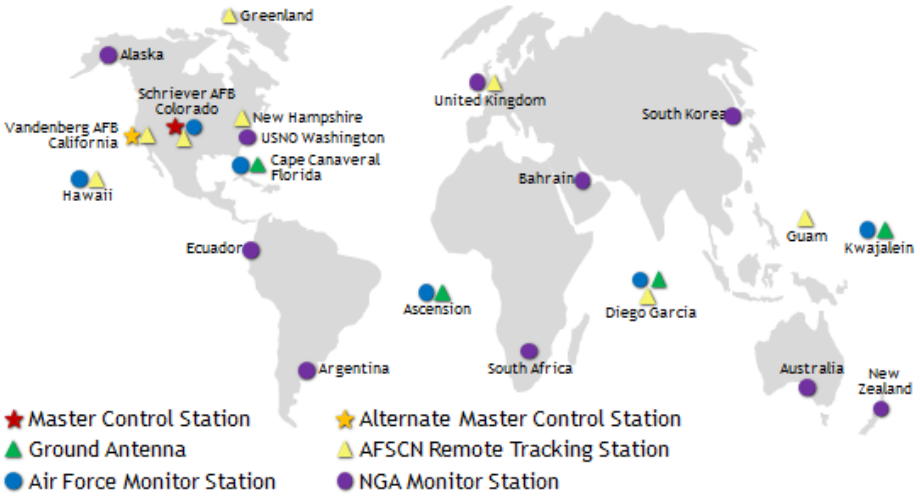

Figure 2.1 GPS GCS (Gps.gov, 2016)

GPS satellites broadcast legacy signals on two carrier frequencies: L1 (1575.42 MHz) and L2 (1227.60 MHz). Carrier frequencies are created by multiplying the fundamental frequency 10.23 MHz for 154 and 120, respectively. These carriers are modulated by two kinds of Pseudo-Random-Noise (PRN) codes, the Coarse-Acquisition (C/A) code with a 1.023 MHz chip-rate and a period of one millisecond, and the Precise (P) code with a 10.23 MHz chip-rate and a period of seven days. The C/A code is available on the L1 carrier only and the P code on both L1 and L2. The C/A code is for civil use, while the P code instead is for military purpose, its access is restricted to authorized users only (using encrypting techniques) and its use is associated with Precise Positioning Service (PPS). A modernized GPS signal with carrier frequency L5 (1176.45 MHz) is designed for safety-of-life applications.

GPS system uses the Code Division Multiple Access (CDMA), i.e. all satellites use the same frequencies and each satellite transmits a different PRN code, so that at the receiver level it is possible to distinguish between tracked satellites. PRN codes are also called “ranging codes”, because the comparison between the received PRN code and its replica generated

inside the receiver, allows computing for the propagation interval of the signal from the satellite to the user (called pseudo-range).

2.1.2. GLONASS

GLONASS is the Russian counterpart of GPS. The full constellation was initially completed in 1995, representing the first generation GLONASS satellites with a design operational life-time of 3 years. In the early 2000s, a plan to restore the GLONASS constellation started. The launch of the modernized Russian navigation satellites, GLONASS-M, started in 2003 (Bhatta, 2011) and finished in 2010, completing the Russian constellation. The first of the latest generation of Russian navigation satellite, GLONASS-K, was launched in 2011 and has a design life-time of 10 years. GLONASS-M and GLONASS-K designs increase satellite reliability. Furthermore, the GLONASS-K is being designed to broadcast integrity data and wide area differential corrections (Kaplan, 2005).

The originally planned Russian's GLONASS space segment consists of 24 satellites, placed on three orbital planes, with eight satellites per plane. The satellites are placed into nominally circular orbits with target inclinations of 64.8^{o} and an orbital radius of 19140 km, about 1060 km lower than GPS satellites. The GLONASS ground track repetition period is 7 days 23 hours 27 minutes. The orbit period of each satellite is 11 h 15m so that, after eight sidereal days, the GLONASS satellites have completed exactly 17 orbital revolutions. Currently (September 2016), 27 satellites compose GLONASS constellation (New.glonass-iac.ru, 2016).

The GLONASS ground segment consists of a network of five Telemetry, Tracking and Command centers (TT&C), the Central Clock situated in Schelkovo (near Moscow), three Upload Stations, two Laser Ranging Stations (SLR), a network of four Monitoring and Measuring Stations. Furthermore, six additional Monitoring and Measuring Stations are planned to be operating on the territory of the Russian Federation and the Commonwealth of Independent States.

Figure 2.2 shows the arrangement of the GLONASS ground segment.

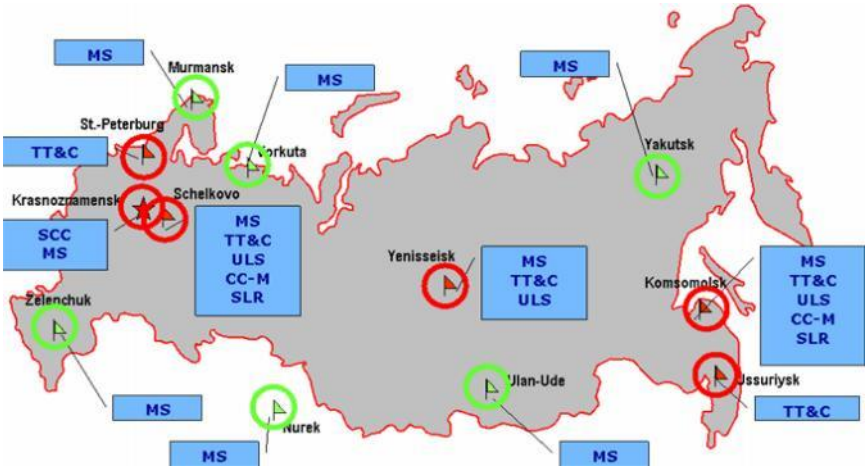

Figure 2.2 GLONASS GCS (New.glonass-iac.ru, 2016)

The Glonass-M satellites transmit signals on two frequency bands: L1 ~ 1.6 GHz and L2 ~ 1.25 GHz. On both the bands, the carriers are modulated by two ranging codes, one associated to a standard positioning service (ST) for all the users and another associated to a precise positioning service (VT) only for authorized users. Both carriers are modulated by signal storing the navigation message.

Unlike GPS, GLONASS system uses the Frequency Division Multiple Access (FDMA) technique, i.e. each satellite transmits on carriers with different frequencies. The sub-bands for L1 frequencies range from 1598.0625 MHz to 1605.3750 MHz with a 0.5625 MHz spacing; the nominal central frequency is at 1602.0 MHz. The sub-bands for L2 frequencies range from 1242.9375 MHz to 1248.6250 MHz with a 0.4375 MHz spacing; the nominal central frequency is at 1246.0 MHz (GLONASS-ICD 2008).

2.1.3. Galileo

In 1998, the European Union (EU) decided to pursue a satellite navigation system independent of GPS, designed specifically for civilian use worldwide (Kaplan, 2005). When completed, Galileo will provide multiple levels of service to users throughout the world. Specifically Galileo will provide four services to worldwide users:

- Galileo Open Service (OS) – Free of charge for all users, featuring excellent positioning and timing performance.
- Galileo Commercial Service – Access to two additional encrypted and guaranteed signals, delivering a higher data throughput rate and increased accuracy.

- Galileo Public Regulated Service (PRS) – provides position and timing to specific users requiring a high continuity of service, with controlled access.
- Support to Search and Rescue Service (SAR) - represents the contribution of the Europe to COSPAS-SARSAT, the international satellite-based search and rescue distress alert detection and information distribution system. Galileo satellites will be able to pick up signals from emergency beacons carried on ships, planes or persons and ultimately send these back to national rescue centers.

The Galileo constellation will be composed by 30 satellites in three orbital planes at an inclination of 56° from the equatorial plane. Each orbital plane consists of 10 satellites, including 9 operational ones and one spare, orbiting at an altitude of 23222 km; the orbital period is around 14 hours and a repetition period of approximately 10 days. Currently (September 2016), only nine Galileo satellites are working properly (Satellite-navigation.eu, 2016).

The heart of the Galileo ground segment will be the two Control Centres. Each Control Centre will manage control functions supported by a GCS and mission functions, supported by a dedicated Ground Mission Segment (GMS). The GMS will use a network of Galileo Sensor Stations (GSS) to monitor the navigation signals of the satellites on a continuous basis (Gsc-europa.eu, 2016). The GMS communicates with the Galileo satellites through a network of Mission Up-Link Stations (ULS). The future development of Galileo ground segment is shown in Figure 2.3.

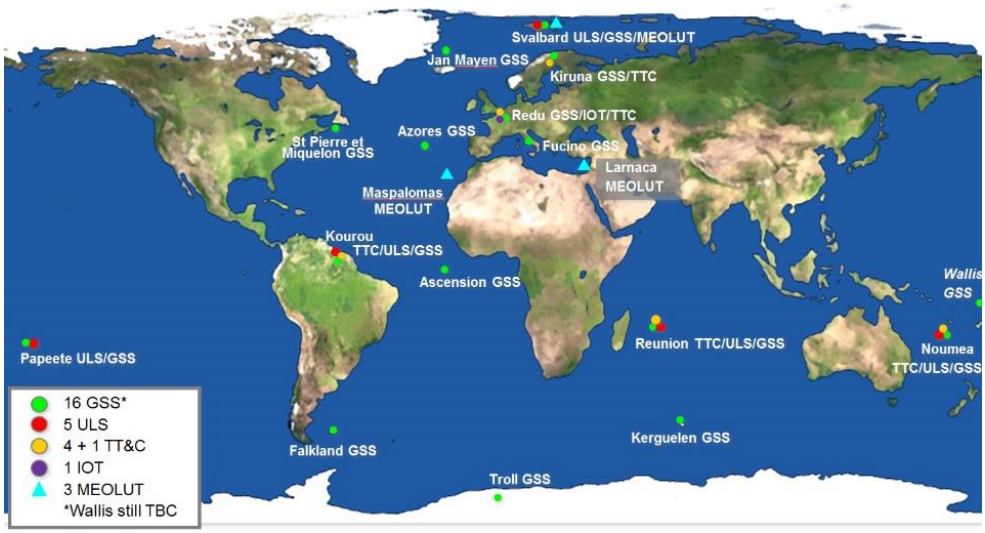

Figure 2.3 GALILEO GCS, available at (GPS World, 2016)

All Galileo satellites transmit six independent signals, on carrier frequencies E1 (1575.420 MHz), E5 (1176.450 MHz) and E6 (1207.140 MHz) and are denoted as L1F, E5a, E5b, E6C, that are open-access, and L1P, E6P, that are restricted-access.
Binary Offset Carrier (BOC) techniques or Binary Phase Shift Keying with Rectangular spreading symbols (BPSK-R) are used to modulate the signals and all satellites adopt the same carrier frequencies with different ranging codes using CDMA transmission (OS SIS IC 1.1, 2010).

2.1.4. BeiDou

BeiDou is the Chinese name for the multistage satellite navigation program designed to provide positioning, fleet-management and precision-time dissemination to Chinese military and civil users.
The Chinese government planned to deploy a regional or worldwide navigation constellation that will consist of five GEO satellite and three IGSO satellites, to provide regional coverage in the Asia-Pacific area, and 27 MEO satellites to provide global positioning services (BDS-ICD 2012, Ge et al. 2012, He et al. 2013, Zhao et al. 2013). At the time of writing (September 2016), the Chinese satellite navigation system BeiDou (BDS) constellation is composed of twenty operational satellites: eight IGSO, five GEO and seven MEO.
The GEO satellites are placed at latitudes 58.75°E, 80°E, 110.5°E, 140°E and 160°E, respectively. The IGSO satellites orbit with an inclination of 55° and cover a longitude band from 90°E to 125°E. The MEO BeiDou satellite orbits have an altitude of 21528 km with an inclination of 55° and have an orbital period of 12 hours and 53 minutes. The repetition period of BeiDou MEO is approximately seven days.
Currently, the BeiDou GCS includes one Master Control Station, two Upload Stations and 30 Monitor Stations located in China.
All the BeiDou satellites transmit navigation signal at three central frequencies which are 1561.098 MHz (B1), 1207.140 MHz (B2) and 1268.520 MHz (B3) (Van Diggelen, 2009; BDS-ICD 2012; He et al, 2013).

2.2. GNSS Fundamentals

GNSS utilizes the concept of one-way time of arrival (TOA) ranging. Satellite transmissions are referenced to highly accurate atomic frequency standards onboard the satellites, which are in synchronism with a time scale adopted by the GNSS. In GNSS adopting CDMA strategy, all satellites transmit on the same frequency, but with specific ranging codes. These codes were selected in order to have low cross-correlation properties. The navigation message provides the necessary parameters for the receiver to compute the satellite position at the time of signal transmission, whereas the ranging code enables the user's receiver to determine the transit time of the signal and thereby obtain the satellite-to-user range (Hoffmann-Wellenhof et al, 1992; Kaplan, 2005). This technique requires that there is a clock also in the user receiver. If satellite and receiver clocks were synchronized then the time of travel, multiplied by speed of light, provides the range satellite-receiver; in this case at the transmission epoch, the user position would belong to the spherical surface centered in the satellite position and with radius equal to the range. Hence, using this technique, ranges to only three satellites would be needed, since the intersection of three spheres yields the three unknowns (e.g., latitude, longitude, and height) as shown in Figure 2.4. However, a crystal clock is usually installed in navigation receivers to minimize the cost, complexity and size of the receiver. For this reason, at least four measurements are necessary to calculate user latitude, longitude, height and receiver clock offset between internal and system time scales (Hoffmann-Wellenhof et al, 1992; Kaplan, 2005).

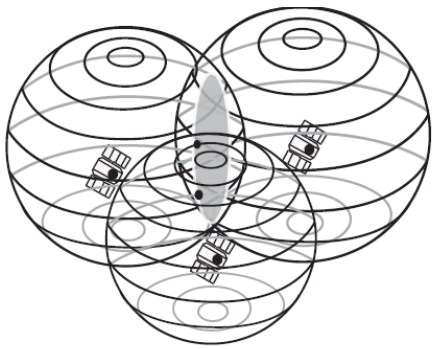

Figure 2.4 User located at one of two points on shaded circle (Kaplan, 2005)

2.3. GNSS Observables

GNSS receivers mainly provide three types of measurement, specifically pseudorange (PR), Doppler shift and carrier phase.

The GNSS observables (PR and Doppler shift) are ranging observables that are computed from measured time or phase differences, based on a comparison between received signals and receiver generated signals.

The PR is the measured range between the receiver and the satellite, equal to the travel time of the signal from the satellite to the receiver, scaled by the speed of light. The PR is obtained using the ranging code C/A and the correlation between the received PRN-code and a replica generated inside the receiver. Since the received signal is referred to the satellite time scale and the local signal is referred to the receiver clock, the measured shift between the two signals contains clock biases (Hoffmann-Wellenhof et al, 1992).

In error-free condition, the equation of PR is expressed as:

$$PR_{true} = d + c\delta t_s - c\delta t_r \tag{2.1}$$

where PR_{true} is the true PR (expressed in m), d is the satellite-receiver distance (m), $c\delta t_s$ and $c\delta t_r$ are satellite and receiver clock offset (m) respectively and c is the speed of light (m/s). However, the measured PR is corrupted by several error sources such as interference, multipath, ionospheric, tropospheric and relativistic effects described in the following section (Hoffmann-Wellenhof et al, 1992; Parkinson et al, 1996). Using Single Point Positioning (SPP), the method adopted in this work, all the error terms are modeled or neglected so there are only four unknowns, which are the three receiver coordinates, included in the d term, and the receiver clock bias $c\delta t_r$, if only one independent GNSS is used for the navigation.

The carrier phase observation contains the difference in phase of the incoming satellite carrier signal and the receiver carrier signal generated with the same frequency. The phase measurement, multiplied by the carrier wavelength, is the most accurate satellite-to-user distance; the integer number of wavelength within the distance is an additional unknown and it cannot be determined in SPP (Parkinson et al, 1996). The carrier phase measurement is expressed as:

$$\lambda \cdot \phi = d + c\delta t_s - c\delta t_r + \lambda \cdot N + \delta d_{orb} - \delta d_{iono} + \delta d_{tropo} + \delta d_{multi} + \varepsilon \qquad (2.2)$$

where

λ is the wavelength of the carrier (m);

ϕ is the phase measurement (expressed as number of cycles);

d is the satellite-receiver distance (m);

$c\delta t_s$ and $c\delta t_r$ are satellite and receiver clock offset (m) respectively;

N is the number of cycles in the satellite–receiver distance;

δd_{orb} is the orbital error (m);

δd_{iono} is the ionospheric error (m);

δd_{tropo} is the tropospheric error (m);

δd_{multi} is the error due to the multipath (m);

ε is the error caused by the noise in the receiver and contains residual errors (m).

GNSS provides the capability for determining three-dimensional user velocity, using the Doppler observable. The relative motion of a satellite and the user produces the Doppler shift that can be considered as a projection of the relative velocity vector onto the line-of-sight vector. Doppler is a measurement of the instantaneous phase rate of a tracked satellite's signal. The equation for Doppler measurement is obtained computing the derivative of PR equation (2.2):

$$\dot{PR} = \dot{d} + c\delta\dot{t}_s - c\delta\dot{t}_r + \delta\dot{d}_{orb} - \delta\dot{d}_{iono} + \delta\dot{d}_{tropo} + \delta\dot{d}_{multi} + \dot{\varepsilon} \qquad (2.3)$$

The velocity accuracy, obtainable using the Doppler measurements, is in the order of some centimeter per second (Hoffmann-Wellenhof et al, 1992) since the errors affecting Doppler measurement are derivatives of the orbital, propagation (atmospheric and multipath) and noise errors.

2.4. GNSS Errors

In section 2.3, the formulation of the pseudorange and carrier-phase measurements is discussed. Several error sources corrupt these measurements and an examination of these error sources is presented within this section.

Satellite and receiver clock offsets directly translate into pseudorange and carrier-phase errors. As satellite signal propagates through the atmosphere, PRN code experiences delays, making the pseudorange larger than it would be if the signal were propagated in a vacuum. The signal carrier is delayed by the troposphere but is actually advanced by the ionosphere. Furthermore, reflections (i.e. multipath) and hardware effects between the user's antenna phase center and receiver code correlation point may delay (or advance) the signal components (Parsons, 2000).

The satellites contain atomic clocks able to control all onboard timing operations, including broadcast signal generation. The MCS determines and transmits clock correction parameters to the satellites for rebroadcasting in the navigation message. These correction parameters are implemented by the receiver using the second-order polynomial:

$$c\delta t_s = a_{f0} + a_{f1}(t - t_{oc}) + a_{f2}(t - t_{oc})^2 + \delta t_r \qquad (2.4)$$

where

a_{f0} is the clock bias (s),

$a_{f1}$is the clock drift (s/s),

a_{f2} is the frequency drift (s/s^2),

t_{oc} is the clock data reference time (s),

t is the current epoch (s),

δt_r is the correction due to relativistic effects (s).

Since the correction parameters for satellite clock offset are computed using a curve-fit of predicted estimates of the actual satellite clock errors, some residual errors remain. The residual clock error, δt_s, results in ranging errors that typically varies from 0.3 to 4 m, according to the type of satellite and the age of the broadcast data (Kaplan, 2005).

The receiver clock offset represents the difference between the time maintained by the receiver and the time determined by the underlying GNSS atomic time scale.

The receiver clock bias is a time-varying error affecting all the range measurements in the same amount for a fixed epoch and is estimated as an unknown, along with the receiver position in the SPP mode. Its drift (time derivative of the clock offset) affects the Doppler measurements and is estimated as an unknown parameter along with the receiver velocity (Kaplan and Leva, 2006).

The orbital error is the difference between the computed and the actual satellite positions. Estimates of ephemerides for all satellites are computed and uplinked to the satellites, with other navigation data, for rebroadcast to the user. These corrections are generated using a curve fit of the control segment's best prediction satellite positions at the time of upload. The residual satellite position error is a vector with typical magnitudes in the range of 1–6 m (Kaplan, 2005). The effective pseudorange and carrier-phase errors due to ephemeris prediction errors can be computed by projecting the satellite position error vector onto the satellite-to-user Line Of Sight (LOS) vector. Ephemeris errors are generally smallest in the radial (from the satellite toward the center of the Earth) direction. The components of ephemeris errors in the along-track (the instant direction of travel of the satellite) and cross-track (perpendicular to the along-track and radial) directions are much larger.
The effective pseudorange or carrier-phase error due to ephemeris prediction errors is about 0.8 m (1σ) (Conley et al, 2006).

The relativistic correction is due to the slight eccentricity of the satellite orbits, bringing a periodic change in the satellite gravitational potential and in the satellite speed in the inertial frame (Conley et al, 2006). The relativistic correction is given by the formula:

$$\delta t_r = F \cdot ecc \cdot \sqrt{a} \cdot \sin(E) \tag{2.5}$$

where
F=-4.442807633·10^{-10} s/m$^{1/2}$,
ecc is the orbit eccentricity,
$\sqrt{a}$ is the square root of the orbital semi-major axis,
E is the eccentric anomaly of the satellite.
Due to rotation of the Earth during the time of signal transmission, the computations for the satellite positions in an Earth-centered Earth-fixed (ECEF) coordinate system cause a relativistic error, known as Sagnac effect. During the propagation time of the signal, a clock

on the surface of the Earth will experience a finite rotation with respect to an Earth-Centered-Inertial (ECI) coordinate system. Clearly, if the user experiences a net rotation away from the satellite, the propagation time will increase, and vice versa. If left uncorrected, the Sagnac effect can lead to position errors of about 30 m (Kaplan, 2005). There are a number of approaches for correcting for the Sagnac effect. One common approach is to avoid the Sagnac effect entirely by working within an ECI coordinate system for satellite and user position computations. An ECI frame can be conveniently obtained by freezing an ECEF frame at the instant of time when a pseudorange measurement set is obtained. The Sagnac effect does not arise in an ECI frame. Importantly, the satellite positions must correspond to the time of transmission, t_s, that is a natural measurement of a GNSS receiver. Then, each satellite position can be computed in terms of its ECEF coordinates (x_s , y_s , z_s) at its time of transmission using the described broadcast ephemerides. Then, each satellite position can be transformed into the common ECI frame using the rotation, obtaining the corrected positions as:

$$\begin{bmatrix} x_s^{ECI} \\ y_s^{ECI} \\ z_s^{ECI} \end{bmatrix} = \begin{bmatrix} cos\dot{\Omega}(t_r - t_s) & sin\dot{\Omega}(t_r - t_s) & 0 \\ -sin\dot{\Omega}(t_r - t_s) & cos\dot{\Omega}(t_r - t_s) & 0 \\ 0 & 0 & 1 \end{bmatrix} \begin{bmatrix} x_s \\ y_s \\ z_s \end{bmatrix} \tag{2.6}$$

where t_s is the time of reception and $\dot{\Omega}$ is the Earth angular velocity. The magnitude of this relativistic effect can range from 0.001 ppm in relative positioning to about 18.7 mm for point positioning (Kaplan, 2005).

One of the main sources of error for GNSS signals is the atmosphere, because GNSS signals are affected by the medium through which the signals travel from the satellites to the receiver antenna; the effects introduced by the atmosphere are delay or advance on the signals and are mainly due to ionosphere and troposphere. Efforts have been carried out to mitigate the effects of the ionosphere and troposphere; such efforts are mainly focused on ionosphere because, even if ionospheric and tropospheric errors are comparable, the variability of Earth's ionosphere is much larger. For this reason, the ionospheric delay is more difficult to model than the tropospheric one. The range of the ionospheric error varies from a few meters up to 30 meters (Langley, 1998), whereas the tropospheric error at the zenith assumes values between two and three meters. Tropospheric error usually does not change by more than

±10%, even for long periods of time, whereas the ionospheric error frequently changes by at least one-order of magnitude during the course of each day (Klobuchar, 1996).
Ionosphere is defined as the ionized region of the upper part of the atmosphere, extending from about 50 km to more than 1000 km. The ionosphere is a dispersive medium: the wave speed depends on the physical properties of the medium and on the frequency of the signal. Due to the complex nature of the ionospheric layer, different methods have been proposed to model it, such as empirical models, numerical maps, analytical models and physical models.
In this research, only single frequency solutions typical for civilian mass-market applications are considered and in this case the ionospheric error can be reduced using suitable models. For GNSS receivers, two models are available to compute real time ionospheric corrections, NeQuick and Klobuchar, both belonging to the class of empirical models.
Klobuchar model is adopted by GPS and it is designed to reach a correction capability of at least 50% of the ionospheric delay (Klobuchar, 1996; Angrisano et al, 2013b). NeQuick model is adopted by Galileo and is able to remove about 70% of the ionospheric code delay (European GNSS Open Service, 2015).

The troposphere is the lower part of the atmosphere and is nondispersive for frequencies up to 15 GHz (Hoffmann-Wellenhof et al, 1992; Kaplan, 2005). Within this medium, the phase and group velocities associated with the GNSS carrier and signal information (PRN code and navigation data) on both L1 and L2 are equally delayed with respect to free-space propagation. This delay is a function of the tropospheric refractive index, which is dependent on the local temperature, pressure, and relative humidity. The range equivalent of this delay can vary from about 2.4 m, for a satellite at the zenith and the user at sea level, to about 25 m for a satellite at an elevation angle of approximately 5º (Hoffmann-Wellenhof et al, 1992; Kaplan, 2005). The tropospheric error is typically divided in two components: a dry (hydrostatic) component, which arises from the dry air, gives rise to about 90% of the tropospheric delay and can be predicted very accurately, and wet (non-hydrostatic) component which arises from the water vapor and is more difficult to predict due to uncertainties in the atmospheric distribution (Hopfield,1971).
Several models can be used to reduce the influence of the tropospheric error, bringing sub-meter accuracy (Spilker, 1997). In this research the Sastamoinen model is used (Sastamoinen, 1993).

One of the most significant errors incurred in the receiver measurement process is multipath. The multipath error is due to the signal arrival at the receiver via multiple paths caused by the reflections during the signal propagation (Parkinson et al, 1996). Multipath errors affect pseudorange, Doppler and carrier-phase measurements in different ways. Multipath errors vary significantly in magnitude depending on the operational environment, satellite elevation angle, receiver signal processing, antenna gain pattern and signal characteristics. Code multipath can vary from few meters in "open-sky" environments to over one hundred meters in signal-degraded scenarios (Parkinson et al, 1996). Carrier phase multipath is generally of centimeter order. Since the Doppler measurement is the derivative of carrier phase measurement, the multipath effect is very small on the velocity estimation (Godha, 2006).

User equipment bias errors introduced by the receiver hardware are often ignored because they are relatively small in comparison to other error sources (Kaplan, 2005). These errors are negligible for carrier phase measurement and are of few decimeters order for code measurement (Conley et al, 2006).

3. GNSS Navigation Solution Estimation

This section discusses the estimation theory used in this research for user position, velocity and time computation.

The estimation process allows obtaining a set of desired unknowns starting from a set of uncertain measures, according to a proper optimization criterion. To estimate the unknown parameters, it is necessary to define a functional relationship between the measures; generally, this relationship is known as measurement model, while the set of unknowns is defined as system state vector (Angrisano, 2010).

If the number of (independent) equations is at least equal to the number of the unknowns, then it is possible to solve the measurement model for the unknown parameters. If the measurements are redundant, the solution can be estimated using an estimation method; otherwise, the solution is unique (if it exists) and there is no possibility for optimization.

Least-squares adjustment is a technique for carrying out objective quality control of surveying measurements by processing sets of redundant observations according to mathematically well-defined rules. The term "redundant observations" implies that the number of available observations is larger than minimum number necessary to determine the unknowns. In particular, WLS method is used in this research and it is introduced in this chapter. In order to improve the navigation solution, the choice of appropriate stochastic model for the GNSS observations plays an important role in satellite navigation. There are several weighting methods adopted for this aim and the most commonly widespread are described in this chapter.

3.1. User Position, Velocity and Time Computation

As described in section 2.3, in GNSS positioning the user position is estimated using the pseudoranges (PR) measurements, while user velocities are computed from the pseudorange rate ($\dot{PR}$) observables.

Starting from the PR measurement equation, applying all the corrections described in Section 2.4 and including all the residual errors in ε_{PR} term, yields:

$$PR = d + c\delta t + \varepsilon_{PR} \tag{3.1}$$

where

d id the geometric range, computed as $d = \sqrt{(x_s - x)^2 + (y_s - y)^2 + (z_s - z)^2}$

$c\delta t$ is the receiver clock offset,

(x_s, y_s, z_s) are the satellite coordinates and (x , y , z) are the receiver coordinates, both in ECEF frame.

The satellite coordinates in the ECEF frame are computed using the ephemeris information contained in the navigation message, as described subsequently, while the receiver coordinates and the receiver offset $c\delta t$ form the state vector must be estimated $\underline{x} = [x, y, z, c\delta t\ ]^T$.

When a single independent GNSS system is used, at least four simultaneous visible satellites are necessary to form a set of equations (3.1) to solve for the unknowns, using an iterative technique based on linearization. The observation equation must be linearized about a nominal value, that is usually the best estimated expressed as $\underline{\hat{x}} = [\mathrm{x}_0, \mathrm{y}_0, \mathrm{z}_0, \mathrm{c\delta t}_0\ ]^{\mathrm{T}}$. By expanding (3.1) in a Taylor series, around the approximate position (Kaplan, 2005), and truncating it at the first order, the following expression is obtained:

$$PR = PR_0 + \left.\frac{\partial PR}{\partial x}\right|_{\hat{x}} (x - x_0) + \left.\frac{\partial PR}{\partial y}\right|_{\hat{x}} (y - y_0) + \left.\frac{\partial PR}{\partial z}\right|_{\hat{x}} (z - z_0) + \left.\frac{\partial PR}{\partial (c\delta t)}\right|_{\hat{x}} (c\delta t - c\delta t_0) \tag{3.2}$$

where

$\left.\frac{\partial PR}{\partial x}\right|_{\hat{x}}$ is the partial derivative of the function with respect to the variable x, evaluated in the approximate point $\underline{\hat{x}}$,

$PR_0 = \sqrt{(\mathrm{x_s} - \mathrm{x_0})^2 + (\mathrm{y_s} - \mathrm{y_0})^2 + (\mathrm{z_s} - \mathrm{z_0})^2} + c\delta t_0$ is the predicted PR.

Applying properly the computations, the equation (3.1) becomes

$$z_{PR} = PR - PR_0 = a_X \Delta x + a_Y \Delta y + a_Z \Delta z + \Delta(c\delta t) \tag{3.3}$$

where

z_{PR} is the difference between the measured and predicted PR,

Δx, Δy, Δz and $\Delta(c\delta t)$ are the incremental components from the approximate position as indicated in (3.2),

$a_X = \frac{x_0 - x_s}{d_0}$, $a_Y = \frac{y_0 - y_s}{d_0}$, $a_Z = \frac{z_0 - z_s}{d_0}$ are the direction cosines of the unit vector, pointing from the approximate user position to the observed satellite.

The linearized measurement model is obtained from a set of equations (3.3):

$$\underline{z}_{PR} = H_{PR} \cdot \underline{\Delta x} + \underline{\varepsilon}_{PR} \tag{3.4}$$

The vector $\underline{\Delta x} = [\Delta x\ \Delta y\ \Delta z\ \Delta(c\delta t)]^T$ is the state vector of the linearized measurement model and has four components if a single GNSS is used. The first three ones are the position offset of the user from the linearization point; the fourth one is the offset of the user time bias from the bias assumed in the linearization point.

The vector $\underline{z}_{PR}$ contains the differences between measured and computed PRs.

Finally, $\underline{\varepsilon}_{PR}$ is the residual errors vector and H_{PR} is the geometry matrix defined as:

$$H = \begin{bmatrix} a_{x1} & a_{y1} & a_{z1} & 1 \\ a_{x2} & a_{y2} & a_{z2} & 1 \\ \vdots & \vdots & \vdots & \vdots \\ a_{xn} & a_{yn} & a_{zn} & 1 \end{bmatrix} \tag{3.5}$$

where a_{xi}, a_{yi} and a_{zi} are the direction cosines as defined previously.

Once the unknowns $\underline{\Delta x}$ are obtained through the chosen estimation method, the user coordinates and the receiver clock offset are obtained as follows:

$$\underline{x} = \underline{\hat{x}} + \underline{\Delta x} \tag{3.6}$$

Since $\underline{z}_{PR}$ is contaminated by unknown random errors, the measurement model (3.4) should be treated as a stochastic equation and the unknowns to be computed should be determined using parameter estimation techniques such as LS estimation (Kuusniemi, 2005; Koch, 2013). After the linearization, the solution is estimated in an iterative procedure until the elements in the correction vector will have a sufficiently small value within a pre-set threshold.

GNSS receivers provide velocity measurements by processing carrier-phase measurements, which enable precise estimation of the Doppler frequency of the received satellite signals. The Doppler shift is produced by the relative motion of the satellite with respect to the user. The satellite velocity vector $\underline{v_s}$ is computed using ephemeris information and a suitable orbital model (Hoffmann-Wellenhof et al, 1992; Kaplan, 2005). The received frequency, f_R, can be approximated by the classical Doppler equation as follows:

$$f_R = f_T \left(1 - \frac{\underline{v} \cdot \underline{a}}{c}\right) \tag{3.7}$$

where

f_T is the transmitted satellite signal frequency,

$\underline{v} = \underline{v_s} - \underline{v_R}$ *i*s the satellite-to-user relative velocity vector, where $\underline{v_s}$ is the velocity of the satellite and $\underline{v_R}$ is the velocity of the user, both referenced to a common ECEF frame.

$\underline{a}$ is the unit vector pointing along the line of sight from the user to the satellite, and

c is the speed of propagation.

The Doppler offset due to the relative motion is computed from (3.7) as:

$$\Delta f = f_R - f_T = -f_T \left(\frac{(\underline{v_s} - \underline{v_R}) \cdot \underline{a}}{c}\right) \tag{3.8}$$

The equation (3.8) is multiplied for the signal wavelength λ obtaining:

$$\dot{d} = -\lambda \cdot (f_R - f_T) \tag{3.9}$$

The transmitted frequency is affected by the satellite clock drift, while the receiver clock drift influences the observed frequency so the pseudorange rate $\dot{PR}$ can be defined as:

$$\dot{PR} = -\lambda \cdot (\hat{f}_R - \hat{f}_T) \tag{3.10}$$

where

λ is the signal wavelength (m)

$\hat{f}_R$ is the received frequency (Hz) given by the relationship $\hat{f}_R = f_R + \Delta f_R$, where f_R is the ideal received frequency and Δf_R is the correction due to the drift of the user clock
$\hat{f}_T$ is the actual transmitted frequency (Hz) expressed as $\hat{f}_T = f_T + \Delta f_T$, where f_T is the nominal transmitted frequency and Δf_T is the correction broadcast by GCS in the navigation message.

Resolving the computations in (3.10), replacing $\lambda \cdot \Delta f_R = c\dot{\delta}t_R$ and $\lambda \cdot \Delta f_S = c\dot{\delta}t_S$, the equation becomes:

$$\dot{PR} = \dot{d} + c\dot{\delta}t_S + c\dot{\delta}t_R \tag{3.11}$$

Applying the appropriate corrections, considering the residual errors in $\varepsilon_{\dot{PR}}$ term and omitting the subscript "R" for the receiver clock drift, the equation for the pseudorange rate is:

$$\dot{PR} = \dot{d} + c\dot{\delta}t \quad + \varepsilon_{\dot{PR}} \tag{3.12}$$

Several approaches can be used in order to compute the receiver velocity; in this research, an immediate method considering the receiver position is used. Rearranging the equation (3.12), the result is:

$$\dot{PR} - \underline{v}_S \cdot \frac{(\underline{r}_S - \underline{r})}{|\underline{r}_S - \underline{r}|} = -\underline{v}_R \cdot \frac{(\underline{r}_S - \underline{r})}{|\underline{r}_S - \underline{r}|} + c\dot{\delta}t \tag{3.13}$$

Reminding that $\underline{a} = \frac{(\underline{r}_S - \underline{r})}{|\underline{r}_S - \underline{r}|}$ and expanding the dot products:

$$\begin{aligned} &\dot{PR} - v_{SX}\frac{x_s - x_0}{d} - v_{SY}\frac{y - y_0}{d} - v_{SZ}\frac{z_s - z_0}{d} = \\ &= \frac{x_0 - x_s}{d}v_{RX} + \frac{y_0 - y_s}{d}v_{RY} + \frac{z_0 - z_s}{d}v_{RZ} + c\dot{\delta}t \end{aligned} \tag{3.14}$$

Reordering the above equation, yields:

$$z_{\dot{PR}} = b_X v_{RX} + b_Y v_{RY} + b_Z v_{RZ} + c\dot{\delta}t \tag{3.15}$$

where

$z_{\dot{P}R}$ is the difference between the measured and the satellite motion-based pseudorange rate,

v_{RX}, v_{RY} and v_{RZ} are receiver velocity components,

$c\dot{\delta}t$ is the receiver clock drift, and

$b_X = \frac{x_0 - x_s}{d}$, $b_Y = \frac{y_0 - y_s}{d}$ and $b_Z = \frac{z_0 - z_s}{d}$ are the direction cosines of the vector $\underline{a}$.

The equation (3.15) is linear for the receiver velocity components and clock drift, which are the unknowns of the problem. The receiver position components must be known a priori, while the satellite position and velocity are determined from ephemeris data. For these reasons, to solve for the receiver velocity components and clock drift at least four simultaneous Doppler measurements are necessary (Kaplan, 2005; Angrisano, 2010).
The Doppler measurement equation is expressed as:

$$\underline{z}_{\dot{P}R} = H_{\dot{P}R} \cdot \underline{v}_R + \underline{\varepsilon}_{\dot{P}R} \tag{3.16}$$

where $H_{\dot{P}R}$ is the design matrix as defined in the formulation for the user position computation and the solution for the velocity and time drift are obtained using the chosen estimation method.

3.2. Weighted Least Square Estimation

In case the number of measurements is larger than the number of unknowns, it is possible to reduce the effect of the observation errors; practically if the measures are redundant, the problem is only to solve an overdetermined linear system equation (Kuusniemi, 2005). The LS technique is the most common estimation procedure in geomatics application, using purely the measurements (Petovello, 2009). Since the measurements are characterized by different accuracy, the WLS approach is used in this research.
A linear measurement model in discrete form can be written as:

$$\underline{z}_k = H_k \cdot \underline{x}_k + \underline{\varepsilon}_k \tag{3.17}$$

where k is related to the k^{th} epoch.

The aim of WLS is to obtain an estimate of the unknowns, $\underline{\hat{x}}_k$, minimizing the weighted sum of squares of deviations, $(\underline{z}_k - H_k \cdot \underline{\hat{x}}_k)$

The cost function to minimize is

$$J_k = (\underline{z}_k - H_k \cdot \underline{\hat{x}}_k)^T \cdot W_k \cdot (\underline{z}_k - H_k \cdot \underline{\hat{x}}_k) \tag{3.18}$$

W is a weighting matrix, usually defined as the inverse of the measurement error covariance matrix, denoted as R:

$$W = R^{-1} \tag{3.19}$$

Assuming uncorrelated measurements, R becomes a diagonal matrix, whose non-zero elements are the measurement error variances.
The WLS solution obtained by setting the derivative of (3.18) to zero and solving for $\underline{\hat{x}}_k$, is given by:

$$\underline{\hat{x}}_k = ({H_k}^T W_k H_k)^{-1} {H_k}^T W_k \cdot \underline{z}_k \tag{3.20}$$

Applying the variance propagation law to the latter formula, the associate covariance matrix is expressed as:

$$C_{\underline{\hat{x}}} = \left({H_k}^T W_k H_k\right)^{-1} {H_k}^T W_k R \quad W_k H_k \left({H_k}^T W_k H_k\right)^{-1} \tag{3.21}$$

Reminding the relationship (3.19), the previous equation becomes:

$$C_{\underline{\hat{x}}} = \left({H_k}^T W_k H_k\right)^{-1} \tag{3.22}$$

In ECEF frame, the state error covariance matrix takes the following form:

$$C_{\underline{\hat{x}}} = \begin{bmatrix} {\sigma^2}_x & \sigma_{xy} & \sigma_{xz} & \sigma_{xt} \\ \sigma_{yx} & {\sigma^2}_y & \sigma_{yz} & \sigma_{yt} \\ \sigma_{zx} & \sigma_{zy} & {\sigma^2}_z & \sigma_{zt} \\ \sigma_{tx} & \sigma_{ty} & \sigma_{tz} & {\sigma^2}_t \end{bmatrix} \tag{3.23}$$

Once the solution is obtained, the residuals can be computed. The vector of residuals $\underline{r}_k$, defined as the difference between the actual and the predicted measurements, is expressed as:

$$\underline{r}_k = \underline{z}_k - H_k \cdot \hat{\underline{x}}_k \tag{3.24}$$

Assuming a correct measurement model, the magnitude of the residuals vector provides an indication about the consistency between the measurements and they can be used to assess the quality of the estimated parameters.

3.3. Weighting Strategies

The computation of positions using GNSS observations requires two important steps: the definition of the functional relationship between the GNSS observations and the unknown parameters, as described previously, and the corresponding stochastic model referring to the statistics of the GNSS observations (Leick et al, 2015). Many researchers have highlighted the importance of the stochastic model, especially for high-accuracy applications (Han, 1997; Barnes et al., 1998; Wang et. al, 1998), recognizing it as a critical component to be enhanced. The parameter estimation used for positioning can only produce reasonable results if the stochastic model resembles reality (Wieser, 2001). For example, in presence of many multipath reflections and low-power signals as it occurs in signal-degraded scenarios, GNSS measurements are biased and noisy, and multiple blunders can occur in the same measurements set; to mitigate the effects of biases or gross errors, weights inversely related to the quality of the received signal should be used.

Assigning equal weights to all measurements is not a realistic assumption, since GNSS measurements are influenced by the orbit, atmospheric and multipath effects, which differ for each satellite and result in unequal precision. For example, measurements obtained from satellite at low elevation or with a low Carrier-to-Noise density power ratio (C/N_0) are prone to large errors due to multipath or ionospheric/tropospheric effects. To this purpose, scientific literature describes several independent variables as indicators of quality: criterions based on satellite elevation, SNR and combinations of them (Satirapod 2004; Realini and Reguzzoni, 2013) have been widely adopted. Some weighting strategies

commonly widespread in GNSS navigation are described in the follows paragraphs.

3.3.1. Signal power based weighting method

The basic measure of GNSS signal quality is its power. The C/N_0 is one of the most important signal quality indicator to be considered in difficult scenarios for satellite navigation. The C/N_0 in GNSS receivers is the ratio of the power level of the signal carrier to that of the noise in a 1 Hz bandwidth (Özlüdemir, 2004). It is a key parameter in analyzing GNSS receiver performance, being strictly related to receiver pseudorange and carrier phase precision (Sükeová et al, 2007).

A model for weighting GNSS observations based on the C/N_0 ratio was proposed in (Langley, 1997; Kuusniemi, 2005): weights are the inverse of measurement variance, whose expression is:

$$\sigma_i^2 = a + b \cdot 10^{\frac{-C/N_0}{10}} \tag{3.25}$$

where C/N_0 is the carrier-to-noise power density ratio expressed in dBHz units, while parameters *a* and *b* have to be chosen according to the local environment. In this research, the described weighting method is indicated as SPW method.

The SNR can be used instead of C/N_0 for the pseudorange observations. The SNR describes the ratio of the signal power and noise power in a given bandwidth, expressed in dB unit (Węzka et al, 2016). It is generally an indicator of the noise level that influences a GNSS observation and can be used as a measure of power for a GNSS signal.

3.3.2. Elevation dependent weighting method

The satellite elevation angle is often used to compute the measurements accuracy matrix. Measurements associated to low elevation angles are generally noisier with respect to measurements associated to high elevation angles; this is a typical feature of multipath and residual tropospheric errors (Kaplan, 2005). For example, the distance that a signal has to travel through the atmosphere is much longer for a low elevation satellite than for a high one.

The most common elevation-dependent variance model used in satellite navigation is (Eueler and Goad, 1991; Petovello, 2003; Angrisano et al, 2013a):

$$\sigma_i^2 = \frac{1}{sin^2(El_i)} \tag{3.26}$$

where El_i is the elevation angle of the i-th satellite and the weights assigned to the measurements increase with their values.

3.3.3. Combining signal power and elevation as a weighting method

Satellite elevation and signal-to-noise ratio can be used synergistically to build a measurement variance model.
A variance model, as function of the satellite elevation and C/N_0, was proposed by Realini (Realini and Reguzzoni, 2013) and is indicated as SPELW method in this research. The variance of the i-th satellite is expressed as:

$$\sigma_i^2 = \begin{cases} \dfrac{1}{sin^2(El_i)} \mathrm{r}_i & if\ C/N_0 < s_1 \\ 1 & if\ C/N_0 \geq s_1 \end{cases} \tag{3.27}$$

where

$$\mathrm{r}_i = 10^{-\frac{C/N_0 - s_1}{B}} \left[\left(\frac{A}{10^{-\frac{s_0 - s_1}{B}}} - 1 \right) \frac{C/N_0 - s_1}{s_0 - s_1} + 1 \right] \tag{3.28}$$

and s_1 is the threshold after which the measurements are considered good and the weights set to 1. The proposed values for the constant s_1, s_0, B and A can be found in (Realini and Reguzzoni, 2013).

3.4. Dilution of Precision

An accurate user position estimate is a function not only of the quality of the range

measurements but also of the user/satellite observation geometry. The dilution of precision (DOP) parameters can be used as indications of the goodness of receiver-satellite geometry. Poor satellite geometry implies navigation accuracy degradation due to its effect of amplifying random errors and biases.

A 2D example of the DOP concept is shown in Figure 3.1; the distance "loci of position" are represented by circles. In case a) the circles related to the two satellites intersect each other approximately with right angle. In case b) the angle between the circles is much smaller. In both cases, error-free circles are indicated and intersect each other at the user's location. Additional circles, indicating the uncertainty of the distance measurements, are included; the error range in both cases is the same. The shaded regions indicate the uncertainty areas of position for both configurations and it is evident the different accuracies obtained. With the same measurement error, the computed position, because of geometry, is less accurate in case b) and is more accurate in case a). This is can be noted comparing the shaded regions. The geometry of b) situation corresponds to a larger DOP than geometry in a) (Kaplan, 2005).

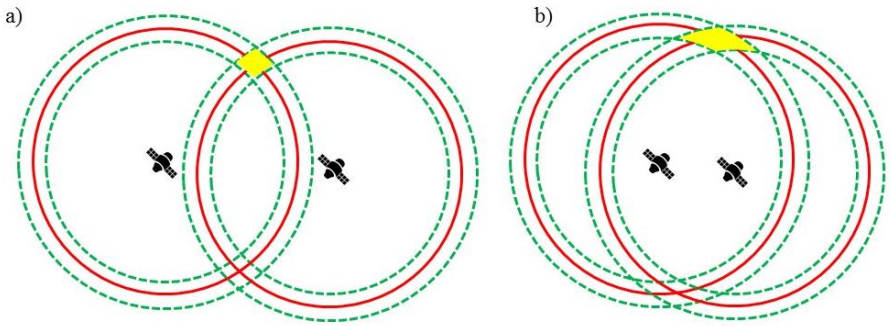

Figure 3.1 Satellite Geometry and Dilution of Position

The DOP parameters can be computed from the design matrix, which contains geometry information:

$$Q_{ECEF} = (H_{ECEF}^{T} H_{ECEF})^{-1} = \begin{bmatrix} q_{xx} & q_{xy} & q_{xz} & q_{xt} \\ q_{yx} & q_{yy} & q_{yz} & q_{yt} \\ q_{zx} & q_{zy} & q_{zz} & q_{zt} \\ q_{tx} & q_{ty} & q_{tz} & q_{tt} \end{bmatrix} \tag{3.29}$$

H is design matrix as described by equation (3.5) and the most used DOP parameters are the GDOP (Geometric DOP), PDOP (Position DOP), and TDOP (Time DOP) expressed as:

$$GDOP = \sqrt{q_{xx} + q_{yy} + q_{zz} + q_{tt}} \tag{3.30}$$

$$PDOP = \sqrt{q_{xx} + q_{yy} + q_{zz}} \tag{3.31}$$

$$TDOP = \sqrt{q_{tt}} \tag{3.32}$$

Additional DOPs, HDOP (Horizontal DOP), EDOP (East DOP), NDOP (North DOP) and VDOP (Vertical DOP), can be obtained by expressing the *H* matrix in local level frame ENU (East North Up):

$$Q_{ENU} = (H_{ENU}^T H_{ENU})^{-1} = \begin{bmatrix} q_E^2 & q_{EN} & q_{EU} & q_{ET} \\ q_{NE} & q_N^2 & q_{NU} & q_{Nt} \\ q_{UE} & q_{UN} & q_U^2 & q_{Ut} \\ q_{tE} & q_{tN} & q_{tU} & q_t^2 \end{bmatrix} \tag{3.33}$$

The HDOP and VDOP formulas are:

$$HDOP = \sqrt{q_E^2 + q_N^2} \tag{3.34}$$

$$VDOP = \sqrt{q_U^2} \tag{3.35}$$

Furthermore, the Q matrix dimension is related to the number of GNSS constellations used to compute position solution. The Q matrices given in (3.29) and (3.33) are valid in case of single GNSS constellation.

4. Benefit of GNSS Multi-constellation

Nowadays, a rapid development of GNSSs is in progress: Galileo and BeiDou are expected to reach their complete capability within 2020, providing significant improvements to the satellite navigation users, if combined to existing full operational GPS and GLONASS

With the increasing number of navigation satellites, more ranging observations, improved user-satellite geometry and increased coverage can be provided in both open sky or obstructed environments.

Many GNSS signals are strongly degraded by natural and artificial obstacles in difficult signal scenarios e.g., urban canyons and mountainous areas. A single GNSS, used as a stand-alone navigation system, in such environments, cannot guarantee an accurate and continuous positioning solution, owing to lack of visible satellites, weak geometry and gross errors. A possible way to overcome this problem is to use the advantages of multi-constellation GNSS. Multi-constellation usage increases satellite navigation availability and integrity, while accuracy still depends on the scenario (Angrisano et al, 2013a; Innac et al, 2016).

Indeed, in (Angrisano et al., 2013a) the authors show the enhancement of the navigation solution in terms of accuracy and continuity, thanks to the GPS and GLONASS combination. In (Gaglione et al, 2016), the performance of the SPP algorithm considering multiple GNSSs are analyzed in open-sky scenario, providing improvements in velocity domain, while GPS-only configuration had better performance with respect to multi-GNSS constellation in the position domain. This is related to the different measurement accuracies in the different systems.

Hence, using multi-constellation, an enhancement in terms of integrity and availability should be possible for any scenario while an accuracy improvement would be evident only for urban canyon scenarios, more or less, when single-frequency positioning is considered.

With the combined use of multiple GNSSs, the differences among the systems must be considered; the most significant difference is the time-offset between the systems, which has to be introduced in the estimation process as an additional unknown for each new GNSS constellation.

In this chapter, the differences between the analyzed GNSS constellations are described and the PVT algorithm for the combination of the four GNSSs is provided.

4.1. Differences between GNSSs

Even if GNSSs are based on the same operational principle, GPS, GLONASS, Galileo and BeiDou have some differences classifiable in three categories: constellation, signal and reference as shown in the Table 4.1.

Table 4.1 GPS, GLONASS, Galileo and BeiDou differences

	Parameter	GPS	GLONASS	Galileo	BeiDou
Constellation	**Number of SV**	24 nominal	24 nominal	27 nominal	35 nominal (3GEO+3IGSO+27 MEO)
	Orbital Planes	6	3	3	3
	Orbital Altitude	20200 Km	19100 Km	23222 Km	35786 km (MEO and IGSO) 21528 km(GEO)
	Orbit Inclination	55 deg	64.8 deg	56 deg	55 deg
	Orbital Period	11 h 58 min	11 h 15 min	14 h 5 min	12 h 52 min
Signal	**Carrier Frequency**	1575.42 MHz, 1227.60 MHz, 1176.45 MHz	1602 +K * 0.5625, 1246 + K *0.4375, (To Be Defined)	1.559-1.592 Mhz, 1.559-1.592 Mhz, 1.559-1.592 Mhz	1561.098 MHz, 1207.140 MHz, 1268.520 MHz
	Multiple Acces	CDMA	FDMA	CDMA	CDMA
	Broadcast Ephemeris	Keplerian	ECEF	Keplerian	Keplerian
Reference	**Reference Frame System**	WGS84	PZ90.02	GTRF	CGCS2000
	Time	GPS Time	GLONASS Time	GST	BDT

The four above mentioned systems adopt different coordinate frames to express the satellite and user coordinates: World Geodetic System 1984 (WGS84) for GPS, Parametrop Zemp 1990 version 2 (PZ90.02) for GLONASS, Galileo Terrestrial Reference Frame (GTRF) for Galileo, China Geodetic Coordinate System 2000 (CGCS2000) for BeiDou. The definition of the coordinate system is detailed in (ICD-GLONASS, 2008; European Union, 2010;

Navstar GPS Directorate, 2012; BDS-ICD, 2012). WGS84 and GTRF datum are based on the International Terrestrial Reference Frame (ITRF), so they differ by only a few centimeters, while a Helmert transformation has to be used to convert coordinates from PZ90.02 to WGS84. The CGCS 2000 datum used by BeiDou is also nominally aligned with the ITRF.

Each GNSS uses a slightly different time base. GPS time (GPST) is established by the Control Segment and is referenced to UTC as maintained by the U.S. Naval Observatory (UTC (USNO)) with zero time-point defined as midnight on the night of January 5, 1980/morning of January 6, 1980. UTC scale is corrected by an integer leap second adjustment upon a recommendation by the International Earth Rotation and Reference Systems Service (IERS) based on astronomical observations of the Earth's rotation.
The GPST is maintained by the Master Control Station (MCS) of the Control Segment (CS). Unlike the UTC (USNO), which applies integer leap second corrections, the GPS time standard operates on a continuous time scale (Navstar GPS Directorate, 2012) and so it is not subject to leap seconds; the navigation message contains the requisite data for relating GPS time to UTC. The accuracy of this data during the transmission interval shall be such that it relates GPS time to UTC (USNO) within 90 nanoseconds (one sigma). GPST is expressed in terms of week number and number of seconds of the week (starting from midnight Saturday/Sunday).

The GLONASS satellites are equipped with clocks whose daily instability is not worse than $5*10^{-13}$ and $1*10^{-13}$ for the GLONASS-M satellites. An accuracy of mutual synchronization of the satellite time scales is not worse than 20 nanoseconds for the GLONASS and eight nanoseconds for the GLONASS-M satellites. GLONASS time is based on GLONASS Central Synchronizer (CS) time. Daily instability of the CS hydrogen clocks in not worse than 2×10^{-15}.
GLONASS time scale is connected to UTC (SU), the UTC as maintained by Russia and is periodically compared with the CS time scale. Difference between GLONASS time and UTC (SU) computed and broadcast to the satellites twice a day by control segment. The error of a scale system linked to the GLONASS UTC (SU) time scale should not exceed 10 nanoseconds. The GLONASS time scale is periodically corrected to integer number of seconds simultaneously with UTC corrections that are performed according to the Bureau International de l Heure (BIH) notification (leap second correction).

Typically, these corrections (1s) are performed once a year (or 1.5 years) at midnight 00 hours 00 minutes 00 seconds UTC from December 31 to January 1 or from March 31 to April 1 or from June 30 to July 1 or from September 30 to October 1 by all UTC users.
The relationship between GPST and GLONASS time is expressed as (GLONASS-ICD, 2008):

$$t_{GPS} = t_{GLO} + \tau_r + \tau_u + \tau_g \tag{4.1}$$

where

t_{GPS} is the GPS time;

t_{GLO} is the GLONASS time;

$\tau_r = t_{UTC(SU)-t_{GLO}}$ broadcast within GLONASS navigation message;

$\tau_g = t_{UTC(USNO)} - t_{GPS}$ broadcast within GPS navigation message;

$\tau_u = t_{UTC(USNO)} - t_{UTC(SU)}$ is the inter-system bias between GPS and GLONASS time that is broadcast in GLONASS navigation message with a time delay and it does not consider the inter-system hardware delay bias which is dependent on the specific receiver (Cai and Gao, 2009; Gioia, 2015).

Galileo System Time (GST) is the reference time scale for the Galileo system and is performed by the Precise Time Facility at the Galileo Control Centre in Fucino, Italy (ESA, 2013; Inside GNSS, 2013). The GST start epoch is 00:00 UT on Sunday 22nd August 1999 (midnight between 21st and 22nd August). At the start epoch, GST was ahead of UTC by 13 leap seconds. Therefore, currently (September 2016) GST is ahead of UTC by 17 seconds. GST is computed independently of the UTC and the offset between these two times is continuously being monitored (European Union, 2010); the Galileo system timing accuracy with respect to the UTC will be within 30 ns (European Union, 2010). Galileo system broadcast the offset between GPST and GST, called Galileo to GPS Time Offset (GGTO), within the navigation message; GGTO is given by the equation below (European Union, 2010):

$$\begin{gathered} GGTO = t_{Gal} - t_{GPS} \\ GGTO = A_{0G} + A_{1G}[TOW - t_{0G} + 604800\big((WN - WN_{0G}) mod 64\big)] \end{gathered} \tag{4.2}$$

where

t_{Gal} is the GST

t_{GPS} is the GPST

A_{0G} and A_{1G} are the constant term and the rate of change of the GGTO, respectively

WN is the Week Number in GST

WN_{0G} is the Week Number of the GGTO reference

TOW is the time of the week

t_{0G} is the reference time for GGTO

The time reference for BeiDou is the BeiDou navigation satellite system Time (BDT). BDT is a continuous time that does not need of leap seconds correction. BDT is realized by composite clocks and is maintained by a time and frequency system (TFS) located at the MCS. The start epoch of BDT was 00:00:00 on January 1, 2006 of Coordinated Universal Time (UTC). BDT is expressed with week and seconds of week (SOW) and is related to the UTC through UTC(NTSC). BDT offset with respect to UTC is controlled within 100 nanoseconds (modulo 1 second). The leap seconds are broadcast in navigation message; in details, BeiDou navigation message broadcasts time parameters relating BDT to UTC, GPS, GLONASS and Galileo time (BDS-ICD, 2012). The BeiDou to GPS Time Offset (BGTO) defines the relationship between BDT and GPST as:

$$\begin{aligned} BGTO &= t_B - t_{GPS} \\ BGTO &= A_{0GPS} + A_{1GPS} \cdot t_B \end{aligned} \tag{4.3}$$

where

t_B is the SOW in BDT

A_{0GPS} is BDT clock bias relative to GPS time

A_{1GPS} is BDT clock rate relative to GPS time.

On this basis, with the combined use of multiple systems, the offset with respect to a time reference systems has to be considered for each component of the multi GNSS system because of the different time scales adopted. While for satellites, equipped with atomic clocks, these offsets are modeled and related correction provided to users by navigation messages, the same approach provides inaccurate results for the receiver side (Gioia, 2014). A more rigorous method is to introduce in the estimation process one additional unknown,

i.e. the inter-system offset, for each new GNSS constellation. More details are provided in the PVT algorithm description.

4.2. Multi-GNSS PVT Algorithm

When observations provided by different GNSSs are used for the navigation solution computation, the measurement model for a single system, as expressed in the equation (3.4), must be changed in order to take into account for the different time reference scales. To solve the problem related to these differences, the approach used in this work is to include the inter-system bias (i.e. τ_u for GLONASS, GGTO for Galileo and BGTO for BeiDou) in the estimation process as an unknown.
In this research, measures ranging from GPS, GLONASS, Galileo and BeiDou are used and the linearized PR measurement equation can be re-written for each system, defined in ECEF frame, as:

$$\begin{aligned} z^G &= a_X^G \Delta x + a_Y^G \Delta y + a_Z^G \Delta z + \Delta(c\delta t^G) \\ z^R &= a_X^R \Delta x + a_Y^R \Delta y + a_Z^R \Delta z + \Delta(c\delta t^G) + \Delta(c\delta t_R^G) \\ z^E &= a_X^E \Delta x + a_Y^E \Delta y + a_Z^E \Delta z + \Delta(c\delta t^G) + \Delta(c\delta t_E^G) \\ z^B &= a_X^B \Delta x + a_Y^B \Delta y + a_Z^B \Delta z + \Delta(c\delta t^G) + \Delta(c\delta t_B^G) \end{aligned} \tag{4.4}$$

where the superscripts “G”, “R”, “E” or “B” indicate that the element is referred to the GPS, GLONASS, Galileo or BeiDou system, respectively. The term $\Delta(c\delta t^G)$ is the increment from the linearization point of the receiver clock offset with respect to the GPS time, while δt_R^G, δt_E^G and δt_B^G are the inter-system time-offset between the two systems as indicated by the superscripts.

The PR measurement model using the observations by the multi-GNSS constellations is shown below:

$$\underline{z} = \begin{pmatrix} \underline{z}_{PR}^G \\ \underline{z}_{PR}^R \\ \underline{z}_{PR}^E \\ \underline{z}_{PR}^B \end{pmatrix} = \begin{bmatrix} H_{PR}^G \\ H_{PR}^R \\ H_{PR}^E \\ H_{PR}^B \end{bmatrix} \cdot \underline{\Delta x} + \underline{\varepsilon}_{PR} = H \cdot \underline{\Delta x} + \underline{\varepsilon}_{PR} \tag{4.5}$$

$\underline{z}$ is the measurements vector with all GNSS pseudorange measurements, corrected by a priori information.

$\underline{\Delta x}$ is the state vector, consisting of the unknown parameters to be estimated through WLS method and it is defined as:

$$\underline{\Delta x} = [\Delta x\ \Delta y\ \Delta z\ \Delta(c\delta t^G)\ \Delta(c\delta t_R^G)\ \Delta(c\delta t_E^G)\ \Delta(c\delta t_B^G)]^T$$

$\underline{\varepsilon}_{PR}$ is the residual errors vector, while H is the design matrix expressed as:

$$H = \begin{bmatrix} a_{x1}^G & a_{y1}^G & a_{z1}^G & 1 & 0 & 0 & 0 \\ \vdots & \vdots & \vdots & \vdots & \vdots & \vdots & \vdots \\ a_{xn}^G & a_{yn}^G & a_{zn}^G & 1 & 0 & 0 & 0 \\ a_{x1}^R & a_{y1}^R & a_{z1}^R & 1 & 1 & 0 & 0 \\ \vdots & \vdots & \vdots & \vdots & \vdots & \vdots & \vdots \\ a_{xn}^R & a_{yn}^R & a_{zn}^R & 1 & 1 & 0 & 0 \\ a_{x1}^E & a_{y1}^E & a_{z1}^E & 1 & 0 & 1 & 0 \\ \vdots & \vdots & \vdots & \vdots & \vdots & \vdots & \vdots \\ a_{xn}^E & a_{yn}^E & a_{zn}^E & 1 & 0 & 1 & 0 \\ a_{x1}^B & a_{y1}^B & a_{z1}^B & 1 & 0 & 0 & 1 \\ \vdots & \vdots & \vdots & \vdots & \vdots & \vdots & \vdots \\ a_{xn}^B & a_{yn}^B & a_{zn}^B & 1 & 0 & 0 & 1 \end{bmatrix} \tag{4.6}$$

where a_{xi}^{gnss}, a_{yi}^{gnss} and a_{zi}^{gnss} are the direction cosines as defined in section 3.1.

Furthermore, in order to obtain the GNSS receiver velocity, the measurement model should include also PR rate observables. Because the systems' time difference is very stable (Cai and Gao, 2009), its derivative can be considered negligible; so expanding the equation (3.16) to all used GNSSs, the Doppler measurement model can be expressed as:

$$\underline{z}_{\dot{P}\dot{R}} = \begin{pmatrix} \underline{z}_{\dot{P}\dot{R}}^G \\ \underline{z}_{\dot{P}\dot{R}}^R \\ \underline{z}_{\dot{P}\dot{R}}^E \\ \underline{z}_{\dot{P}\dot{R}}^B \end{pmatrix} = \begin{bmatrix} H_{\dot{P}\dot{R}}^G \\ H_{\dot{P}\dot{R}}^R \\ H_{\dot{P}\dot{R}}^E \\ H_{\dot{P}\dot{R}}^B \end{bmatrix} \cdot \underline{v}_R + \underline{\varepsilon}_{\dot{P}\dot{R}} = H_{\dot{P}\dot{R}} \cdot \underline{v}_R + \underline{\varepsilon}_{\dot{P}\dot{R}} \tag{4.7}$$

where $\underline{z}_{\dot{P}R}$ is the measurements vector consisting of all GNSS pseudorange rate measurements corrected by the satellite motion component, $\underline{v}_R$ and $\underline{\varepsilon}_{\dot{P}R}$ are the same vectors as defined in (3.16) and $H_{\dot{P}R}$ is the design matrix computes as:

$$H = \begin{bmatrix} a_{x1}^G & a_{y1}^G & a_{z1}^G & 1 \\ \vdots & \vdots & \vdots & \vdots \\ a_{xn}^G & a_{yn}^G & a_{zn}^G & 1 \\ a_{x1}^R & a_{y1}^R & a_{z1}^R & 1 \\ \vdots & \vdots & \vdots & \vdots \\ a_{xn}^R & a_{yn}^R & a_{zn}^R & 1 \\ a_{x1}^E & a_{y1}^E & a_{z1}^E & 1 \\ \vdots & \vdots & \vdots & \vdots \\ a_{xn}^E & a_{yn}^E & a_{zn}^E & 1 \\ a_{x1}^B & a_{y1}^B & a_{z1}^B & 1 \\ \vdots & \vdots & \vdots & \vdots \\ a_{xn}^B & a_{yn}^B & a_{zn}^B & 1 \end{bmatrix} \tag{4.8}$$

where b_{xi}^{gnss}, b_{yi}^{gnss} and b_{zi}^{gnss} are the direction cosines of the vector $\underline{a}$ as defined in section 3.1 for the velocity computation and finally the receiver velocity is estimated using WLS method.

In order to process GNSS data in SPP, a customized PVT algorithm, developed in MatLab® environment, is used in this research and shown in Figure 4.1. All the software belongs to a Toolbox developed by PANG (PArthenope Navigation Group – http://pang.uniparthenope.it). The main inputs of the algorithm are GNSS observables, i.e. pseudorange and Doppler shift, and GNSS ephemerides. The ephemerides are used to compute satellite position, velocity and clock offset; different orbital propagators are implemented for the various GNSSs considered due to the different parameterization of the ephemerides. The mathematical models for the computation of GNSS satellites position and velocity can be found in (ICD-GLONASS, 2008; European Union, 2010; Navstar GPS Directorate, 2012; BDS-ICD, 2012).

The raw PR measurements are corrected for the satellite clock error, as described in Section 2.4, using the parameters broadcast within GNSS navigation message and applying the equation (2.4). The Sagnac correction is applied to the satellites position and velocity, and atmospheric corrections are used to remove tropospheric and ionospheric effects from the raw PRs using Saastamoinen and Klobuchar models, respectively. Finally, the corrected measurements are used in the WLS estimator in order to have the state vector $\underline{\Delta x}$ containing

the corrections to the receiver position and clock offset, as described in the section 3.1. Then, the position solution $\underline{\hat{x}}$ is computed updating the predicted position $\underline{x}_0$ with the corrections vector $\underline{\Delta x}$.

GNSS ephemerides are used to compute the satellites velocity in the orbital propagator which also provides the correction for the satellite clock drift, calculated using the derivative of the equation (2.4). Satellites position and velocity are corrected from Sagnac effect while clock error is removed by the raw PRs rate. Finally, the corrected PR rate observables are used in the WLS for the receiver velocity computation.

After the navigational solution computation, the error analysis is performed in position and velocity domain comparing the estimated solution with respect to the reference one.

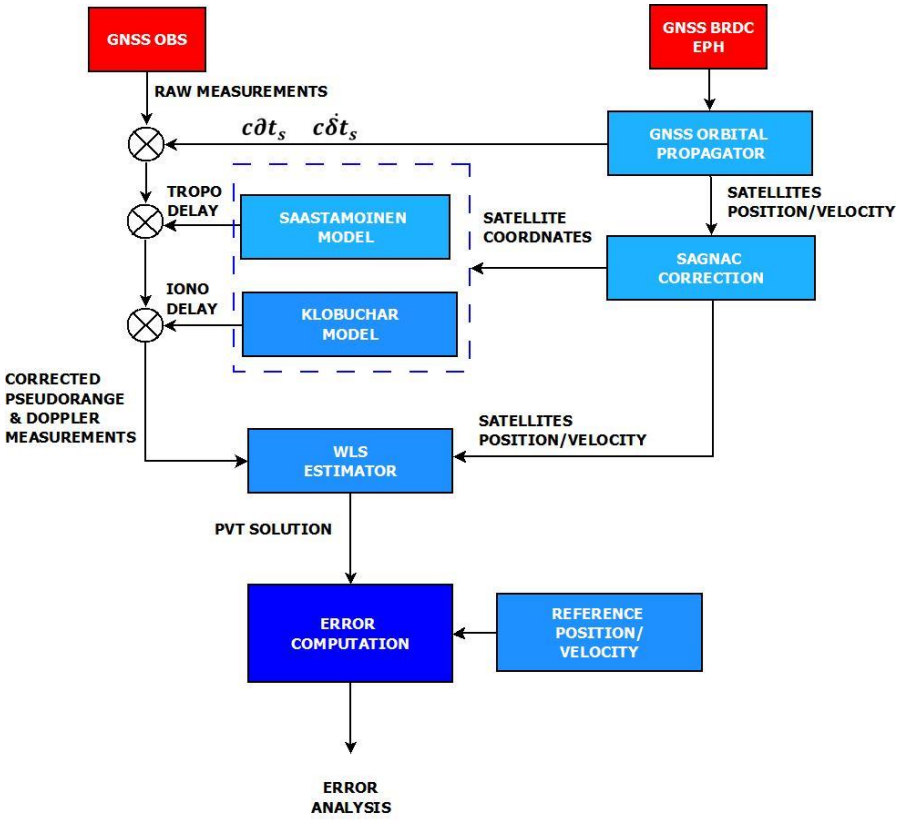

Figure 4.1 PVT algorithm description

5. Reliability Theory

In signal-degraded scenarios gross errors strongly affect the measurements, decreasing the accuracy of the navigation solution. Therefore, integrity monitoring becomes an important task for the applications conducted in these scenarios. Integrity, as defined in the International Civil Aviation Organisation's GNSS Standards and Recommended Practices (SARPS), is the ability of the system to recognize and point out any system dysfunctions that can compromise the required performance for the operation that you are carrying out (ICAO SARPS, 2004). In this context, the reliability test is carried out as a method to monitor system integrity when the position estimate is used in safety-critical applications. For this reason, RAIM was introduced referring to integrity monitoring of GNSS navigation signals performed by a receiver independent of external reference systems, except for the navigation signals themselves. Significant efforts have been made to develop and analyze RAIM methods and algorithms over the past decade (Hein et al, 1997; Ryan and Lachapelle, 2000; Ochieng et al, 2002; Lee, 2001). A variety of RAIM schemes have been proposed in the literature. The common principle includes performing a self-consistency check among redundant measurements using a statistical hypothesis test of LS residuals (Brown, 1992).

In this chapter, the concept of integrity and the mathematical models, that are the basis of the RAIM, are provided as well as the developed RAIM algorithm described.

5.1. Integrity

The integrity problem is important for many applications and its function becomes critical especially when the GNSS is used as a stand-alone navigation method in safety-critical applications. The integrity parameters can be used as indicators about the reliability of the navigation solution at a particular epoch.

The integrity is defined in terms of the following parameters:

- *alert limit* corresponds to the maximum allowable error in the user position solution before an alarm is to be raised within the specific time to alert;
- *time to alert* is the time from when an alarm condition occurs until when the alarm is received at the user level;
- *integrity risk* is defined as the probability, during any continuous period of operation, that the computed vertical or horizontal positioning error exceeds the corresponding

alert limit and the user is not informed within the specified time to alert (Kaplan, 2005).

When the system generates an excessively large error without producing a timely warning about degraded solution for the users, the solution output from the system is called Misleading Information (MI). If the potential consequence of MI can potentially impose life threatening situation then the term Hazardously Misleading Information (HMI) is used (Petovello et al, 2008). The Probability of Hazardously Misleading Information (PHMI) is referred to the probability that the true position lies outside the maximum error bound determined by the user. The integrity is confirmed if the PHMI is below the allowable integrity budget (Blanch et al, 2011).

The system integrity can be guaranteed by comparing protection level and the corresponding alert limit: when the protection level is smaller than the alert limit, the integrity is ensured. In the opposite situation, the system should provide a warning message to the user about possible misleading information (Winit, 2013).

5.2. Traditional RAIM Algorithm

GNSSs broadcast integrity information to the users within the navigation message, but this information is not timely enough for real time applications since it is available after a delay. An integrity monitoring algorithm is required to detect and exclude faulty satellite measurements from a set of measurements that will be used to compute navigation solutions. To achieve this, RAIM was proposed in 1986 to perform an integrity check on the satellite navigation system (Lee, 1986; Brown, 1992; Lee and Cashin, 2010).

In the classical RAIM approach, measurement errors are assumed normally distributed; such assumption is not true in degraded signal environments. If only a single blunder is present within the measurement set, methods for outlier identification work properly. However, it is more difficult to detect outliers when there are two or more of them (Brown, 1998).

When using RAIM to detect a faulty measurement in a single GNSS constellation, the algorithm requires a minimum of five satellites in view in order to detect the presence of an unacceptably large position error for the desired application. To perform a fault elimination process, at least six satellites are required. When using range measurements from two GNSS constellations, five satellites in any combination between the two systems are required to obtain a position solution. This further complicates RAIM schemes as at least seven satellites from two GNSS constellations are required if an FDE algorithm is applied on these

measurements (Hewitson and Wang, 2006a, O'Keefe et al, 2011; Angrisano el al, 2013a; Gioia, 2015). However, the use of a priori inter-system time-offset parameters as measurements or constraints would result in the reduction of number of satellites required.
Epoch by epoch, the RAIM verifies the availability of the FDE algorithm and then proceeds with the protection level computation. If the requirements are not satisfied by the computed Protection Level (PL), the RAIM will notify the user. If the PL is under the expected threshold and the FDE algorithm is applied, it can be possible to exclude the blunder from the measurement set before the position computation.
The inputs to the RAIM algorithm are the measurement geometry, the measurement noise and the maximum allowable probabilities for a false alert and a missed detection. The output of the algorithm is the Horizontal Protection Level (HPL), which is the radius of a circle, centered at the true aircraft position that is assured to contain the indicated horizontal position with the given probability of false alert and missed detection. If the aircraft is in a phase of flight requiring vertical guidance, Vertical Protection Level (VPL) is output as well; however, VPL is generally associated with differential-based systems.
In all, a RAIM algorithm is based on the self-consistency of measurements and its main goal is to protect against excessive solution errors.
Horizontal position error $\underline{e}$ is defined as the difference between the estimated position $\underline{\hat{x}}$ and the true position $\underline{x}$**:**

$$\begin{aligned}
&\underline{e} = \underline{\hat{x}} - \underline{x} \\
&\underline{e} = (H^T H)^{-1} H^T \underline{z} - \underline{x} \\
&\underline{\mathrm{e}} = (\mathrm{H^T H})^{-1} \mathrm{H^T}\left(\mathrm{H}\underline{\mathrm{x}} + \underline{\varepsilon}\right) - \underline{\mathrm{x}} \\
&\underline{e} = (H^T H)^{-1} H^T H \underline{x} + (H^T H)^{-1} H^T \underline{\varepsilon} - \underline{x} \\
&\underline{\mathrm{e}} = (\mathrm{H^T H})^{-1} \mathrm{H^T} \underline{\varepsilon}
\end{aligned} \qquad (2.1)$$

The last equation of (2.1) represents the relationship between measurement errors and the position ones.
In the LS case a quality control is performed testing the residuals $\underline{r}$, as described in 3.2:

$$\underline{r} = \underline{z} - \underline{\hat{z}} = \underline{z} - H \cdot \underline{\hat{x}} \qquad (5.2)$$

where $\underline{\hat{z}}$ is the vector of the predicted measurements.

The residuals represent the level of agreement of the measurements to each other and so they are suitable to assess the quality of the LS solution.
The relationship between residuals and measurements errors can be obtained combining the equation (5.2) with the expression of the LS solution:

$$\begin{aligned} \underline{r} &= \underline{z} - H \cdot \underline{\hat{x}} \\ \underline{r} &= \underline{z} - H(H^T H)^{-1} H^T \cdot \underline{z} \\ \underline{r} &= (I - H(H^T H)^{-1} H^T) \cdot \underline{z} \\ \underline{r} &= (I - H(H^T H)^{-1} H^T)(H \cdot \underline{x} + \underline{\varepsilon}) \\ \underline{r} &= (I - H(H^T H)^{-1} H^T) \cdot \underline{\varepsilon} \end{aligned} \tag{5.3}$$

So the residual vector can be used to test the internal consistency among the observations (Kuang, 1996) and to check the validity of the assumptions underlying the used functional and stochastic models.

5.3. Reliability Testing

This section briefly describes hypothesis testing methodology that is the basis for the reliability theory applied to GNSS. Since the GNSS observables cannot be directly subjected to such testing, the statistical analysis in GNSS is not direct but the pseudoranges must first be involved in the LS estimation of the position and user clock bias.
The LS estimation is based on the assumption that all the gross and systematic errors have been eliminated before the adjustment, so only remaining random errors affect the samples. The local and large disturbances are considered as gross errors, blunder or outliers, whereas smaller and global deviations are considered as systematic errors. Generally, errors can be assigned to the functional or to the stochastic model according to their origin which usually is unknown.
Systematic effects or gross errors depict the inability of the functional model to describe the real situation. The presence of a blunder will bias the navigation solution and it is important to detect any anomalies among the observations and remove them.
In satellite navigation, reliability refers to the controllability of observations, namely the ability of a system to detect blunders and to estimate the effects of undetectable blunders on the estimated parameters. Reliability is quantified using the failure probabilities of the components as a function of time (Angrisano et al, 2013a; Innac et al, 2016). Statistical tests

are used to compare results with a given standard. In most cases, assumptions have to be made about whether a set of measurements belongs to a certain distribution, usually a normal distribution with a given standard deviation.

Reliability monitoring is based on a statistical test of the observation residuals, with the aim of detecting and excluding measurement errors. A statistical test uses a null hypothesis H_0 (denoting a fault-free situation), related to the probability distribution of a random variable. For any null hypothesis, there is an infinite number of alternative hypotheses (H_a) that is a statement that directly contradicts the null hypothesis. The null hypothesis is the reference level from which any deviation of the alternative hypotheses has to be detected by statistical tests (Kuang, 1996; Kuusniemi, 2005; Gioia, 2015).

Hypothesis testing is used to verify the hypothesis assumption about the actual probability distribution of the error through the use of test statistics. Hypothesis testing is conducted through four steps:

- define H_0 using a decisional variable D related to the value for specific parameters characterizing a population in case of null hypothesis being true;
- fix the criteria for a decision indicated by the level of significance α;
- state the test statistic that will be used to conduct the hypothesis test and calculate the value of the test statistic, using the sample data;
- get a decision, based on a comparison of the calculated value of the test statistic and the critical value of the test.

A statistical test could involve two types of potential errors, identified as type I and type II errors. A type I error is defined as the error due to the rejection of the null hypothesis H_0, when H_0 is actually true. The probability of committing type I error is called "significance level" α. The probability of making the correct decision is the "confidence level" (1-α). Type II error is defined as the acceptance of the null hypothesis when in fact is false. The probability of committing this type of error is (1- β). The probability of making the correct decision is the "power of the test" β. Graphical interpretation of the abovementioned parameters is provided in Figure 5.1. Under null hypothesis and alternative hypothesis, the probability density functions of a chosen statistic take the same form but have different mean values as shown in Figure 5.1. The power of the test β indicates the smallest difference δ that can be detected if the test has been executed at a significance level α. In order to decrease the probability of both types I and II error, the internal reliability will be increased and the difference between H_0 and H_a will be larger (Kuang, 1996; Kuusniemi, 2005; Gioia, 2015).

The selection of the probability levels "α" and "1-β" should be based on the cost of committing either type I or type II error. Thus depending on the testing purpose and on the cost of making a wrong decision of either type, a compromise between the confidence level and the power of the test can be reached.

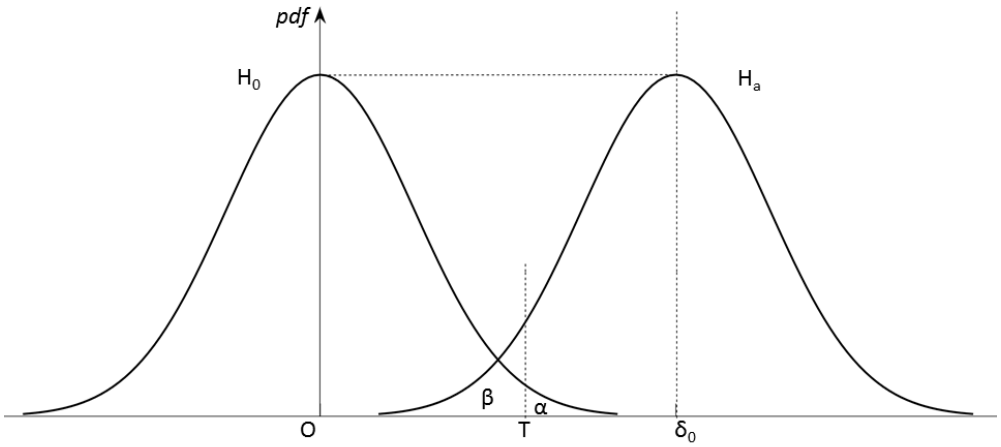

Figure 5.1 Type I Error α and Type II Error β in a One-Tailed Test

5.3.1. Global and Local Test

Reliability refers to the consistency of the results provided by a system; internal and external reliability are respectively the ability to detect gross errors and verify the effect of an undetected blunder on the solution (Kuusniemi, 2005; Gioia, 2015).

In order to detect a blunder influencing the measurements, the residuals could be statistically tested using two different tests: Global and Local test.

Global Test (GT) is carried out to verify the measurement set consistency, testing the null hypothesis H_0 that states the adjustment model is correct and the distributional assumption meets the reality, as opposed to the alternative H_a (Kuang, 1996; Leick et al, 2015). If GT fails, a Local Test (LT) could be performed for failure detection.

In the GT, the statistical variable D is used to test the null hypothesis and is based on the quadratic form of the residual $\underline{r}$ weighted through the weighting matrix W:

$$D = \underline{r}^T W \underline{r} \tag{5.4}$$

Assuming Gaussian measurement errors, the statistical variable is tested against a threshold obtained from chi-square (χ^2) test statistic, which is a function of degrees of freedom (DoF) and significance level α:

$$T_G = \chi^2_{1-\alpha,DoF} \tag{5.5}$$

The parameter DoF is the redundancy of the system, defined as the difference between the measurements number m and the number of the unknowns n. Figure 5.2 shows a central χ^2 density function for four degrees of freedom (DoF=4) representing the null hypothesis of the GT.

If the statistical variable exceeds the threshold, the sum-of-squares of the residuals does not follow the expected distribution, consisting of a sum of squares of zero-mean Gaussians, and the null hypothesis is rejected in favor of H_a. The hypothesis testing in GT is conducted as:

$H_0 : D \leq T_G \Rightarrow$ No integrity failure

$H_a: D > T_G \Rightarrow$ Integrity failure

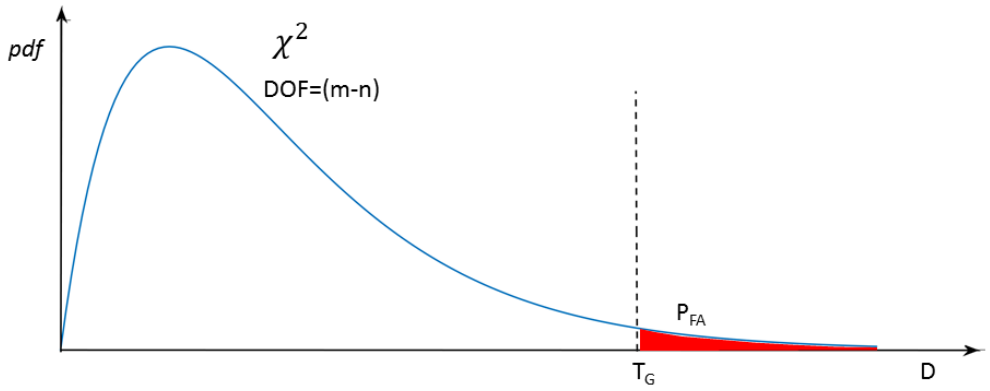

Figure 5.2 Central χ2 density function for four degrees of freedom in the Global Test

If H_0 is rejected and H_a accepted, the result of GT is an inconsistency in the measurement set and the blunder should be identified and mitigated through the Local Test (Baarda, 1968; Kuusniemi, 2005; Angrisano et al, 2013a).

In the LT, the statistical variable $\underline{w}$ is the vector containing the standardized residual of the i^{th} satellite:

$$w_i = \left| \frac{r_i}{\sqrt{(C_r)_{ii}}} \right|, i = 1{:}m \tag{5.6}$$

where r_i denotes the i^{th} element of residual vector $\underline{r}$, $(C_r)_{ii}$ the i^{th} diagonal element of the residual covariance matrix C_r computed as:

$$C_r = W^{-1} - H(H^T W H)^{-1} H^T \tag{5.7}$$

with the weighting matrix W and the design matrix H expressed as described previously in the chapter 3.

The standardized residuals are assumed to be normally distributed and they are tested against the threshold defined as:

$$T_L = N^2_{1-\alpha/2} \tag{5.8}$$

where T_L is defined as the abscissa corresponding to the probability value $(1 - \alpha/2)$ of a normal distribution. The hypothesis testing in LT is conducted as:

$$H_0 : w_i \leq T_L => w_i \text{is not an outlier}$$

$$H_a : w_i > T_L => w_i \text{is an outlier}$$

The measurement is identified as a blunder and will be rejected if the local test statistic exceeds the threshold, in which case an alternative hypothesis, H_a is chosen. Conversely, after a GT failure, if the LT does not fail, the solution is unreliable because there is an inconsistency between the GT and LT.

Knowing the assumption model on which these tests are based, a single blunder within the measurement set is not realistic in degraded signal conditions. Furthermore, this kind of data snooping can actually also work with multiple blunders if is performed iteratively.

5.4. Statistical Reliability

As described in the previous section, reliability concerns the controllability of observations that is the ability to detect outliers and estimate the impact of undetectable outliers on the solution. Reliability comprises the internal and external reliability.

Internal reliability identifies a detectable blunder on each measurement through statistical reliability testing of LS residuals on an epoch-by-epoch basis. External reliability is quantified by the effect of undetectable outliers on the estimated parameters.
The smallest bias of the measurement is called Minimum Detectable Blunder (MDB) and it is used as a measure of internal reliability. A non-centrality parameter is selected on the basis of some predefined values for α and β and the MDB can be computed as:

$$MDB_i = \frac{\delta}{\sqrt{(C_r)_{i,i}}} \tag{5.9}$$

where δ is the non centrality parameter of the unbiased and biased normal distributions and it is defined as:

$$\delta = N_{1-\frac{\alpha}{2}} + N_{1-\beta} \tag{5.10}$$

External reliability describes the effect of the smallest detectable blunder on the estimated parameters and is computed as:

$$e_i = (H^T W H)^{-1} H^T W MDB_i \tag{5.11}$$

where H is the design matrix, W the weight matrix and MDB_i is a column vector containing all zeros except for the MDB of the i^{th} observation in the it^{h} position. The external reliability is also called Position Protection Level (PPL) and can be computed assuming that the first three elements of the state vector are the coordinates:

$$PPL = \sqrt{e_1^2 + e_2^2 + e_3^2} \tag{5.12}$$

Since protection levels are not equal for different measurements, PPLs are computed for all measurements and the largest one is selected.

5.5. Fault detection and exclusion

FDE is an important part of navigation integrity monitoring and reliability assurance. Reliability monitoring can test all types of observables but, in this discussion, only pseudoranges are monitored in order to mitigate the error in the navigation solution in urban canyon scenario.

There are several approaches to provide assurance of integrity of the navigation system. In this research, the adopted method is based on snapshot schemes using LS estimation techniques. These schemes are based upon assessment of single epoch solutions with only current redundant measurements being used in the self-consistency check. The adopted snapshot approaches are extendable into a filtering method.

System integrity monitoring can be extended when dynamic information is available as in Kalman filter (Hewitson et al, 2004; Ryan and Lachapelle, 1999). If the state and observation model assumptions are correct, Kalman filter could provide optimal estimations of the navigation parameters. On the other hand, erroneous assumptions about the system state dynamics could create inconsistency between the measurements, so the outlier is due to the process model information and is not present in the measurement model (Gioia, 2015). For this reason, the use of Kalman filter is not convenient in the degraded signal conditions considered in this work and the LS approach is chosen. The following discussion is focused on single-epoch RAIM and FDE algorithms.

5.5.1. Geometry Check in pre-RAIM

In order to stay within the requirements, a geometry check is crucial in signal-degraded environments where the poor satellite geometry implies large DOP values and the navigation accuracy degradation. In this case, the performance of the integrity monitoring algorithms is degraded too and large errors can occur before the outliers are detected. Before RAIM application in a safety-critical application, a geometry check must be performed to screen out bad geometries, which could imply erroneous detections.

The method adopted to evaluate the geometry detection was based on a Protection Radius parameter computation as follow:

$$Protection\ Radius = slope_{max} \cdot \lambda \tag{5.13}$$

where λ is the noncentrality parameter of a noncentral chi-squared distribution and the slope parameter is the ratio between the position error (horizontal or vertical) and the test statistic (Parkinson et al, 1996; Brown and Chin, 1997) and is defined as follows:

$$slope_i = \frac{HRE_i}{test\ statistic_i} \tag{5.14}$$

In the slope definition, the stochastic perturbation is omitted and a deterministic error on the pseudorange, between the user and the i^{th} satellite, is considered. This deterministic pseudorange error causes in the navigation solution the Horizontal Radial Error (HRE) defined as:

$$HRE_i = \sqrt{A_{1,i}^2 + A_{2,i}^2} \tag{5.15}$$

where the index i is between 1 and m, and where the matrix A is:

$$A = (H^T H)^{-1} H^T \tag{5.16}$$

For failure detection purposes the measurement whose bias error causes the largest slope is the most difficult to detect and it produces the largest position error for a given test statistic. The $\text{slope}_{\text{max}}$ corresponds therefore to the most-difficult-to-detect measurement.
A geometric interpretation of the Protection Radius parameter is provided in Figure 5.3.

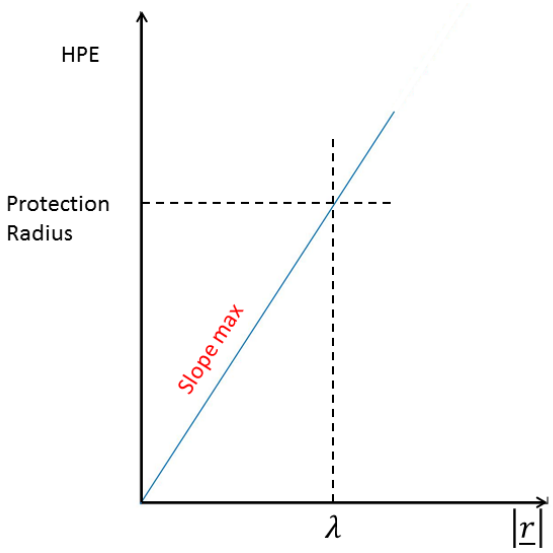

Figure 5.3 Protection Radius parameter computed as a function of Horizontal Position Error (HPE) and test statistic $|\underline{\boldsymbol{r}}|$

5.5.2. Observation Testing with Subsets

The analysis of LS residuals can help to localize a large error. However, the LS procedure can mitigate the effects of multiple blunders in the measurement set simultaneously as their localization based on the statistical testing can become difficult. To solve this problem, a possible approach is the computation of several LS adjustments by removing and including one or more suspected observations from the set (Kuusniemi, 2005).

Subset testing is a RAIM–FDE method for the detection and the exclusion of faulty measurements and is based uniquely on the Global Test (Innac et al,2016; Angrisano et al, 2013a; Kuusniemi, 2005), which is used to find the measurement subset without blunders. If a measurement set does not pass the GT, all the possible combinations of measurements are checked, specifically all the possible subsets from (m – 1) to (n + 1) measurements. The subset with the smallest test statistic and the largest number of observations is used to compute the navigation solution.

The scheme is shown in Figure 5.4. The Observation Testing Subset is computationally heavy because several combinations have to be checked.

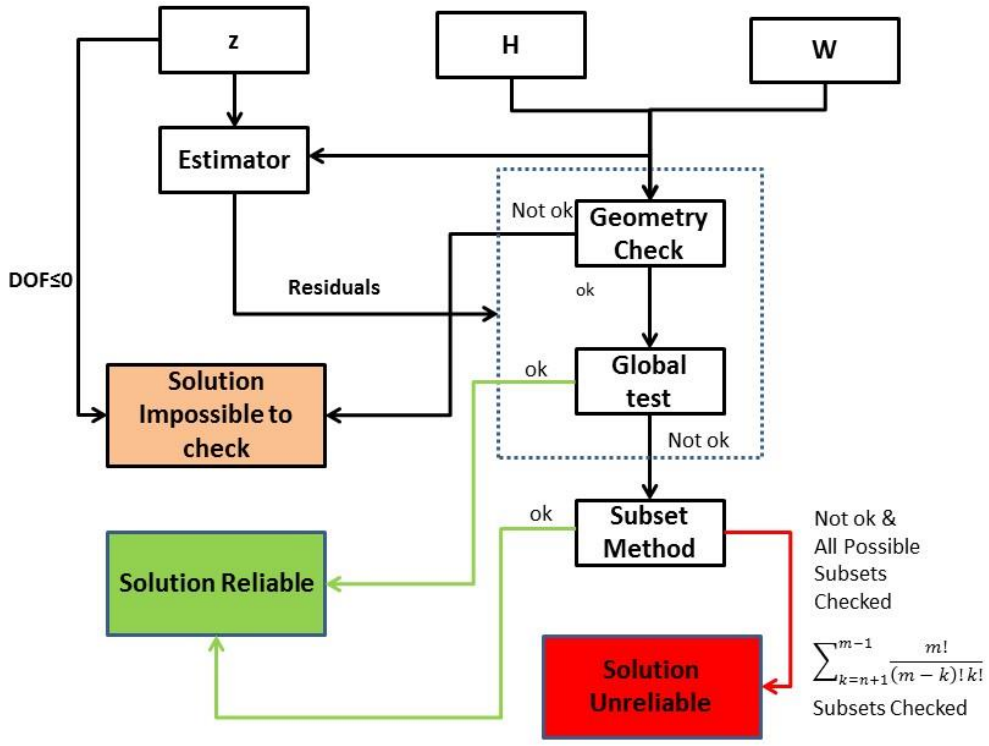

Figure 5.4 Subset Testing Algorithm (where m is the number of measurements, n is the number of unknowns and k is the number of excluded measurements)

6. Fuzzy Logic Theory

Fuzzy logic is a technique developed by Lotfi Zadeh in the middle 1960s (Zadeh, 1965). It is one of the most widespread theories in control systems and was developed for data processing using fuzzy sets, as opposed to the classical computations involving (crisp) sets (Tanka and Niimura, 1996; Syed and Cannon, 2005; Sairo, 2006; Ross, 2009). It provides a way to obtain precise conclusions from vague or imprecise information and to mimic the process of decision making and the ability to work with approximate data typical of humans. Fuzzy logic allows modeling expert's knowledge and experience in complex systems using a higher level of abstraction with respect to exact mathematical formulae and strict implication, accounting for vagueness. Fuzzy logic has several advantages such as: flexibility in computation that eases its incorporation in an existing software/algorithm; simple integration with conventional computational techniques to yield precise and robust results; acceptance of imprecise data due to its fuzzy reasoning.

Thanks to its properties, fuzzy logic has been of widespread use in countless applications, ranging from controlling consumer products or medical instrumentation, to industrial process control, to decision-support systems, to portfolio selection and more (Hess, 1996; Rostovsky et al, 2016). Among others, several authors (Lin et al, 1996; Wieser and Brunner, 2002) used the idea of fuzziness in the GNSS context in order to improve the position accuracy, especially when GNSS is used as a stand-alone navigation system in critical conditions (urban canyons, dense vegetation environments or indoor).

A fuzzy controller maps numerical input variables to numerical output variables, but it operates with *fuzzified* linguistic variables, which represent some property (for example, the "SNR", or the "satellite elevation" for GNSS measurements) and terms (e.g., "high" and "low"), rather than numbers. It uses rules rather than formulas in order to transfer properties. In this research fuzzy logic is used as a method to set the weighting matrix used in WLS estimation. In order to improve the accuracy of positioning, two quality measures of the received signals (SNR and satellite elevation) are *fuzzified* and integrated, then a rule base is used to obtain an aggregated fuzzy weight, finally *defuzzified* in a numerical value.

In the next sections, the concept of fuzzy logic is described, including an introduction to fuzzy sets, logical operators applied to the fuzzy sets, fuzzy rules and *defuzzification* method. Finally, the fuzzy controller design adopted in the PVT algorithm is shown.

6.1. Fuzzy set Theory

A classical set A is a collection of entities *x*, which are called the *members* of the set. The set can be defined by listing all the members, defining a property which the members share or by means of the so called *characterizing function* (Wieser, 2002):

$$\mu_A(x) = \begin{cases} 1 & if\ x \in A \\ 0 & if\ x \notin A \end{cases} \tag{6.1}$$

The fact, that an arbitrary entity is either completely an element of A or it is not at all in A, is linked to the possible values of the characterizing function, which are 1 (membership) and 0 (non-membership). In order to solve the problem due to the presence of a crisp boundary in the classical set, the fuzzy logic could be a valid alternative approach.

For example, one of the most commonly used cases of a fuzzy set is the set of tall people and it is shown in Figure 6.1. The universe of discourse is all potential heights, from 150 to 200 cm, and the word tall would correspond to a curve that defines the degree to which any person is tall; this curve represents the characterizing function. If the set of tall people is given in the well-defined (crisp) boundary of a classical set, it is possible to say all people taller than 175 cm are officially considered tall. However, this classification it is not applicable talking about real people because it is not reasonable to call one person short and another one tall when they differ in height by a few centimeters. For this reason, using fuzzy logic it is possible to choose a smoothly varying curve that passes from not-tall to tall. In this way, two people are tall to some degree, but one could be significantly less tall than the other. This degree of membership to the set “tall” is given by the curve as shown in the Figure 6.1.

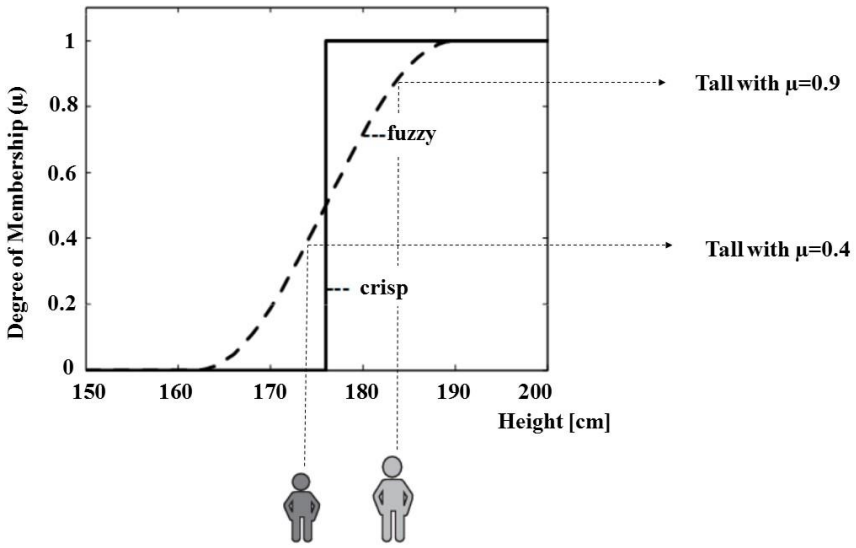

Figure 6.1 Two definitions of the set of "tall people", a crisp set and a fuzzy set.

To properly design a fuzzy controller, two concepts need to be introduced: the linguistic variable (LV) and the linguistic term (LT). A linguistic variables represents a concept that is measurable in some way (like SNR or satellite elevation), while a linguistic term is a quantification of that concept (for example “low”, “medium” or “high”). A linguistic term is a fuzzy set, and the related linguistic variable defines its domain. For example, a numerical variable like “height” may have a range from 1 to 2 meters – its domain – and fuzzy sets defined on it – categories – may be short (“low height”), normal (“medium height”) and tall (“high height”). Most notably one single height value can belong to more than one category with a different degree: fuzzy sets normally overlap.

Fuzzification of a variable means to define a set of overlapping categories (fuzzy sets) on its domain, and for each of them a *membership function* (MF) μ(x), which assigns a value between 0 and 1 to each element *x* of the domain to that category. Intuitively, the membership value of an element *x* to a category *C* represents the degree of belonging of *x* to *C*. Formally, a fuzzy set F (or a LT) is generally expressed as a collection of the elements *x* of a universe of measurements U with an associated MF:

$$F = \{(x, \mu_F(x))\} = \bigcup_{x_i \in U} \mu_F(x_i)/x_i, x \in U \tag{6.2}$$

where the x_i are the finite elements of a discrete universe, and the symbol "/" denotes "related to x_i" (Berkan and Trubatch, 1997). If the membership value is 1, the element x is fully included in the set; if it is 0, x is fully excluded; values of μ between 0 and 1 indicate partial membership. Each numerical input variable needs to be *fuzzified* before it can be used in a fuzzy controller, and the most critical aspect is determining the shape and the parameters of the MFs.

Any function which maps an input value from a (classical) set U onto a non negative real number could theoretically be used as a MF. However, it makes sense to limit the range of possible degree of membership to the interval [0,1]:

$$0 \leq \mu_F(x) \leq 1, \quad \forall x \in U \tag{6.3}$$

The maximum value of $\mu_F(x)$ is called *height* of F. Fuzzy sets with a height of 1 are called *normal*. The classical set U of all possible input values for which the MF is defined, is called the *domain* of the fuzzy set (Wieser, 2002). The *support* S is composed by all values of U which correspond to a non-zero degree of membership to F and is defined as:

$$S(F) = \{x \in U | \mu_F(x) > 0\} \tag{6.4}$$

The *tolerance* T of the fuzzy set F is the closed interval T which corresponds to full membership and is expressed as:

$$T(F) = \{x \in U | \mu_F(x) > 1\} \tag{6.5}$$

There are several alternative ways to transform a measurement into fuzzy categories. A frequent approach is to use triangular, Gaussian or trapezium-shaped MFs. The simplest fuzzy MF is the so-called triangular function, written as:

$$\mu_F(x) = \begin{cases} 0 & x \leq a \\ \dfrac{x-a}{b-a} & a < x \leq b \\ \dfrac{c-x}{c-b} & b < x \leq c \\ 0 & c < x \end{cases} \tag{6.6}$$

where a, b and c are the parameters of MF with a triangular shape as shown in Figure 6.2.

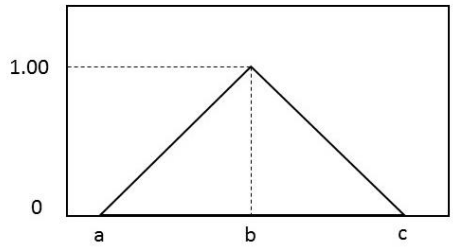

Figure 6.2 Example of a triangular MF

6.2. Basic operations on fuzzy sets

Fuzzy logic involves a number of logical operations that are a generalization of classical sets (Kaufmann and Gupta, 1985). The standard logical operations are AND, OR and NOT that are the operations also used in the conventional Boolean logic.

In defining each of the operations, two fuzzy sets, A and B, each belonging to finite set U, of real numbers, are assumed.

The MF of the union of two fuzzy sets A and B with MFs μ_A and μ_B, respectively, is defined as the maximum of the two individual MFs and is expressed as:

$$\mu_A \cup B(x) = (\mu_A(x) \vee \mu_B(x)) = \max\left(\mu_A(x), \mu_B(x)\right) \quad x \in U \tag{6.7}$$

This corresponds to fuzzy OR operator and the union of A and B is the smallest fuzzy set that contains all elements held in both sets.

The MF of the intersection of two fuzzy sets A and B with their MFs is defined as the minimum of the two individual MFs and is indicated as:

$$\mu_A \cap B(x) = (\mu_A(x) \wedge \mu_B(x)) = \min\left(\mu_A(x), \mu_B(x)\right) \quad x \in U \tag{6.8}$$

meaning that it is the largest fuzzy subset containing elements held in both A and B and it corresponds to fuzzy AND operator.

The MF of the complement of a fuzzy set A with its MF is defined as the negation of the specified MF and is expressed as:

$$\mu_{\overline{A}}(x) = 1 - \mu_A(x) \tag{6.9}$$

where $\overline{A}$ is the complement of the fuzzy set A. In Fuzzy set theory, the complement operator is the equivalent of the NOT operation in Boolean algebra.

Figure 6.3 provides the plot of two fuzzy sets A and B applied together to create one fuzzy set using the logical operator just described.

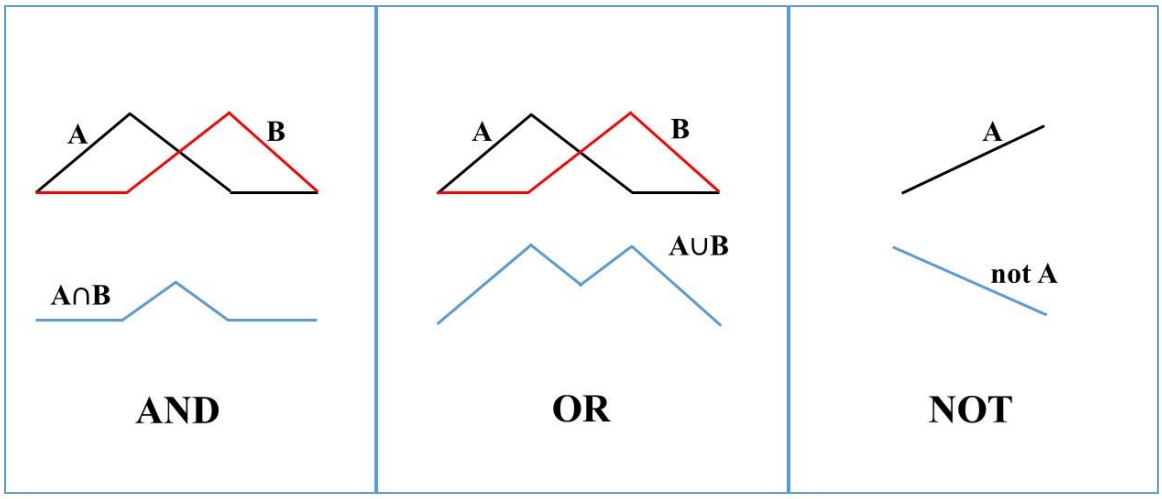

Figure 6.3 Geometric interpretation of AND, OR and NOT operators on two fuzzy sets A and B

6.3. Fuzzy rules

After the fuzzification, fuzzy rules can be defined. The fuzzy rules are IF-THEN statements involving LVs and LTs, logically linked by OR/AND connectives. The rules are based on expert's knowledge about interpreting the input parameters, and are expressed as:

If $INPUT_1$ is LT_{11} and $INPUT_2$ is LT_{12} then OUTPUT is LT_1

where $INPUT_1$ and $INPUT_2$ are the input LV and OUTPUT is the output LV, while LT_{11}, LT_{12} and LT_1 are LT. The if-part of the rule is the *antecedent*, while the then-part of the rule is the *consequent*.

An example in GNSS context is:

If elevation is low and SNR is medium then weight is low

Interpreting a collection of fuzzy rules consists of two parts: applying an implication operator and aggregating the results. For both parts more than one option is feasible, so the following is referred to the most common choices. If the individual premises are combined by a logical "and", the truth value of the compound premise is the minimum of the individual truth values; if the individual premises are combined by a logical "or", the truth value is its maximum. The implication operator builds the fuzzy set of each consequent combining the memberships specified by its antecedent (Bandemer and Nather, 1992), usually with the minimum function, and then the aggregator function merges the fuzzy sets of the consequents, usually with the maximum function. A graphical example of the evaluation of two fuzzy rules with two input variable and one output is shown in Figure 6.4: the implication and aggregation steps are shown.

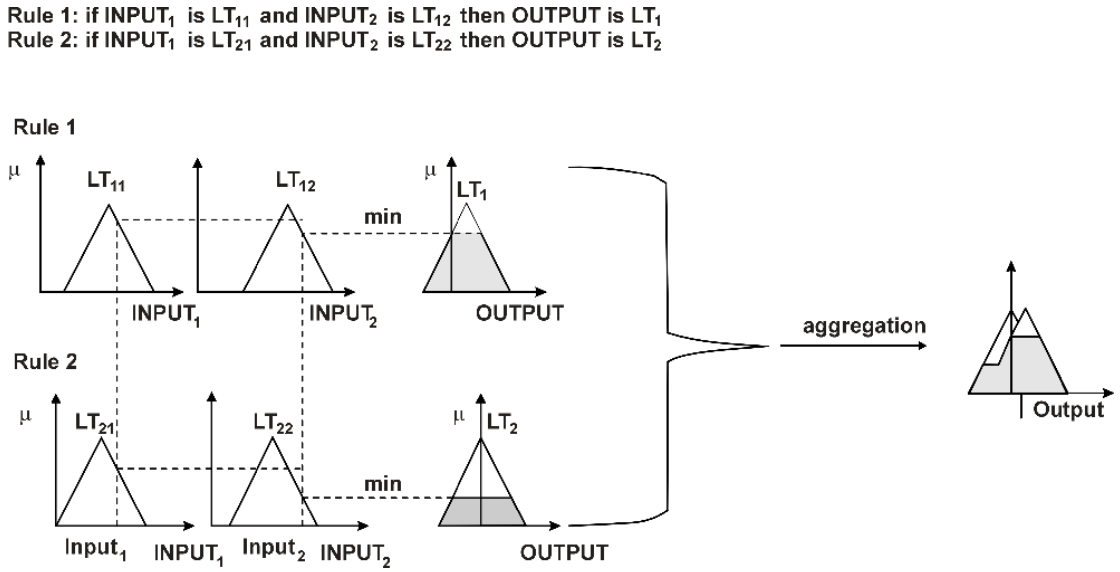

Figure 6.4 Example of the evaluation of two fuzzy rules with two input variable and one output. The implication and aggregation steps are shown

6.4. Defuzzification

The last step of a fuzzy system is *defuzzification* that is the reverse transformation in which the MF resulting from the aggregated fuzzy outputs is replaced by a single number. The fuzzy conclusion or output is still a LV that needs to be converted to the crisp variable via the defuzzification process (Bai and Wang, 2006). There are many ways of defuzzifing the aggregate fuzzy output. The most commonly used criterion is centroid defuzzification: the center of gravity (COG) of the area below the MF is projected into the domain axis to obtain

the final output value. This method is similar to the formula for computing the center of gravity in physics. The main advantages of this method are its simple computation, producing a unique result and it is not very sensitive to small changes in the input values generating only small changes in the defuzzied value of the result variable.

The COG of the area bounded by the MF curve is calculated to be the most crisp value of the fuzzy quantity. Obtained the aggregated fuzzy output indicated as "O*", the related center of the gravity is computed as:

$$COG(O^*) = \frac{\int \mu_{O^*}(x) \cdot x dx}{\int \mu_{O^*}(x) dx} \tag{6.10}$$

The geometric interpretation of the COG computed for the aggregated fuzzy output "O*" is shown in Figure 6.5.

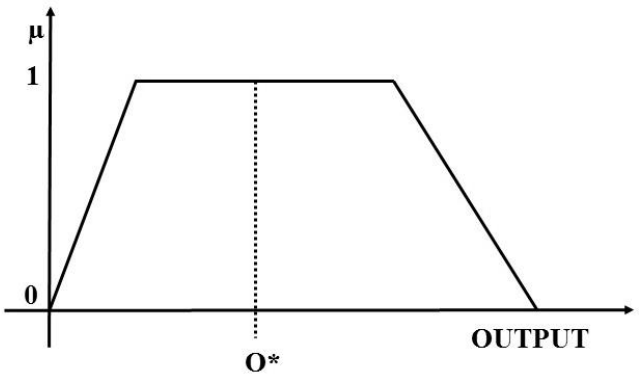

Figure 6.5 Center Of Gravity method

The other defuzzification methods are the maximum-height method or the average of support one. Using the first one, the domain value which corresponds to the maximum membership value is selected as output value. The result depends on the rule with maximum truth value of the premise only and it may not be unique. Using the latter one, the mean of the support of the result fuzzy set is used as output value. This value is linked to the active rules but not on their respective truth values (Wieser, 2002).

6.5. Fuzzy controller design for GNSS measurements weighting

In order to estimate the quality of GNSS pseudorange measurements used in the PVT algorithm, the proposed fuzzy controller was designed using the Matlab® Fuzzy Logic

Toolbox (The Mathworks Inc, 2005; Zadeh, 1995). The PVT algorithm developed in the MatLab® environment is detailed in section 4.2.

The scheme of the adopted fuzzy inference system (FIS), which is the process of formulating the mapping from a given input to an output using fuzzy logic, is shown in Figure 6.6.

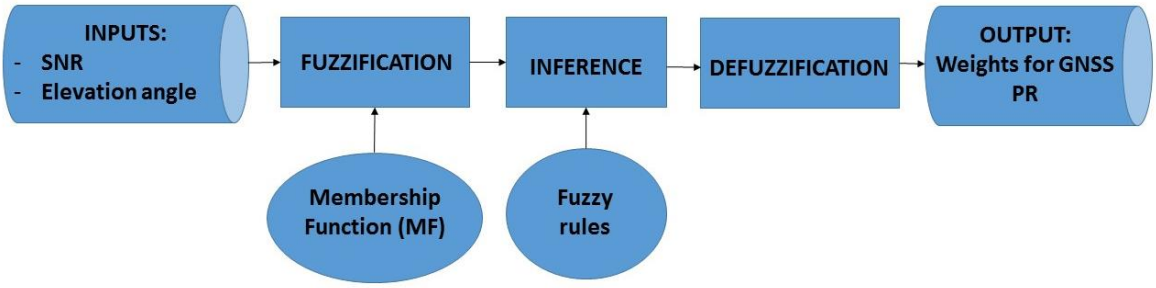

Figure 6.6 Fuzzy Inference System (FIS) to compute weighting coefficients for GNSS PR used in the WLS estimation

The input LVs are the *SNR* and *elevation angle* for each satellite, each characterized by five LT and trapezoidal MFs, labelled “very low”, “low”, “medium”, “high” and “very high”; while the output LV is the weight (ranging from 0 to 1) to be used in the weighting matrix W, characterized by five triangular functions named as the input LTs. Figure 6.7 shows the MFs for input (up) and output (down) LVs for GPS measurements. For example, since the accuracy of GLONASS satellite measurements is lower than GPS ones, different coefficients have been assigned to GPS and GLONASS (Moaiied and Mosavi, 2016). To obtain these coefficients, different fuzzy systems are used related to the GNSS constellation: the same LVs, LTs and fuzzy rules are considered, only lower weights are assigned to GLONASS measurements than to GPS ones.

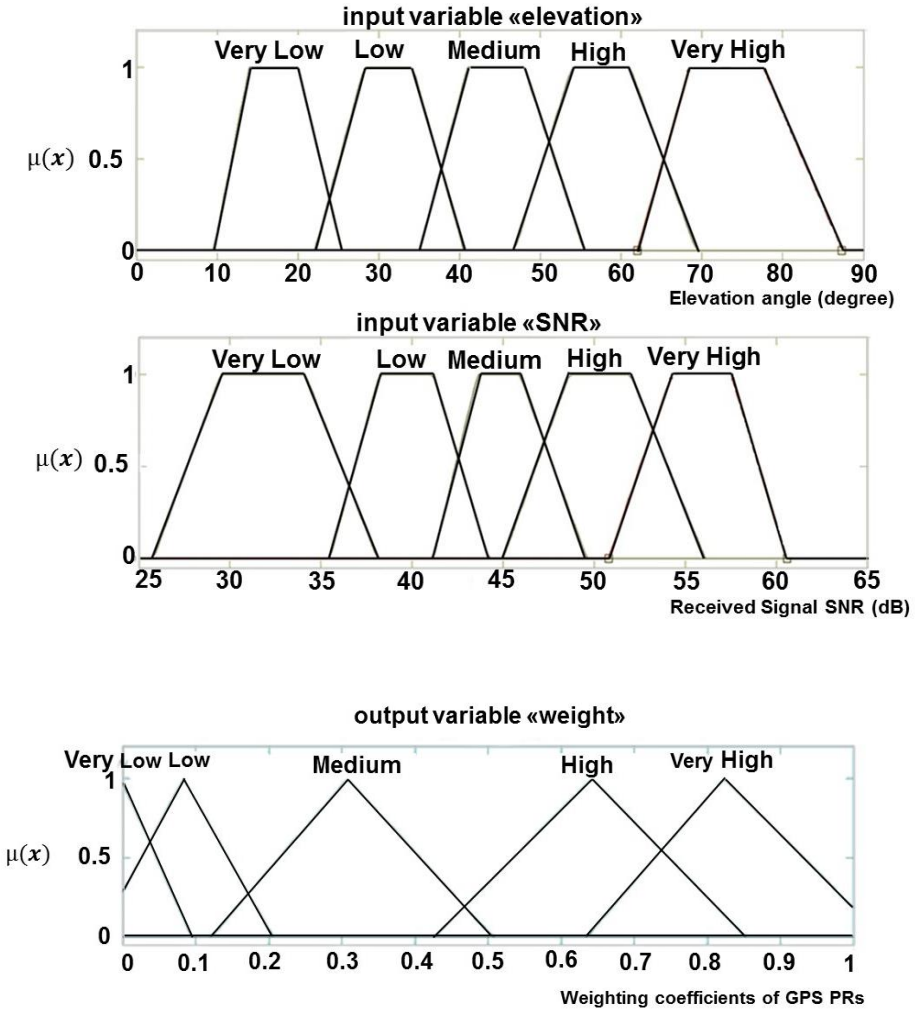

Figure 6.7 Membership functions of fuzzy system's input (elevation angle and SNR in the first two boxes) and output (weight in the latter box) for GPS PR

Twenty-five rules are built on the two inputs and one output LVs, shown in Figure 6.8.

1. If (elevation is Very Low) and (SNR is Very Low) then (weight is Very Low)
2. If (elevation is Very Low) and (SNR is Low) then (weight is Very Low)
3. If (elevation is Very Low) and (SNR is Medium) then (weight is Low)
4. If (elevation is Very Low) and (SNR is High) then (weight is Medium)
5. If (elevation is Very Low) and (SNR is Very High) then (weight is High)
6. If (elevation is Low) and (SNR is Very Low) then (weight is Very Low)
7. If (elevation is Low) and (SNR is Low) then (weight is Low)
8. If (elevation is Low) and (SNR is Medium) then (weight is Low)
9. If (elevation is Low) and (SNR is High) then (weight is Medium)
10. If (elevation is Low) and (SNR is Very High) then (weight is High)
11. If (elevation is Medium) and (SNR is Very Low) then (weight is Low)
12. If (elevation is Medium) and (SNR is Low) then (weight is Medium)
13. If (elevation is Medium) and (SNR is Medium) then (weight is Medium)
14. If (elevation is Medium) and (SNR is High) then (weight is High)
15. If (elevation is Medium) and (SNR is Very High) then (weight is High)
16. If (elevation is High) and (SNR is Low) then (weight is Medium)
17. If (elevation is High) and (SNR is Very Low) then (weight is Medium)
18. If (elevation is High) and (SNR is Medium) then (weight is Medium)
19. If (elevation is High) and (SNR is High) then (weight is High)
20. If (elevation is High) and (SNR is Very High) then (weight is Very High)
21. If (elevation is Very High) and (SNR is Low) then (weight is Medium)
22. If (elevation is Very High) and (SNR is Very Low) then (weight is Medium)
23. If (elevation is Very High) and (SNR is High) then (weight is High)
24. If (elevation is Very High) and (SNR is Very High) then (weight is Very High)
25. If (elevation is Very High) and (SNR is Medium) then (weight is High)

Figure 6.8 The rule base of the two-input (SNR and elevation) and one-output (GNSS measurements weight) fuzzy controller

As stated in section 6.3, the implication operator uses the minimum function, the aggregator uses the maximum, while defuzzification is done by computing the centroid of the aggregated area. Defuzzified output values are the weighting coefficients of PRs to be used in the WLS estimation of the SPP algorithm.

7. Test and Results

This chapter describes the tests carried out to assess the performance of the methods presented. Details about the adopted equipment, the operational environments and the algorithm performance are discussed.

In signal-degraded environments, the presence of obstacles blocks or strongly degrades the GNSS signals. In these situations, the multi-constellation approach enhances the solution availability and the continuity but it is not necessarily able to provide accurate PVT solutions because of the frequent presence of gross errors. A quality check on the measurements should be performed, so in this research two approaches are tested in order to improve the accuracy of the navigation solution. These approaches consist of:

- assigning weights, inversely related to the quality of the received signal in order to mitigate the effects of biases or gross errors;
- identifying and rejecting erroneous observables through a FDE algorithm improved by the use of the proposed weighting schemes.

As described in sections 1.2 and 6.5, this research proposes a technique based on fuzzy logic to compute the weighing matrix for the measurements set. To measure the performance of the proposed fuzzy weighting scheme (FWLS), two static tests are introduced and the results analyzed, then a vehicular test is considered and the obtained results are assessed. In all the tests a High-Sensitivity (HS) receiver is used.

Several configurations are compared, firstly considering only GPS and later combining two GNSS (specifically GPS and GLONASS). The configurations differ from each other for the weighting matrix (as described in 3.3 and 6.5) used in WLS to compute the position solution:

- assigning equal weights to all GPS measurements (briefly indicated as GPS EW);
- GPS with weights computed as function of elevation angle ($1/\sin^2(el)$, briefly indicated as GPS EL);
- GPS with weights computed using the signal power based weighting method as defined in section 3.3.1 (GPS SPW);
- GPS with weights computed combining satellite elevation and signal-to-noise ratio parameters as described in section 3.3.3 (GPS SPELW);
- GPS with Fuzzy weights as described in 6.5 (GPS FWLS);

- assigning equal weights to all measurements provided by the GPS/GLONASS constellation (briefly indicated as GG EW);
- GPS/GLONASS with weights computed as function of elevation angle ($1/\sin^2(el)$, GG EL);
- GPS/GLONASS with weights computed using SPW method (GG SPW);
- GPS/GLONASS with weights computed using SPELW method (GG SPELW);
- GPS/GLONASS with Fuzzy weights (GG FWLS).

Besides these comparisons, the Subset algorithm is applied in order to verify the enhancement obtained thanks to the different weighting schemes. The advantages of the proposed weighting methods in the RAIM are analyzed, comparing the following configurations:

- the basic configuration GPS EW without RAIM functionality (GPS EW);
- GPS with Subset RAIM functionality and weights computed using the SPELW method (GPS Sub/SPELW);
- GPS with Subset RAIM functionality and using Fuzzy weights (GPS Sub/FWLS);
- GPS/GLONASS without RAIM functionality (GG EW);
- GPS/GLONASS with Subset RAIM functionality and weights computed using the SPELW method (GG Sub/ SPELW);
- GPS/GLONASS with Subset RAIM functionality and Fuzzy weights (GG Sub/FWLS).

The obtained results are compared with a reference solution in order to carry out the error analysis: the Key Performance Indicators (KPIs) used to characterize the performance of the system are Root Mean Square (RMS) and mean and maximum errors for both horizontal and vertical components of the position. Furthermore, two additional parameters are considered: the solution and reliability availability. The solution availability is considered when no RAIM is being performed and it is defined as the time percentage when the navigation solution is computed. The reliability availability is the time percentage when the RAIM algorithm defines the solution as reliable.

7.1. Static Tests

Two different data collections in static mode were carried out on 1st and 12th of July 2016 (the duration of the tests are shown in Table 7.1). The antenna was placed on two points located at Centro Direzionale of Naples (Italy), where the presence of skyscrapers blocks many GNSS signals and leads to multipath effects; hence, the operational environment represents a typical signal-degraded case. The coordinates of the points, where the receiver was located, are known with high accuracy, and are considered as references for the computation of errors. The static receiver does not limit the validity of the analysis because the data are processed epoch-by-epoch, simulating real-time processing.

The receiver used is a NV08C-CSM from NVS Technologies AG, able to provide single frequency (L1) GPS, GLONASS, GALILEO, BeiDou, and SBAS measurements, connected to a patch antenna. The NV08C-CSM is an HS receiver, so it is characterized by the ability to acquire and track weak GNSS signals. However, while the increased tracking capability of HSGNSS is advantageous, severe interference effects due to a poor signal conditions lead to large measurements errors. The devices used for the static tests in all are shown in Figure 7.1.

Figure 7.1 Static Test Equipment and operational scenario

The characteristics of the scenario are evident from Figure 7.2 which shows the positions where the data collections were carried out.

The known coordinates of the reference points are shown in Table 7.1.

Table 7.1 Information about reference points and description of the data collections carried out

	Coordinate Information			Data Collection	
Name	Latitude (deg)	Longitude (deg)	Height (m)	Date	Duration (minute)
Point 1	40.857161	14.284020	59.9456	01/07/2016	108
Point 2	40.857139	14.283787	59.9497	12/07/2016	77

Figure 7.2 Location of the considered points, situated at Centro Direzionale of Naples (Italy)

In the next paragraphs, the results for the two static tests are shown, analyzing the previously mentioned configurations and conducting the error analysis to evaluate the performance of the proposed approaches.

7.1.1. Static Test 1

To verify the improvement due to the combination of two GNSS constellations (GPS and GLONASS), the satellite availability and the satellite geometry are analyzed for the static

test campaign. Figure 7.3 shows the number of available GNSS satellites during the data collection on 1st of July 2016, while the satellite geometry is analyzed plotting the behavior of the Position Dilution of Precision (PDOP) during the session in Figure 7.4.

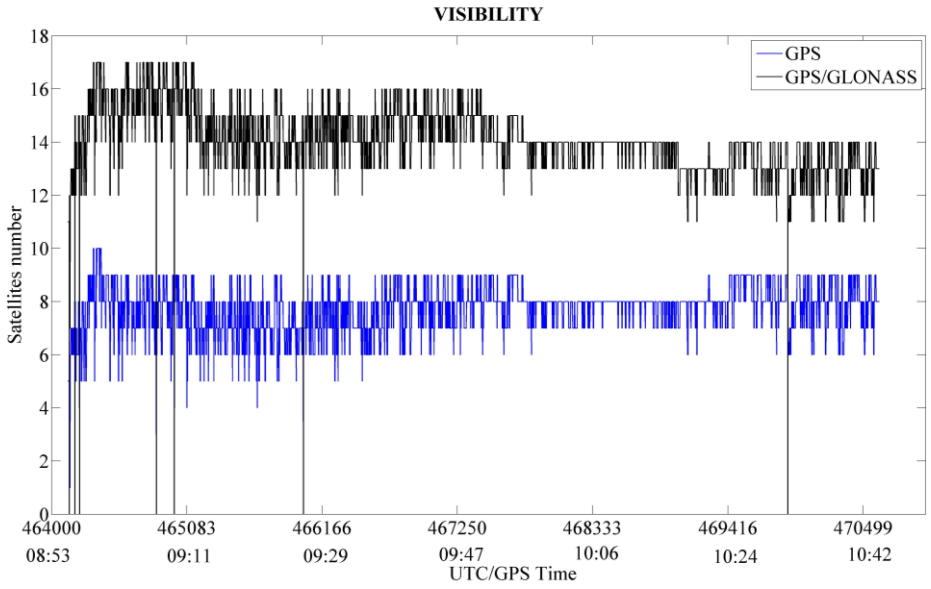

Figure 7.3 Number of available GNSS satellites during the data collection carried out on 1st of July 2016 and used for navigation solution computation

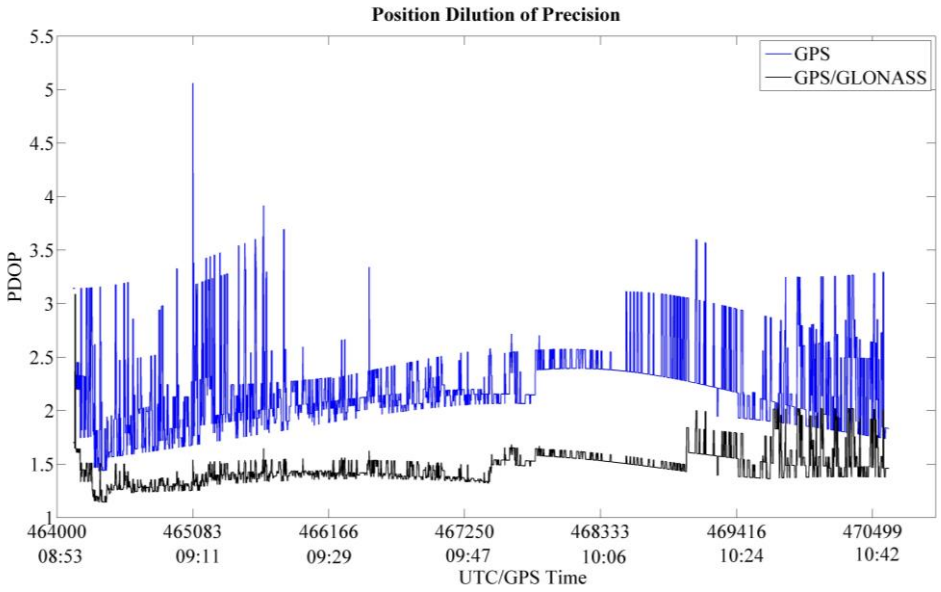

Figure 7.4 PDOP values computed epoch-by-epoch and plotted as function of the time for the data collection on 1st of July 2016

Figure 7.3 shows that the number of GPS satellites varies from 0 to 10, with an average of circa 7 satellites for epoch. In the multi-constellation case (GPS/GLONASS) the mean number of satellites is 14, varying from 0 to 17. Moreover, in some epochs there are not enough satellites to compute the navigational solution at all due to the degraded situation of the environment.

PDOP is commonly used as a measure of satellite geometry and is the combination of both the horizontal and vertical components of the position error caused by satellite geometry (as described in 3.4): lower values indicate a higher probability of obtaining good position accuracy. During the observation period, PDOP varies from a minimum value of 1.4 to a maximum of 5, with an average of 2.3 for the GPS configuration, while for the multi-constellation case the mean value of PDOP is 1.5, passing from a minimum of 1.2 to a maximum value of 3.1. This behavior shows how the combination of different GNSS measurements improves the satellites availability and the related geometry, decreasing the mean value of PDOP as shown in Figure 7.4.

Table 7.2 summarizes the statistical parameters of the error analysis for horizontal (H) and vertical (Up) components of position for the GPS only configuration during the static session carried out on 1st of July 2016. Due to the signal-degraded environment, very large errors affect the static test: without specific algorithms able to detect and remove the blunders, the accuracy of the navigation solution is compromised. However, the use of quality indicators for the computation of the weighting matrix in WLS can improve the accuracy, as shown by Table 7.2. In fact, all adopted weighting schemes show a better behavior compared to the basic configuration (equal weights to all measurements).

Table 7.2 Summary Results for Horizontal (H) and Vertical (Up) component of the position obtained using only GPS constellation for static test carried out in point 1

	H Mean Error [m]	**Up Mean Error [m]**	**H RMS [m]**	**Up RMS [m]**	**H Max Error [m]**	**Up Max Error [m]**
GPS EW	33.86	61.73	60.66	85.25	362.98	328.48
GPS EL	21.37	46.45	37.74	63.38	185.88	225.02
GPS SPW	28.28	49.30	55.24	71.25	340.97	306.70
GPS SPELW	14.02	27.91	27.38	41.38	156.45	192.71
GPS FWLS	7.72	13.27	15.16	20.64	114.08	137.81

From the analysis of the statistical parameters, it can be noted that the weights as function of elevation angle (EL) provide a better accuracy with respect to the SPW method, based on

the SNR, in terms of all analyzed KPIs for horizontal and vertical components of the position. However, the SPELW method and Fuzzy Weights (FWLS) outperform all the other ones, being able to exploit both the elevation angle and the SNR information. Specifically, FWLS provides the best performance in terms of all considered figures of merit for the horizontal and vertical components: horizontal RMS decreases from circa 27 meters for SPELW configuration to circa 15 meters for FWLS, while vertical RMS decreases of circa 20 meters; the horizontal and vertical maximum errors decrease of circa 50 meters.

The qualitative analysis is carried out comparing the identified two best methods to the basic configuration. In Figure 7.5 the green points are relative to the horizontal position errors obtained assigning equal weights to all GPS PR, the black ones to the SPELW method and the magenta ones to the FWLS. The horizontal position errors are computed with respect to the known coordinates of the reference point 1.

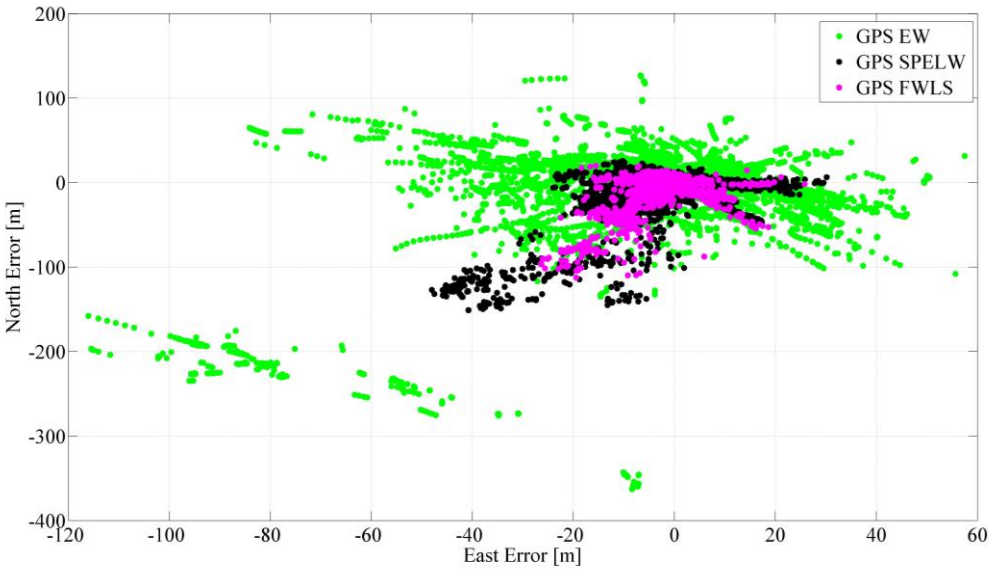

Figure 7.5 Horizontal Position Errors obtained using Equal Weigths, the SPELW method, and Fuzzy Logic for the GPS configuration

Looking at the figure, it is evident that FWLS has the best performance, however, both the resulting point clouds relative to SPELW and FWLS are concentrated around the origin (reference truth). GPS EW is characterized by the highest errors since it gives equal weights to all measurements, including the blunders, degrading by consequence the solution.

Horizontal and vertical position errors, obtained using the different configurations, are plotted as a function of time in Figure 7.6. The color convention is the same as in the previous plot.

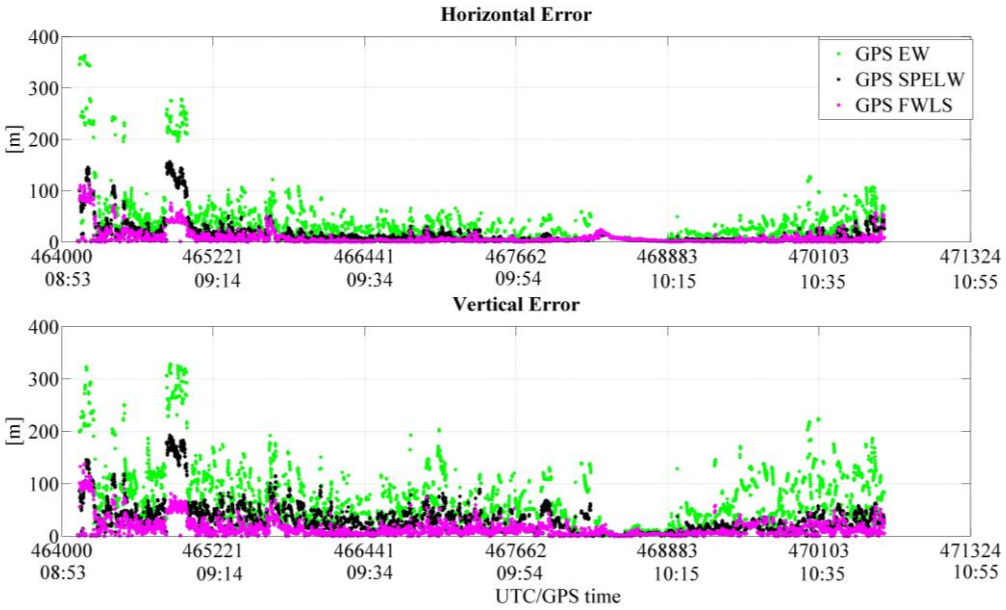

Figure 7.6 Horizontal and Vertical Errors as a function of time for Equal Weights, SPELW, and Fuzzy weights for the GPS configuration using the data collected during the static test 1

The qualitative analysis confirms the results summarized in Table 7.2: FWLS provides the best behavior compared to the other configurations for the horizontal and vertical components.

The same error analysis is carried out for the GPS/GLONASS configuration in order to show the enhancement of fuzzy logic also for GLONASS measurements. Indeed, as described in section 6.5, different fuzzy systems are developed based on the GNSS system at hand, so the weights assigned here for GLONASS measurements are lower than for GPS. The statistical parameters of the error analysis for horizontal (H) and vertical (Up) components of position for GPS/GLONASS (GG) configuration are reported in Table 7.3.

Table 7.3 Summary Results for Horizontal (H) and Vertical (Up) component of the position obtained using GPS and GLONASS systems

	H Mean Error [m]	**Up Mean Error [m]**	**H RMS [m]**	**Up RMS [m]**	**H Max Error [m]**	**Up Max Error [m]**
GG EW	46.01	121.05	63.82	153.87	301.11	580.01
GG EL	31.37	82.66	38.32	94.84	147.73	273.62
GG SPW	37.83	103.37	56.67	137.83	268.99	542.61
GG SPELW	17.81	54.06	22.88	65.17	100.64	301.23
GG FWLS	10.21	25.41	14.91	35.67	107.19	407.95

Also for this case, the weights as function of elevation angle (EL) offer a better accuracy with respect to the SPW method, in terms of all analyzed figures of merit for horizontal and vertical components of the position. However, FWLS shows the best behavior in terms of horizontal and vertical mean and RMS errors; vertical mean error and RMS for FWLS are almost half of the resulting equivalents of SPELW. The only exception concerns the maximum errors. In fact, a value of circa 400 m can be noted for vertical maximum error of the GG FWLS configuration: in this case, the quality index obtained using the fuzzy logic highly de-weights a satellite that it is not faulty unlike the SPELW method. Indeed, GG EL configuration shows the lowest value of vertical maximum error.

The next figures provide the same qualitative analysis conducted previously, showing the performance only for the best two methods (GG FWLS and GG SPELW) with respect to the basic configuration (GG EW). Figure 7.7 shows the horizontal position errors for the three configurations, while horizontal and vertical errors as function of time are plotted in Figure 7.8.

The use of fuzzy logic in the stochastic model clearly improves the performance with respect to the baseline and the SPELW method (combining signal power and elevation angle parameters): the magenta cloud is the smallest, except for the presence of 3 points very far from the cloud. This confirms the analysis of the statistical parameters summarized in the Table 7.3 highlighting the presence of some blunders in the GLONASS measurement set at the beginning of the data collection and around 10:00 am as shown in Figure 7.8. As expected, the vertical error has values larger than the horizontal one due to the satellite geometry, but the behavior of FLWS is the best when considering both vertical and horizontal components of position.

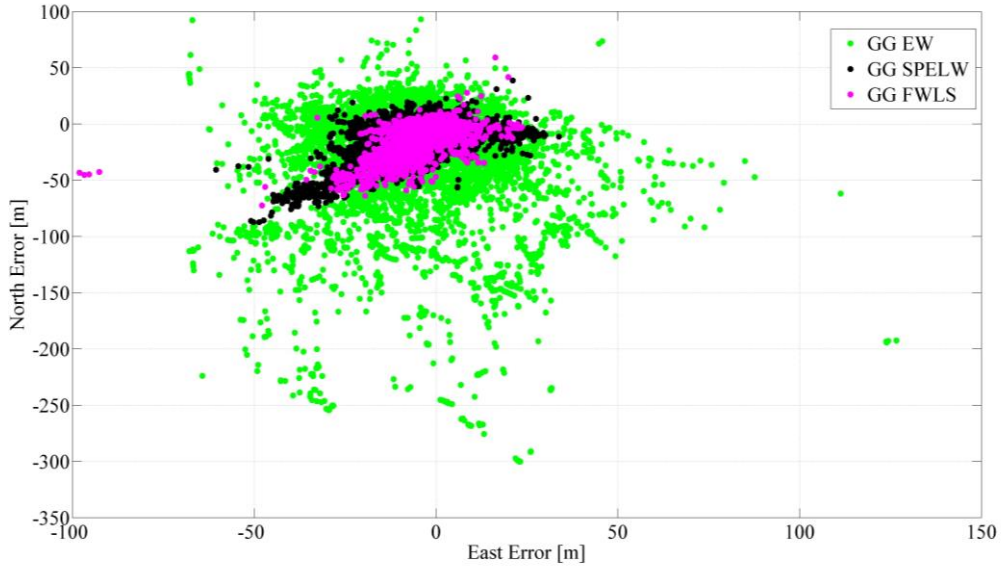

Figure 7.7 Horizontal position errors obtained using Equal Weigths, the SPELW method, and the Fuzzy Logic process for GPS/GLONASS configuration

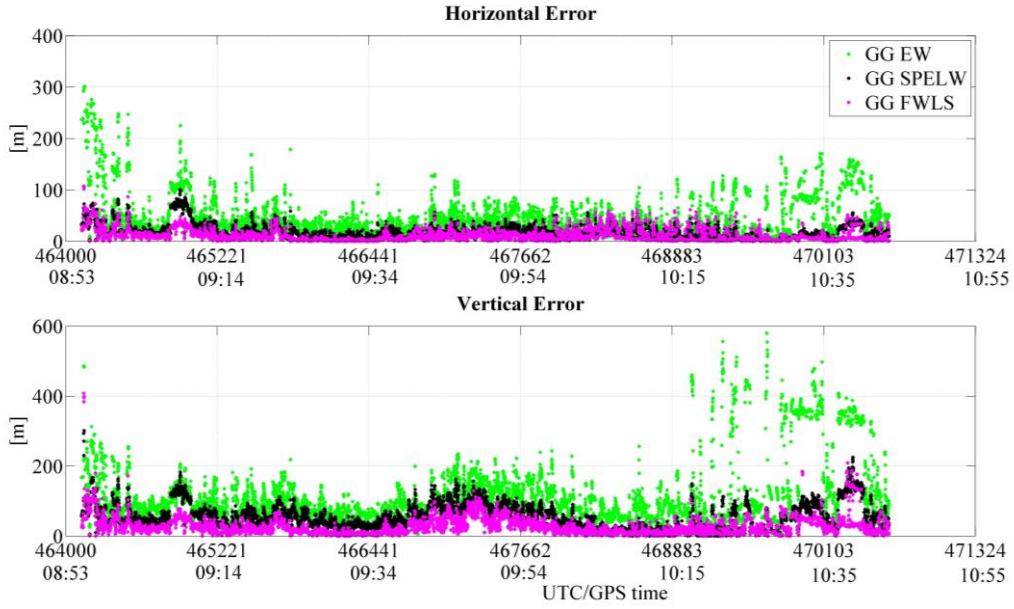

Figure 7.8 Horizontal and Vertical Errors as a function of time for Equal Weights, the SPELW, and Fuzzy weights for GPS/GLONASS configuration

Because the data are collected in a typical signal-degraded scenario, the use of a quality control algorithm is necessary to improve the performance of the PVT algorithm, removing the influence of the large errors. For this reason, the Subset algorithm is applied as an FDE

and since the statistical variable, computed as in equation (5.4), includes the W matrix, then the enhancement of the different weighting methods in the FDE algorithm is verified.

For a fast comparison, only the results of the weighting methods with the best performance in the previous results are shown for GPS and GPS/GLONASS configurations (Sub/FWLS and Sub/SPELW). They are compared to the basic configurations obtained assigning equal weights to GNSS observations and without the use of Subset algorithm (GPS EW and GG EW). For the configurations obtained using the Subset algorithm, only the reliable epochs are considered and epochs deemed not reliable are fully discarded reducing simultaneously the availability.

The statistical parameters of the error analysis for horizontal (H) and vertical (Up) components of position, obtained using only GPS pseudoranges are presented in Table 7.4. To verify the improvement in terms of availability thanks to the Subset method, the reliability availability (R.A.) is also shown in Table 7.4. The figures of merit for GPS EW are computed in all the available epochs (99.83%) while for the two configurations using the RAIM algorithms the error analysis is carried out only in the reliable epochs.

Table 7.4 Summary results for Horizontal (H) and Vertical (Up) component of the position obtained using only GPS and applying the Subset algorithm as an FDE

	H Mean Error [m]	**Up Mean Error [m]**	**H RMS [m]**	**Up RMS [m]**	**H Max Error [m]**	**Up Max Error [m]**	**S.A. [%]**	**R.A. [%]**
GPS EW	33.86	61.73	60.66	85.25	362.98	328.48	99.83	N.A.
GPS Sub/SPELW	5.17	6.94	11.75	20.15	124.80	257.99	N.A.	60.00
GPS Sub/FWLS	4.82	6.56	11.63	18.52	109.67	224.63	N.A.	62.02

From the table, the improvement obtained applying the Subset algorithm is clear with an important reduction of all the figures of merit for position horizontal and vertical components. This is due to its capability to detect and remove the large errors present in a measurement set, enhancing the accuracy and reliability of the navigation solution. The GPS Sub/FWLS configuration has the best performance for all the KPIs analyzed. In detail, comparing GPS Sub/FWLS with GPS Sub/SPELW, a decrease of decimeter order for the vertical and the horizontal mean errors and the horizontal RMS can be noted, and of meter order for the vertical RMS. In addition, maximum errors are also reduced using the fuzzy

logic, varying from around 125 m to 110 m for the horizontal component and from 258 m to 225 m for the vertical.

The use of the fuzzy system in the Subset algorithm guarantees a higher reliability availability (62%) with respect to the SPELW method (60%).

These results are recapped in the next two figures and only the navigation solutions declared reliable from the Subset algorithm are illustrated. In Figure 7.9 the green points represent the horizontal position errors, obtained assigning equal weights to all GPS PR without the application of a RAIM/FDE algorithm, the black ones the GPS Sub/SPELW and the magenta ones the GPS Sub/FWLS configurations. The horizontal and vertical errors, as function of time for the three considered configurations, are shown in Figure 7.10 using the same color convention. The qualitative analysis shows that GPS Sub/FWLS has the best behavior both for horizontal and vertical components in the position domain, except in some epochs where this configuration shows errors slightly higher than the baseline. For example looking at the Figure 7.10, higher errors are visible around 9:03 and 10.30 am in the horizontal domain. This behavior is due to an erroneous measurement rejection in the presence of multiple blunders; in these epochs, instead, the solution provided by the GPS Sub/SPELW is therefore unreliable. However, FWLS and SPELW applied to the RAIM/FDE provide similar performance for most of the time, except for a few epochs where the GPS Sub/FWLS works better than the SPELW method.

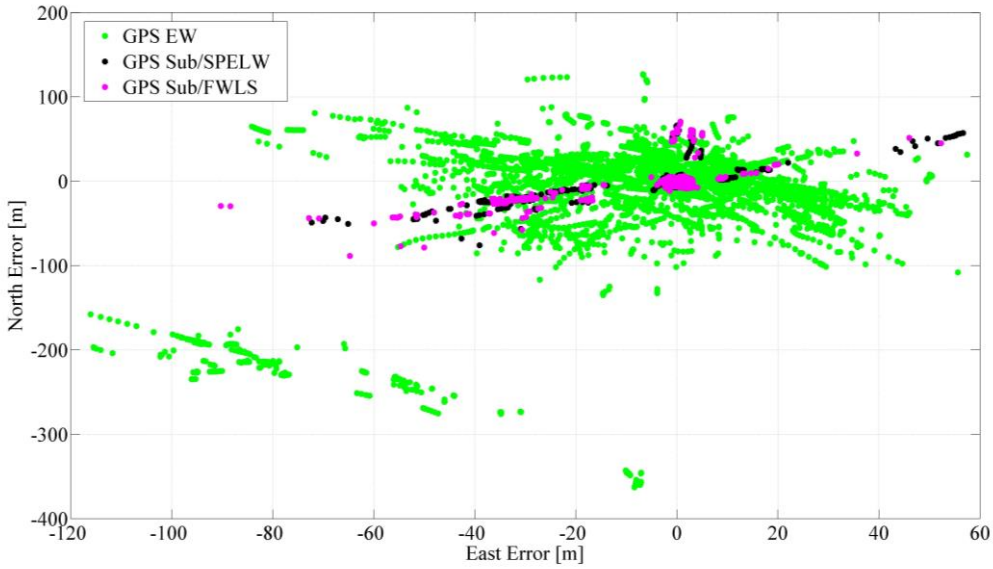

Figure 7.9 Horizontal position errors for the tree considered configurations: the baseline obtained assigning equal weights to GPS observations and without the use of Subset algorithm (GPS EW), and the solutions computed using the SPELW method (GPS Sub/SPELW) and the fuzzy system (GPS Sub/FWLS) within the Subset algorithm

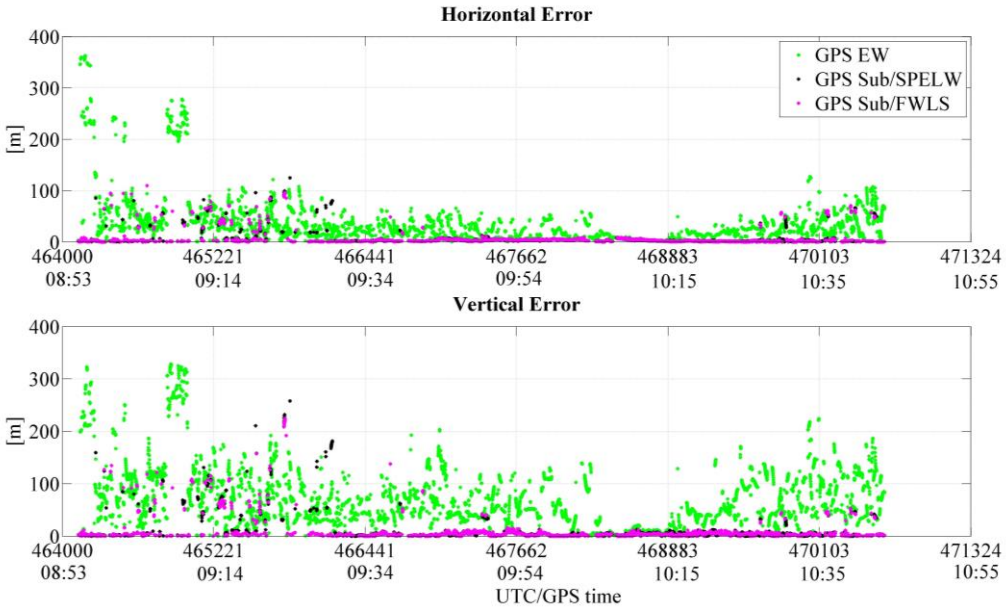

Figure 7.10 Horizontal and vertical errors as function of the time: comparison between the baseline (GPS EW), and the configurations obtained applying the Subset algorithm using the SPELW method (GPS Sub/SPELW) and fuzzy weights (GPS Sub/FWLS)

For a multi-constellation configuration, Table 7.5 summarizes the KPIs for the conducted accuracy and reliability analysis, obtained combining the Subset algorithm and the two weighting schemes.

Table 7.5 Statistical paramenters of the error analysis for Horizontal (H) and Vertical (Up) component of the position obtained using the multi-constellation approach (GPS/GLONASS) and applying the Subset algorithm

	H Mean Error [m]	**Up Mean Error [m]**	**H RMS [m]**	**Up RMS [m]**	**H Max Error [m]**	**Up Max Error [m]**	**S.A. [%]**	**R.A. [%]**
GG EW	46.01	121.05	63.82	153.87	301.11	580.01	99.83	N.A.
GG Sub/SPELW	7.22	13.34	16.01	32.90	160.88	326.94	N.A.	62.63
GG Sub/FWLS	5.41	10.43	12.52	25.38	124.86	307.42	N.A.	65.46

Also for the multi-constellation case, the usage of RAIM/FDE improves the accuracy of the navigation solution, enhancing considerably all the indicators of accuracy performance. Using the RAIM/FDE, the number of available/reliable epochs (indicated by R.A. and used for the error analysis) is lower than the S.A. considered for the configuration with “no

RAIM", but this latter parameter also includes the epochs that are no reliable or with no redundancy. However, even if the availability performance decreases for GG Sub/SPELW and GG Sub/FWLS configurations, an evident improvement in terms of accuracy can be noted.

In the Table 7.5, the configuration that provides the best performance for all the considered parameters is the multi-constellation GPS/GLONASS using the Subset algorithm and assigning fuzzy weights to the GNSS measurements. An enhancement of meter order is evident for the horizontal mean error and RMS using the FWLS setup and it is higher for vertical component. In fact, vertical mean error increases from around 10.4 m for GG Sub/FWLS configuration to 13.3 m for GG Sub/SPELW, while a reduction of around 7 meter is obtained for vertical RMS thanks to the fuzzy logic. Furthermore, the use of the fuzzy logic in the computation of the weight matrix W improves the performance of the RAIM/FDE algorithm as it can be noted from the analysis of the reliability availability that varies from 62.63% for GG Sub/SPELW configuration to 65.46% for the GG Sub/FWLS.

The investigation of the performance of the three considered configurations is carried in the Figure 7.11 and Figure 7.12. The green points refers to the horizontal and vertical position errors obtained assigning equal weights to all GNSS PR without the application of a RAIM/FDE algorithm, the black and the magenta ones, respectively, to GG Sub/SPELW and GG Sub/FWLS configurations. Only the reliable epochs are plotted for the configurations using the Subset algorithm.

The performance of the two weighting methods in the horizontal and vertical plane are compared with the baseline configuration (GG EW). Using quality checks and fuzzy logic in the W matrix clearly improves the performance with respect to the baseline case. In the horizontal domain the magenta cloud is the smallest, confirming the results obtained in the previous cases. GG Sub/SPELW and GG Sub/FWLS schemes seem to provide similar performance and the relative clouds are smaller and near to the origin of the figure (reference truth) with respect to the baseline configuration. The number of markers for the configurations using Subset algorithm is lower because of the limited reliability (the R.A.) defined by the method. From a qualitative analysis, the cloud relative to the FWLS solutions (magenta dots) is the most concentrated with respect to the other ones.

The vertical and horizontal errors for the two configurations with the different W matrix (Figure 7.12) are lower than the baseline configuration with a slight improvement for the GG Sub/FWLS. These results confirm the enhancement of the fuzzy system, which provides

a valid approach to modify the stochastic model of both GPS and GLONASS observations. Furthermore, it allows an efficiency improvement of the RAIM/FDE algorithm as well.

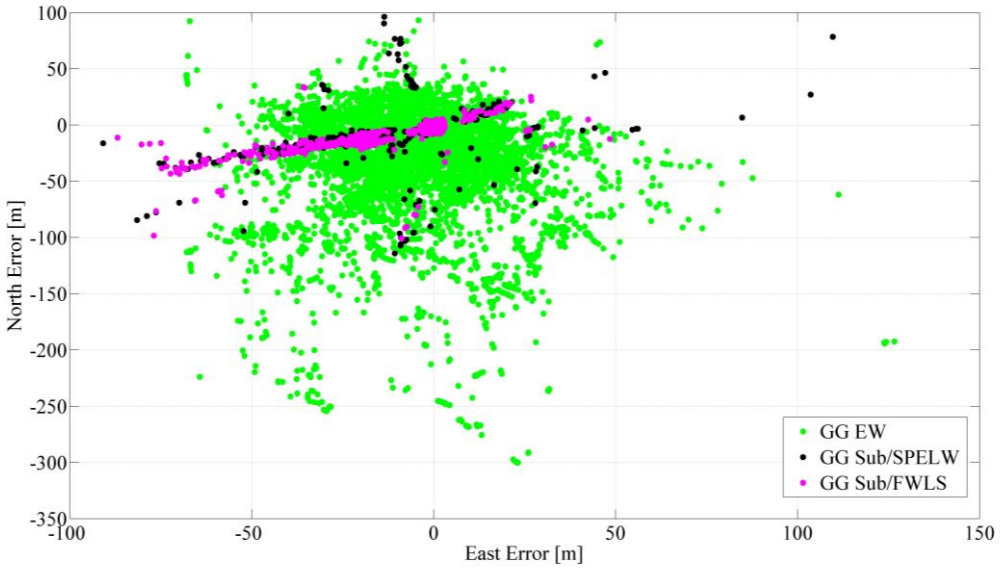

Figure 7.11 Horizontal position errors obtained using Equal Weigths (without RAIM functionality), and the SPELW method and the Fuzzy Logic process for the GPS/GLONASS configuration when applying the Subset algorithm

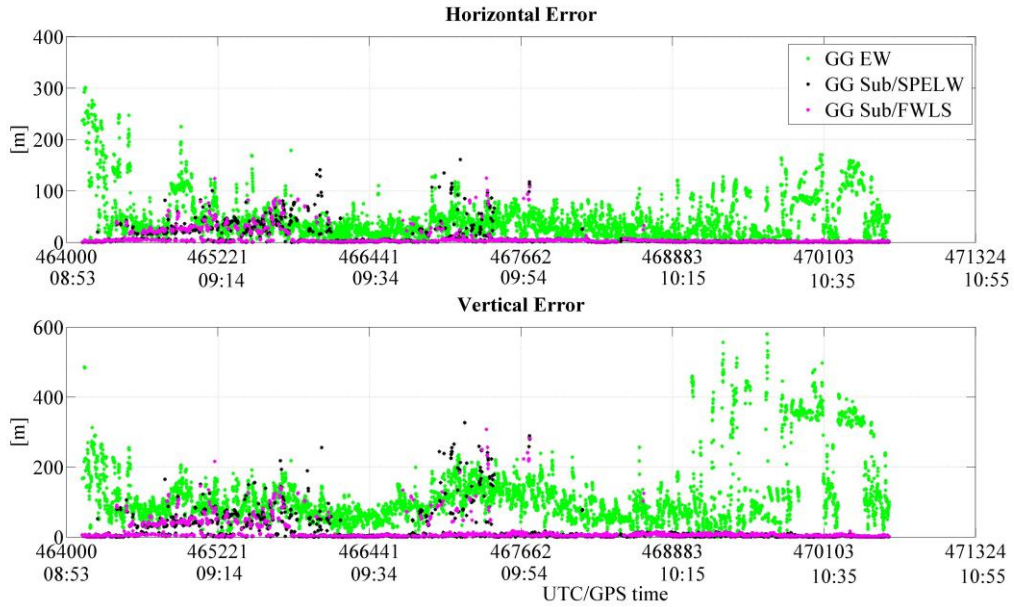

Figure 7.12 Horizontal and vertical position errors during the data collection obtained using Equal Weigths (without RAIM functionality), and the SPELW method and the Fuzzy Logic process for the GPS/GLONASS configuration when applying the Subset algorithm

7.1.2. Static Test 2

The analysis described in the previous section is repeated for the statistic session gathered on 12th of July 2016 in point 2 of CDN. Firstly, the number of available GNSS satellites and the satellite geometry during the observation period are shown in Figure 7.13 and Figure 7.14, respectively.

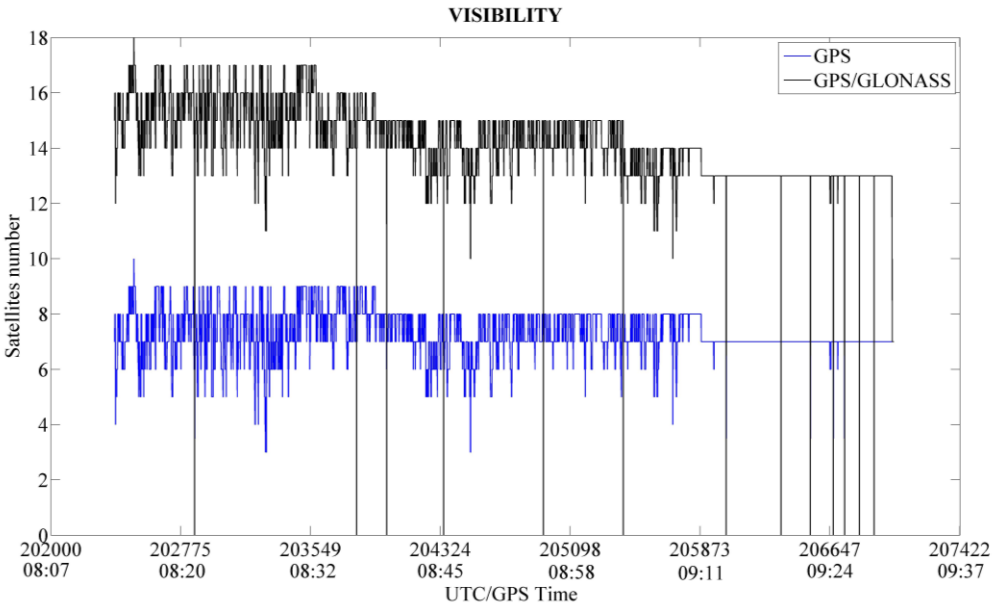

Figure 7.13 Available GNSS satellites during the data collection carried out on 12th of July 2016

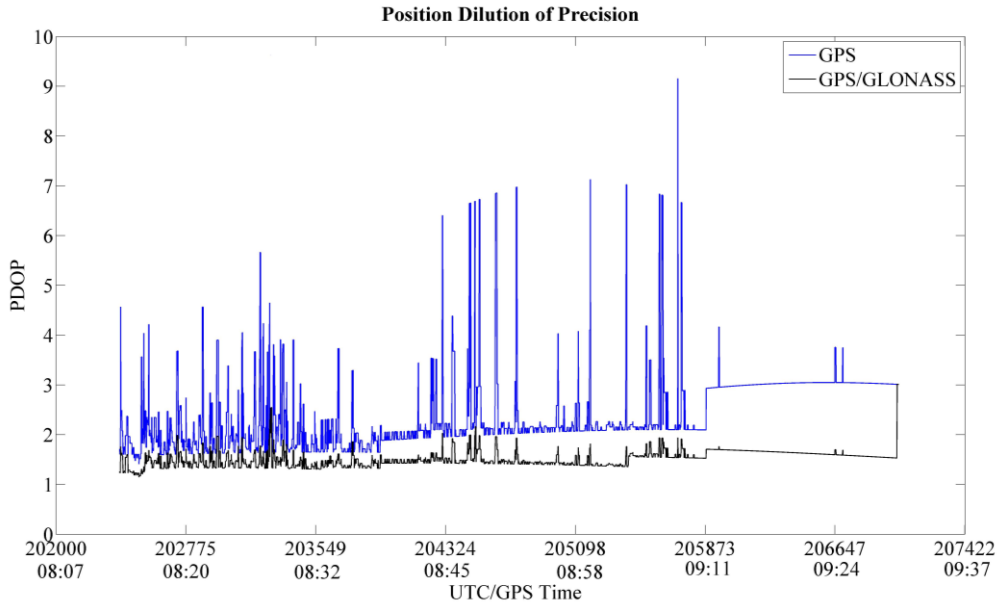

Figure 7.14 PDOP plotted as function of the time for the data collection on 12th of July 2016

The number of available GPS satellites varies from 0 to 10, with an average of circa 7, while thanks to the inclusion of GLONASS measurements the number of satellites is increased varying from 0 to 18, with an average of circa 14. In some epochs, the number of satellites is not sufficient to compute the navigational solution. Furthermore, using only GPS satellites, a poor satellite geometry is evident for some epochs, as shown in Figure 7.14. In fact, PDOP varies from 1.4 to 9.6 with an average of 2.4 for the GPS only case, but PDOP values higher than 8 indicate a poor satellite geometry and a low probability of obtaining a good position accuracy. On the other side, thanks to the combination of the two GNSS constellations, PDOP decreases fluctuating from 1.1 to 3 with a mean value of 1.5. This fact confirms that the use of a multi-constellation allows to provide better satellite availability and to improve the satellite geometry.

The performance comparison between the considered configurations is shown in Table 7.6 analyzing the KPIs on vertical and horizontal components of the position, obtained using only GPS PR.

Table 7.6 Summary Results for static test carried out in point 2 of CDN on 12th of July 2016 (only GPS PR are used)

	H Mean Error [m]	Up Mean Error [m]	H RMS [m]	Up RMS [m]	H Max Error [m]	Up Max Error [m]
GPS EW	37.19	95.49	51.87	123.18	429.44	869.82
GPS EL	31.96	88.94	44.02	114.26	428.94	846.79
GPS SPW	34.40	89.84	47.53	115.37	434.39	872.01
GPS SPELW	27.38	76.55	38.48	99.92	444.09	846.49
GPS FWLS	23.82	65.20	35.93	89.08	454.53	836.31

The Table 7.6 shows that the elevation dependent weighting method has better performance compared to the basic configuration (GPS EW) in terms of all considered figures of merit for the horizontal and vertical component. On the other hand, the SPW method, based on SNR, remains worse than EL, outperforming the basic configuration, except for the horizontal and vertical maximum errors. Both methods based on the use of a single quality parameter (EL and SPW) have higher KPI values with respect to FWLS and SPELW (except for horizontal maximum error), thus providing a lower accuracy.

From Table 7.6, it is evident that also in this case GPS FWLS outperforms the other configurations for all the considered figures of merit, except for the horizontal maximum error. This is due to the influence of blunders that are not be correctly weighted since characterized by conflicting inputs (for example a satellite with a low elevation angle but high SNR value) that do not satisfy the fuzzy rules. Comparing SPELW and FWLS configurations, the latter shows an improvement of circa 10 meters in terms of RMS and maximum error on the vertical component, but FWLS has a higher horizontal maximum error with respect to the former.

The horizontal position errors for Equal Weights, SPELW and FWLS configurations are shown in Figure 7.15, while horizontal and vertical position errors obtained using the several configurations during the static session are plotted in Figure 7.16. The navigation solutions are computed using measurements from only GPS constellation. The green markers are relative to the configuration obtained assigning equal weights to all measurements, the black ones to the SPELW method and the magenta ones to the FWLS.

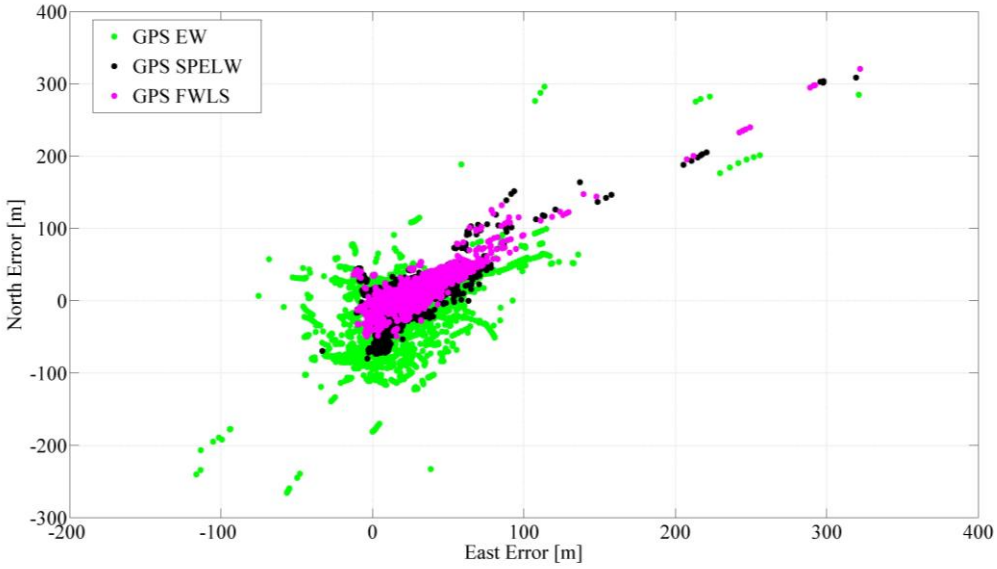

Figure 7.15 Horizontal Position Errors for Equal Weights (GPS EW in green points), SPELW (black) and Fuzzy Weights (magenta) configurations, obtained using the GPS PR measurements

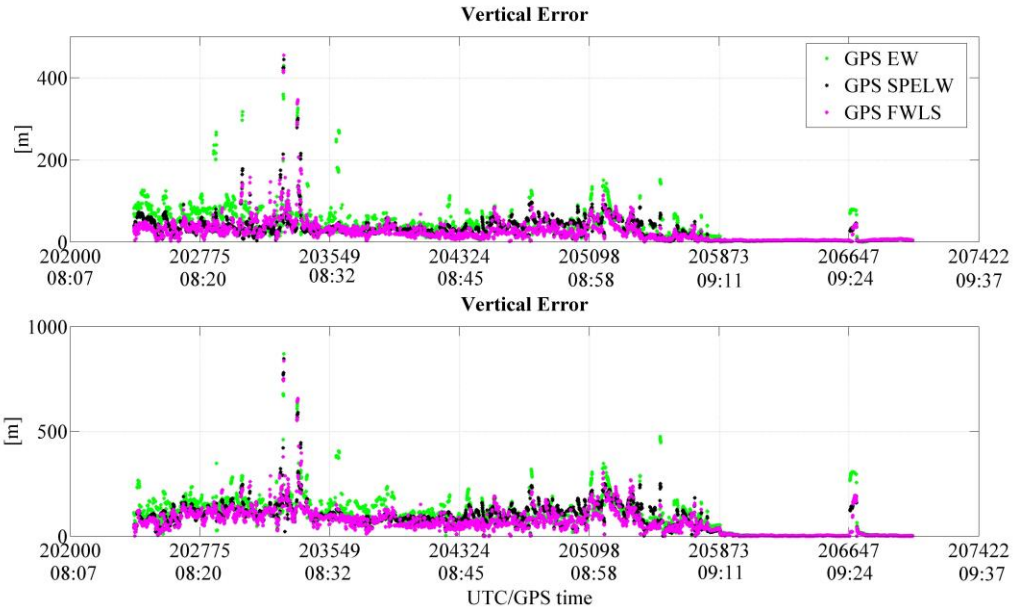

Figure 7.16 Horizontal and Vertical Errors as a function of time for all considered configurations: Fuzzy Logic (GPS FWLS), SPELW (GPS SPELW) and Equal Weights (GPS EW)

The qualitative analysis of the Figure 7.15 shows that the solution clouds relative to GPS SPELW and GPS FWLS configurations are more concentrated with respect to the GPS EW one, even if some sparse measurements are not well weighted, degrading the horizontal solution in the North-East direction.

From Figure 7.16, it can be noted that GPS FWLS provides the best behavior compared to the other configurations for horizontal and vertical components, except for some epochs with very large errors, confirming the statistical analysis shown in Table 7.6.

The effectiveness of fuzzy logic to weight GLONASS measurements is verified also in this statistic test and the assessment of the statistical parameters of the error analysis for the multi-constellation case (GG) is summarized in Table 7.7.

Table 7.7 Summury results for Horizontal (H) and Vertical (Up) component of the position obtained using GPS and GLONASS observables

	H Mean Error [m]	**Up Mean Error [m]**	**H RMS [m]**	**Up RMS [m]**	**H Max Error [m]**	**Up Max Error [m]**
GG EW	40.97	150.46	60.41	166.58	1958.27	2821.43
GG EL	32.30	125.12	49.29	148.85	1850.06	4001.03
GG SPW	34.75	121.26	43.77	129.84	177.04	323.52
GG SPELW	23.32	89.43	28.66	96.94	156.57	392.00
GG FWLS	15.75	59.70	21.07	71.28	105.11	294.55

The test is also characterized by very large errors without applying RAIM/FDE: this is due to large errors that influence GLONASS measurements, inherently noisier, compromising the accuracy of the navigation solution. In fact, using the Elevation dependent weighting method, the vertical maximum errors increase from circa 2.8 km for the basic configuration to around 4 km, therefore highlighting the presence of blunders.

However, the use of the other quality indicators for the computation of the weighting matrix in WLS improves the accuracy, as shown by Table 7.7. Analyzing the statistical parameters, it is evident that the SPW method, based on the SNR, provides better accuracy with respect to the weights as function of elevation angle (EL), in terms of all analyzed KPIs for horizontal and vertical components of the position, except for the horizontal mean error. However, GG SPELW and GG FWLS configurations outperform all the other ones, being able to combine both elevation angle and SNR. Precisely, FWLS provides the best performance in terms of all considered figures of merit for the horizontal and vertical components: horizontal mean error decreases from circa 23 meters for the SPELW configuration to circa 15 meters for FWLS, while vertical error decreases with circa 20 meters. Finally, the horizontal and vertical maximum errors decrease with circa 50 meters and 100 meters, respectively, using FWLS with respect to the SPELW method.

A more detailed performance evaluation is carried out in the follow figures, showing the results only for the best two methods (GG FWLS and GG SPELW) with respect to the basic configuration (GG EW). Figure 7.17 illustrates the horizontal position errors for the three configurations, while horizontal and vertical errors as function of time are plotted in Figure 7.18. Due to the presence of the largest errors of the GG EW configuration, Figure 7.19 shows additionally the horizontal and vertical errors only for GG FWLS and GG SPELW configurations only in order to have a clear representation. The same color convention as in the previous plots is used.

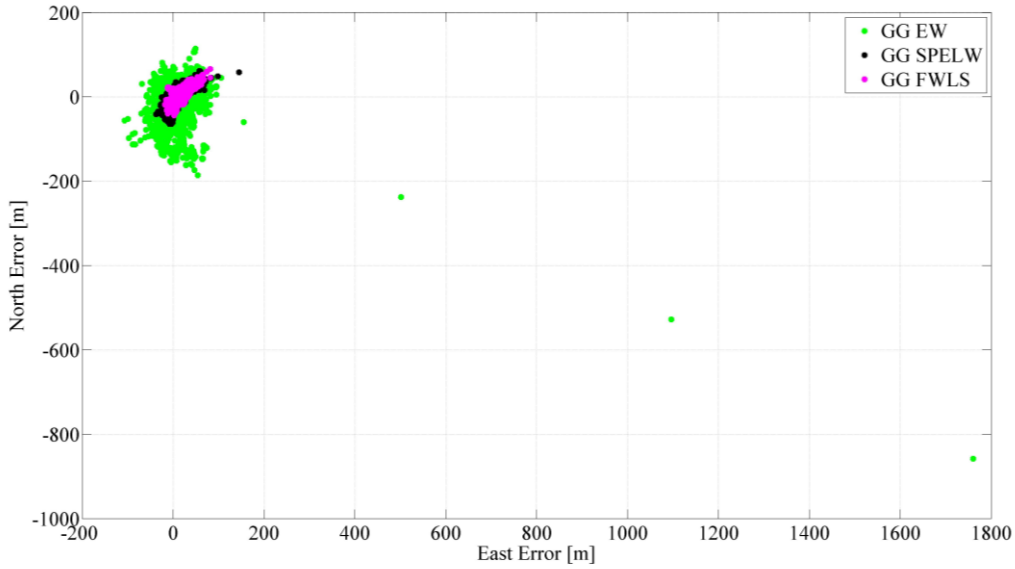

Figure 7.17 Horizontal position errors obtained using Equal Weigths, the SPELW method, and the Fuzzy Logic process for the GPS/GLONASS configuration

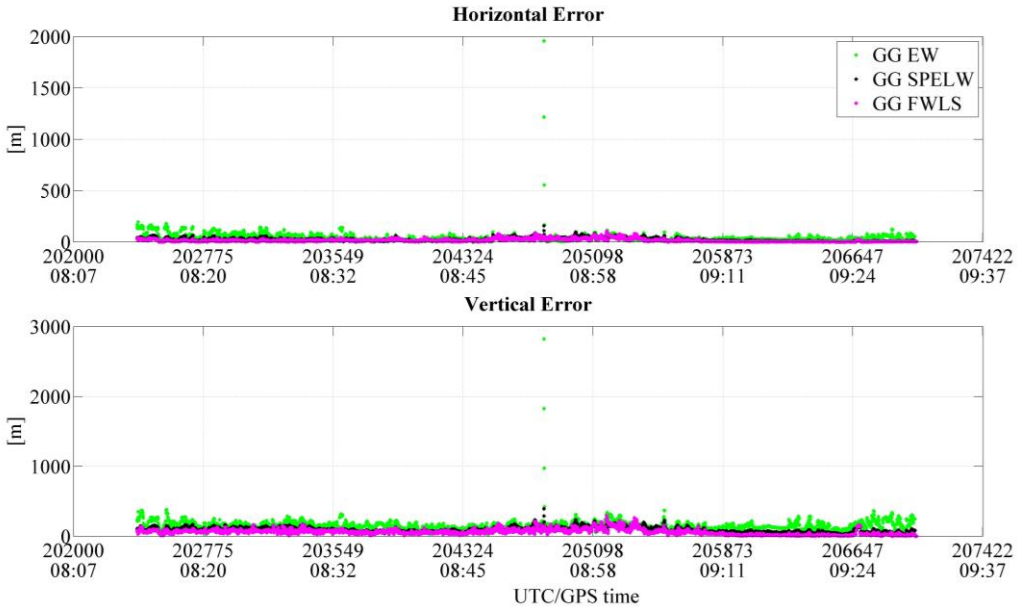

Figure 7.18 Horizontal and Vertical Errors as a function of time for Equal Weights, SPELW, and Fuzzy weights for the GPS/GLONASS configuration

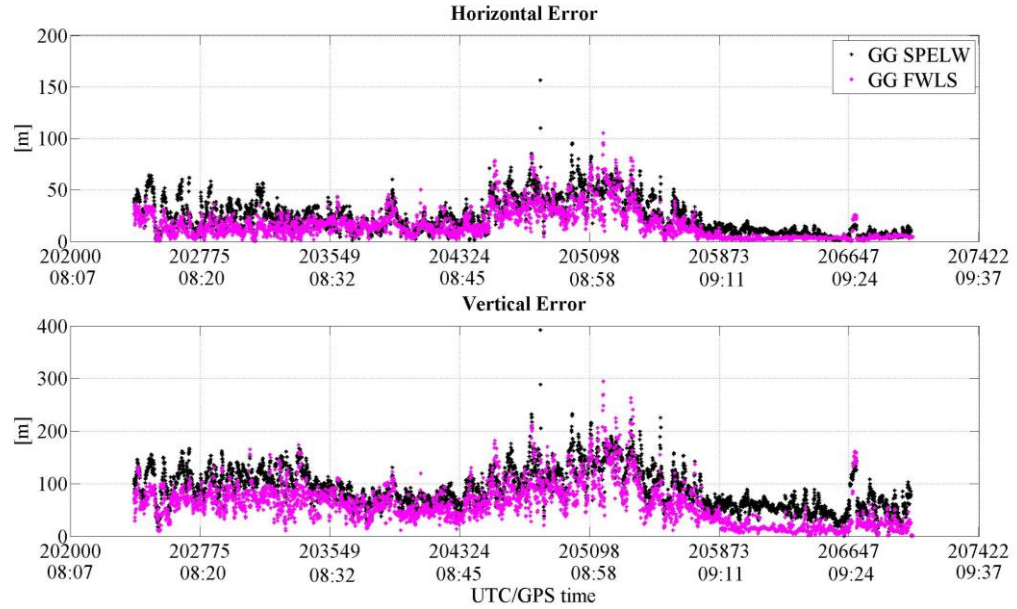

Figure 7.19 Details of Figure 7.18 showing horizontal and vertical errors as a function of time only for GG SPELW and GG FWLS configurations

The spread of the result clouds in Figure 7.17 provides an immediate representation of the magnitude of the error and allows a simple performance comparison between the configurations considered. From Figure 7.17 and Figure 7.18, it clearly emerges that the configuration without a quality control is characterized by large errors: the maximum horizontal error reaches almost 2 km and vertical maximum error exceeds 1.5 km. Moreover, in Figure 7.17 the clouds relative to the configurations obtained using the weighting schemes

integrating both quality indicators (elevation angle and SNR) are significantly reduced with respect to the baseline configuration, removing the presence of large errors for horizontal and vertical components (as confirmed in Figure 7.18). Furthermore, the magenta cloud is more concentrated and smaller than the other ones. This fact is confirmed by Figure 7.19 where the GG FWLS has better performance than the GG SPELW that has horizontal and vertical maximum errors of circa 157 meters and 392 meters, respectively - higher than those ones obtained using fuzzy logic. However, in some epochs the FWLS setup gives higher errors due to the presence of blunders that are difficult to be weighted since characterized by contrasting inputs similarly as in the configuration with GPS only.

These results are consistent with the ones obtained in the static test case 1, confirming the capability of the fuzzy logic to be an alternative approach for the computation of the weights assigned to both GPS and GLONASS measurements.

Due to the presence of the large errors that degrade the accuracy of the navigation solution, the application of the FDE is required. Therefore, the proposed weighting schemes having the best performance (SPELW and FWLS) are used in the Subset algorithm in order to verify the repeatability of the results obtained in the static test 1. The analysis is conducted for both GPS only and multi-constellation cases and only the reliable epochs are considered for the configurations using the Subset algorithm.

Firstly, the results for GPS only case are analyzed comparing with the basic configuration (without the application of the RAIM/FDE and assigning equal weights to the GPS measurements) with respect to the ones computed using the SPELW method (GPS Sub/SPELW) and the fuzzy system (GPS Sub/FWLS) in the Subset algorithm. The results are summarized in the Table 7.8 showing also the solution and reliability availability parameters for the analysis of RAIM/FDE performance improvements.

Table 7.8 Summury results for Horizontal (H) and Vertical (Up) component of the position obtained using only GPS and when applying the Subset algorithm

	H Mean Error [m]	**Up Mean Error [m]**	**H RMS [m]**	**Up RMS [m]**	**H Max Error [m]**	**Up Max Error [m]**	**S.A. [%]**	**R.A. [%]**
GPS EW	37.19	95.49	51.87	123.18	429.44	869.82	99.44	N.A.
GPS Sub/SPELW	18.46	45.78	29.95	79.06	149.96	423.53	N.A.	48.45
GPS Sub/FWLS	12.97	26.42	22.78	47.18	114.62	305.31	N.A.	41.89

For all the considered configurations with the application of the RAIM/FDE technique, the error decreases with respect to the “no RAIM” case, which is characterized by horizontal and vertical mean errors of 37.2 m and 95.5 m, respectively, and by horizontal and vertical RMS errors of 51.2 m and 123.2 m, respectively.

The horizontal and vertical mean errors obtained with the SPELW method in the Subset testing are, respectively, 18.5 m and 45.8 m with horizontal RMS of circa 30 m and vertical RMS of circa 79 m.

The mean horizontal and vertical absolute errors obtained with the GPS Sub/FWLS configuration are, respectively, equal to 13 m and 26 m with horizontal RMS of 22.8 m and vertical RMS of 47.2 m, providing the best performance among all the considered setups. This behavior is evident in Figure 7.20 representing the horizontal position errors for the three configurations: the magenta results cloud related to the application of fuzzy logic is the smallest. Furthermore, GPS Sub/FWLS and GPS Sub/SPELW configurations have similar clouds but the former has a lower number of spikes than the latter.

Looking the Figure 7.21 where horizontal and vertical errors are plotted during the observation time, it is possible to note that the basic configuration has the highest horizontal and vertical errors that, respectively, reach 429.44 m and 869.82 m. SPELW and FWLS configurations have similar behavior both on horizontal and vertical planes, with the horizontal and vertical maximum error of 149.96 m and 423.53 m for the former configuration, while they decrease of circa 35 m and 118 m, respectively, for the GPS Sub/FWLS configuration.

About the reliability availability, the SPELW method improves the performance of the Subset algorithm giving a higher value of 48.45% with respect to the 41.89% for the FWLS.

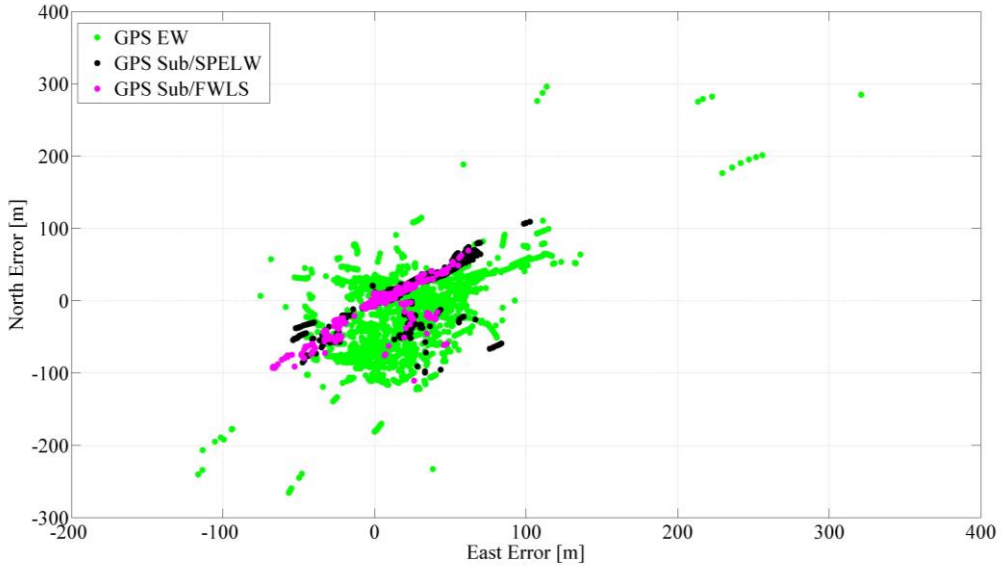

Figure 7.20 Horizontal position errors for the tree considered configurations: the basic one obtained assigning equal weights to GPS observations and without the use of Subset algorithm (GPS EW), the ones computed using the SPELW method (GPS Sub/SPELW) and the fuzzy system (GPS Sub/FWLS) in the Subset algorithm

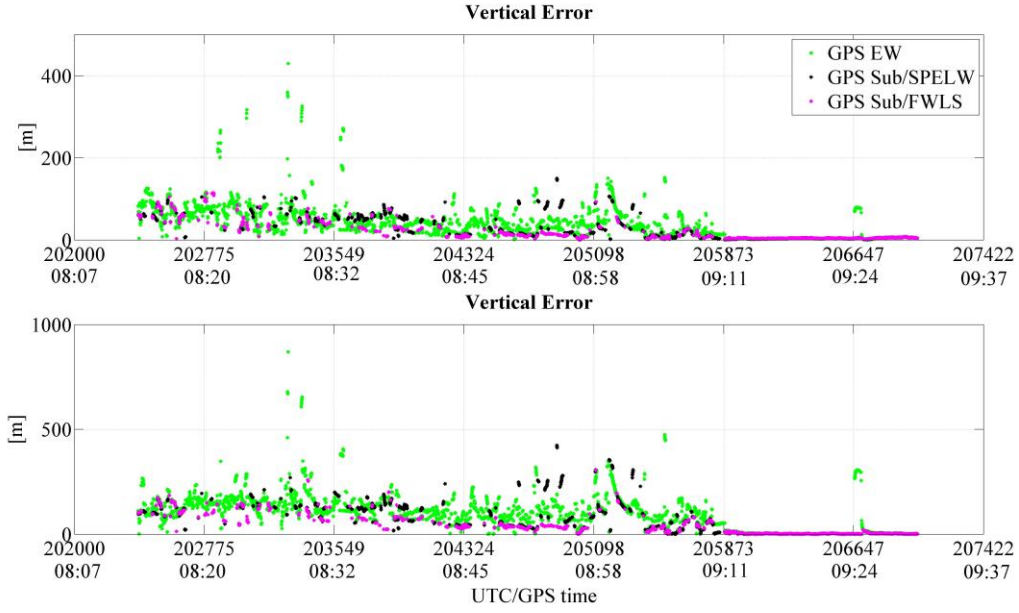

Figure 7.21 Horizontal and vertical errors as function of the time: comparison between the baseline (GPS EW), and the configurations obtained applying the Subset algorithm using the SPELW method (GPS Sub/SPELW) and fuzzy weights (GPS Sub/FWLS)

For the multi-constellation case, Table 7.9 summarizes the statistical parameters for accuracy and reliability analysis, provided by the use of the Subset algorithm joint with the two

weighting schemes. The error analysis is carried out only at reliable epochs for the two configurations using the Subset method.

Table 7.9 Summary results for Horizontal (H) and Vertical (Up) component of the position obtained for multi-constellation case (GPS/GLONASS) and applying Subset algorithm

	H Mean Error [m]	**Up Mean Error [m]**	**H RMS [m]**	**Up RMS [m]**	**H Max Error [m]**	**Up Max Error [m]**	**S.A. [%]**	**R.A. [%]**
GG EW	40.97	150.46	60.41	166.58	1958.27	2821.43	99.72	N.A.
GG Sub/SPELW	16.61	42.74	27.47	70.69	154.97	309.96	N.A.	53.87
GG Sub/FWLS	15.22	40.62	24.62	65.09	137.79	295.29	N.A.	56.17

The test session is characterized by high solution availability and the inclusion of GLONASS observables provides only a slight improvement in terms of solution availability, which is improved by 0.3 % with respect to the GPS only configuration. The use of the FLWS in the Subset algorithm guarantees a higher reliability availability (56.2 %) with respect the GG Sub/SPELW configuration (53.9%).

Since there are large errors influencing the GLONASS measurements, the horizontal and vertical maximum errors exceeding 1.5 km are evident for the basic configuration and they are reduced using the Subset algorithm providing an accurate navigation solution for both the analyzed configurations. In detail, the mean horizontal and vertical errors obtained with the SPELW method in the Subset testing are, respectively, 16.7 m and 42.7 m with horizontal RMS of 27.5 m and vertical RMS of 70.7 m. Instead, the GG Sub/FWLS configuration has the best performance for all the figures of merit. In fact, the mean horizontal and vertical errors obtained using the FWLS setup are, respectively, equal to 15.2 m and 40.6 m with horizontal RMS of 24.6 m and vertical RMS of 65.1 m.

The performance of the configurations with RAIM/FDE is compared to the baseline, using the classical representation for the horizontal component as in the previous analysis, i.e. East and North errors in order to have a clear amplitude of the clouds as shown in Figure 7.22. The same color convention is also used in these plots. For the configuration with RAIM functionality, only reliable epochs are considered.

Figure 7.22 shows that the result clouds relative to the configurations using RAIM are significantly reduced with respect to the baseline. Therefore, the use of fuzzy logic in the

computation of the W matrix, used for the computation of the Subset statistic variable as well, provides the best performance. In fact, the magenta result cloud is the smallest and is more concentrated near to the origin of the plot (reference truth). Because of the highest errors characterizing the basic configuration, in order to have a fair comparison, in Figure 7.23, the horizontal and vertical errors are plotted only for the two configurations with the application of the Subset method. The configurations obtained using SPELW and FWLS methods have similar behavior during the data collection both on horizontal and vertical channel. However, FWLS is able to provide a more accurate position solution with lower maximum errors. Indeed, horizontal and vertical maximum error of 154.97 m and 309.96 m for GG Sub/SPELW configuration, while they are 137.79 m and 295.29 m, respectively, for the GG Sub/FWLS.

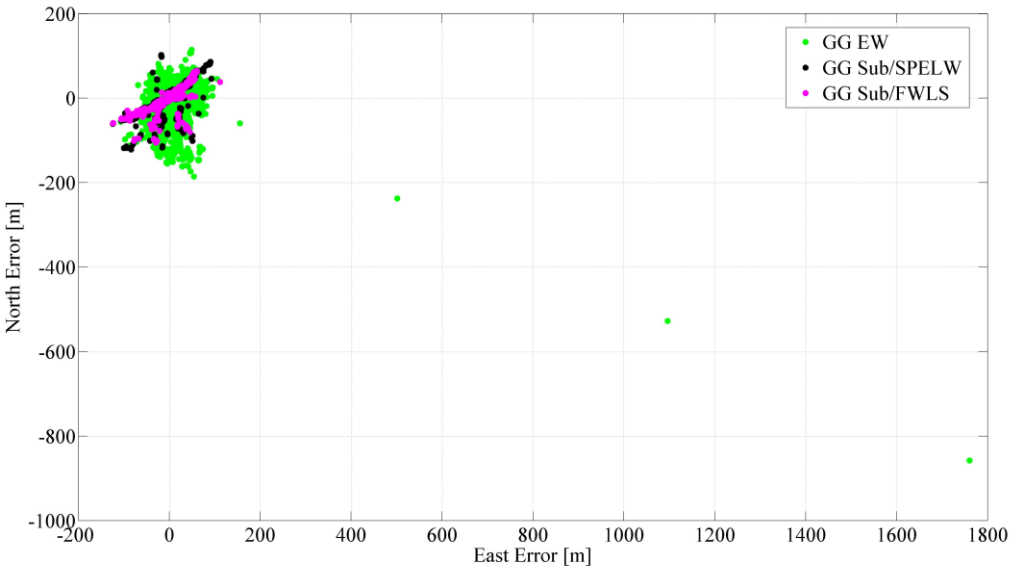

Figure 7.22 Horizontal position errors obtained using Equal Weigths (without RAIM), the SPELW method, and the Fuzzy Logic process for the GPS/GLONASS configuration and applying the Subset algorithm

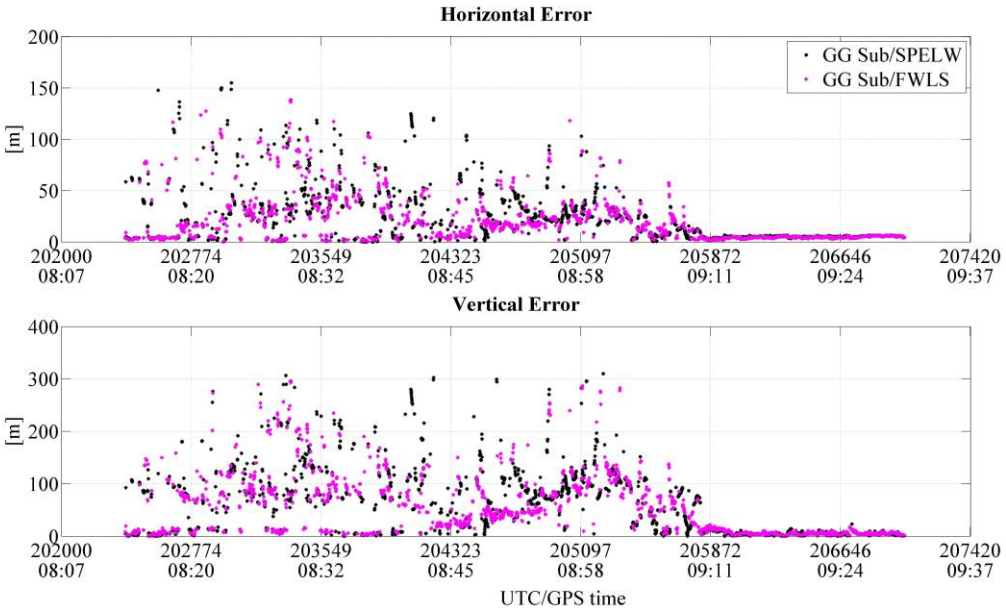

Figure 7.23 Horizontal and vertical position errors obtained using the SPELW method and the Fuzzy Logic process for the GPS/GLONASS configuration and applying the Subset algorithm

7.2. Vehicular Test

In this paragraph, the vehicular test is described. The data collection was carried out in a vehicle in downtown Helsinki (Finland) on 23rd of February 2016 in the morning (around 11:23 am local time). The scenario is characterized by the presence of medium high buildings along the entire trajectory that can block GNSS signals or cause multipath errors during the session, so the operational environment may be considered as a lightly degraded signal scenario. The route was travelled in circa 55 minutes and the trajectory is shown in Figure 7.24.

Figure 7.24 Vehicular Test Trajectory

The receiver used is a u-blox M8 that is a multi-GNSS receiver capable of receiving and processing signals from multiple GNSSs. During the data collection, the receiver was connected to a patch antenna.

In order to perform the error analysis, a reference solution is achieved using a high-grade inertial unit combined with a professional GNSS receiver from NovAtel Inc. (specifically a tactical grade INS) and post-processing procedures via the Inertial Explorer software. In particular, the device used for the reference solution computation is the NovAtel SPAN (Synchronous Position, Attitude and Navigation) system. NovAtel's SPAN tightly couples precision GPS receiver with robust Inertial Measurement Units (IMUs) in order to obtain reliable, continuously available measurements including position, velocity and attitude even though there are short periods of time when no GPS satellites are available. Data from the SPAN were post-processed with the NovAtel Inertial Explorer software using the tightly coupled strategy and the double difference technique; so the reference trajectory has centimeter level accuracy.
All the devices are placed in the car as shown in the Figure 7.25.

Figure 7.25 Vehicular Test Equipment

7.2.1. Vehicular Test Results

In this section, the results of the GNSS positioning are presented and the error analysis in position domain is shown. A SPP is obtained using the pseudorange measurements epoch-by-epoch and computing the weights used in the WLS estimation through the methods described in Sections 3.3 and 6.5. Then, the Subset algorithm is applied to remove the possible blunders and improve the accuracy of the navigation solution. Several configurations are compared and analyzed as described at the beginning of this chapter.
The number of visible GPS and GPS/GLONASS satellites are shown in Figure 7.26, while the corresponding PDOP values are plotted in Figure 7.27. Partial and total GNSS outages, where the solution cannot be computed, characterize the test (e.g. around 10:13 or 10:23

am). These outages are caused by the presence of tunnels during the route. At the beginning, the number of visible satellites is large and the PDOP value low as the receiver is in an open area (the test started in a parking lot for the initialization of the SPAN). Going inside the downtown area, the number of visible satellites decreases, varying between 10 and 0 for GPS and between 0 and 9 for GLONASS; the PDOP values increase noticeably, reaching peaks of 28 for GPS only case and 27 for the GPS/GLONASS combination. These high values of PDOP correspond to the poor geometries immediately after the outages. However, including the GLONASS satellites yields great benefits in both visibility and geometry, in fact the total number of GNSS available satellite varies from 0 to 19 with an average of circa 14 and the values of PDOP are lower than for the GPS only case.

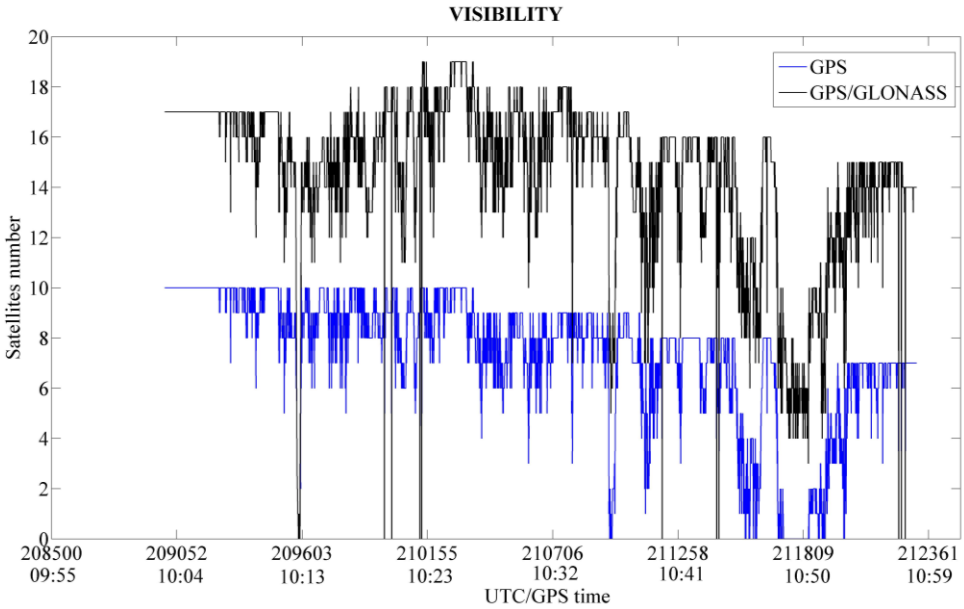

Figure 7.26 Number of available GNSS satellites during the vehicular test carried out on 15th of September 2016

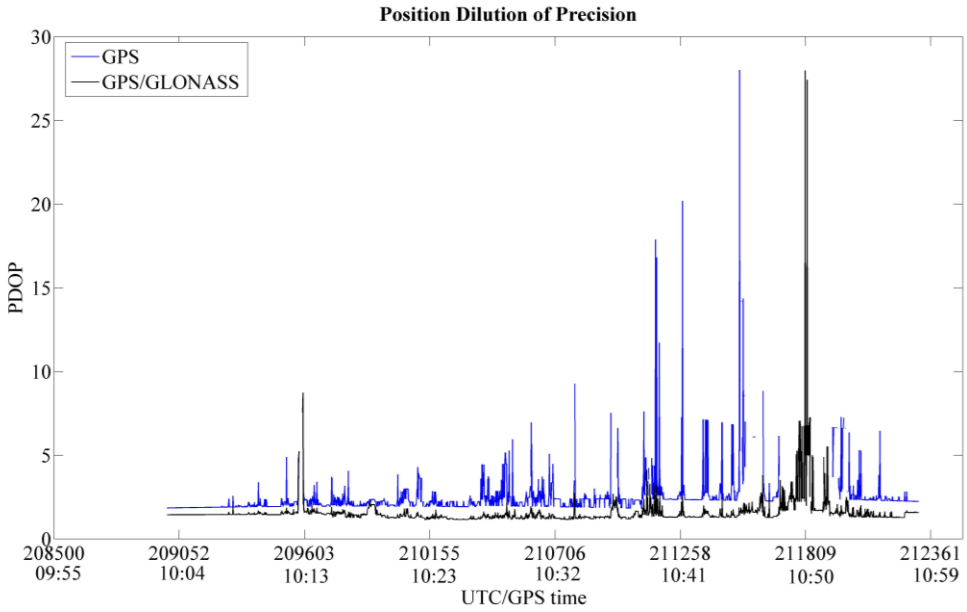

Figure 7.27 PDOP values computed epoch-by-epoch for the vehicular test carried out on 15th of September 2016

The Table 7.10 summarizes the comparison between the considered configurations providing the error statistics for horizontal (H) and vertical (Up) components of position, computed using only GPS observables.

Table 7.10 Summary Results for Horizontal (H) and Vertical (Up) component of the position obtained using only GPS constellation

	H Mean Error [m]	**Up Mean Error [m]**	**H RMS [m]**	**Up RMS [m]**	**H Max Error [m]**	**Up Max Error [m]**
GPS EW	11.11	17.69	19.05	36.53	151.40	294.30
GPS EL	8.71	11.85	14.47	23.45	93.71	155.34
GPS SPW	8.13	11.25	13.70	23.41	93.71	155.61
GPS SPELW	7.20	9.03	12.00	18.67	93.71	125.30
GPS FWLS	5.75	6.30	10.23	15.19	93.71	125.48

From the table, it can be highlighted that the SPW method, based on the SNR parameter, provides a slightly better accuracy with respect to the EL one, in terms of all analyzed KPIs for horizontal and vertical position components. However, SPELW and Fuzzy Weights (FWLS) outperform all the other ones. In particular, FWLS provides the best performance in terms of all considered figures of merit (except for vertical maximum error): horizontal RMS decreases from circa 12 meters for the GPS SPELW configuration to circa 10.2 meters for the GPS FWLS, while vertical RMS drops by circa 3.5 meters. The use of fuzzy logic

reduces the horizontal and vertical mean errors of circa 1.4 meters and 2.7 meters, respectively, with respect to the GPS SPELW configuration. Moreover, all the weighted configurations show better behavior with respect to the basic configuration for all the analyzed KPIs. This is due to the presence of the blunders or the poor geometries influencing the navigation solution accuracy that can be improved by adopting a proper weighting scheme.

The qualitative analysis is performed comparing the two best methods to the baseline one. In Figure 7.28 the green points are relative to the horizontal position obtained assigning equal weights to all GPS observables, the magenta ones to the FWLS and the black ones to SPELW method. The red markers are relative to the coordinates of the reference, obtained using the SPAN. Horizontal and vertical position errors, computed with respect to the reference solution, are plotted as a function of time in Figure 7.29. The color convention is the same as in the previous plots.

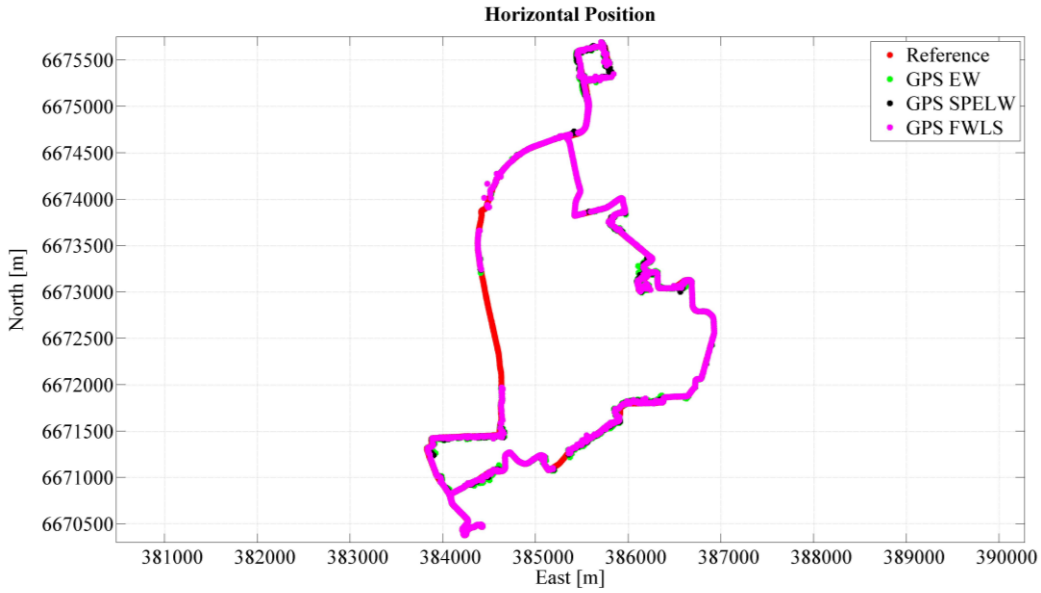

Figure 7.28 Horizontal Positions obtained using Equal Weigths, the SPELW method, and the Fuzzy Logic for the GPS configuration

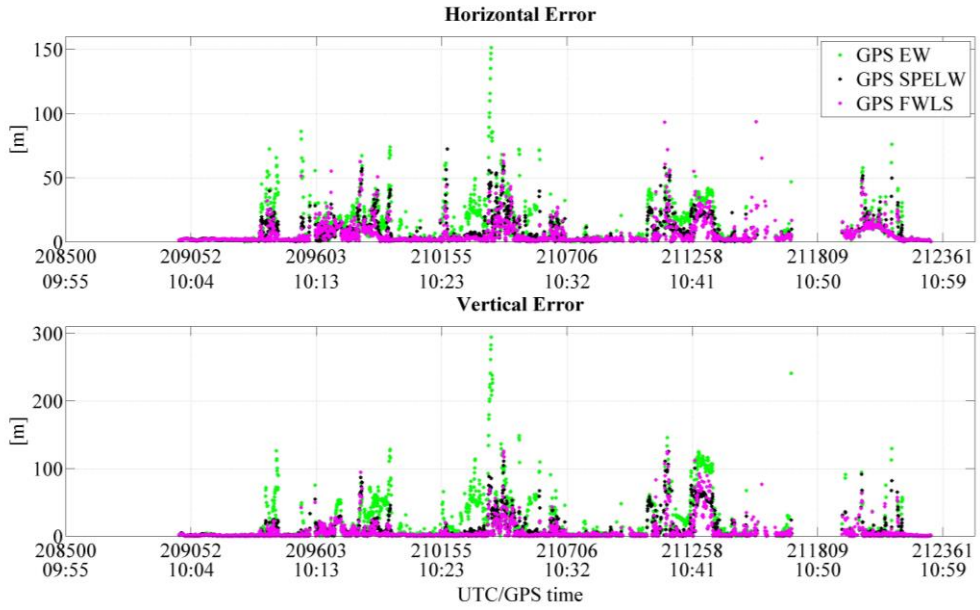

Figure 7.29 Horizontal and Vertical Errors as a function of time for Equal Weights, the SPELW, and Fuzzy weights for the GPS configuration

Figure 7.28 shows that FWLS has the best performance, however, both the trajectories relative to SPELW and FWLS are coinciding with the red reference route, even if the two configurations are characterized by higher errors usually placed after total outages. However, GPS EW is characterized by the highest errors since it gives equal weights to all the measurements, including the blunders, therefore degrading the solution accuracy. The Figure 7.29 also confirms this behavior: GPS EW configuration has the highest horizontal and vertical errors that are 151.4 m and 294.3 m, respectively. At the beginning of the test, GPS FWLS and GPS SPELW configurations have similar performance, then during the test, FWLS has a better behavior with respect to the SPELW on horizontal and vertical domains, and only at circa 10:41 an improvement, provided by the GPS SPELW, is evident. GPS FWLS and GPS SPELW configurations have the same values of horizontal maximum error (equal to 93.7 m) while there is a difference of 0.2 m for the vertical maximum error.

The same error analysis is carried out for the multi-constellation configuration (indicated as GG), using combined pseudoranges ranging from GPS and GLONASS constellations, and the results are shown in the Table 7.11.

Table 7.11 Summary Results for Horizontal (H) and Vertical (Up) components of the position obtained for multi-constellation case

	H Mean Error [m]	**Up Mean Error [m]**	**H RMS [m]**	**Up RMS [m]**	**H Max Error [m]**	**Up Max Error [m]**
GG EW	12.38	21.58	27.24	37.30	1042.30	737.64
GG EL	9.94	17.48	31.45	28.00	1532.26	359.17
GG SPW	9.09	14.23	16.50	24.33	384.82	265.33
GG SPELW	7.91	13.10	13.46	21.52	199.38	223.73
GG FWLS	5.67	7.01	9.76	14.25	202.27	204.73

In the multi-constellation case, the weights computed using the SPW method offer a better accuracy with respect to the GG EL configuration, in terms of all analyzed figures of merit, except for the vertical maximum error. GG EL and the basic configurations are characterized by the highest errors: in particular, on the horizontal plane a maximum error of circa 1.5 km is obtained for GG El configuration and of circa 1.0 km for the baseline. However, GG FWLS shows the best behavior with an enhancement in the meter order for horizontal and vertical mean and RMS errors, except for the horizontal maximum error, where a slight improvement in the meter order is obtained using the SPELW method.

A further analysis is carried out, comparing only FWLS and SPELW methods. Figure 7.30 shows the horizontal positions for the two configurations with respect to the basic configuration and the reference solution, while horizontal and vertical errors as function of time are plotted in Figure 7.31 (the horizontal maximum error influencing the baseline configuration is not shown in the figures for clarity). The same color convention as in the previous plots is used.

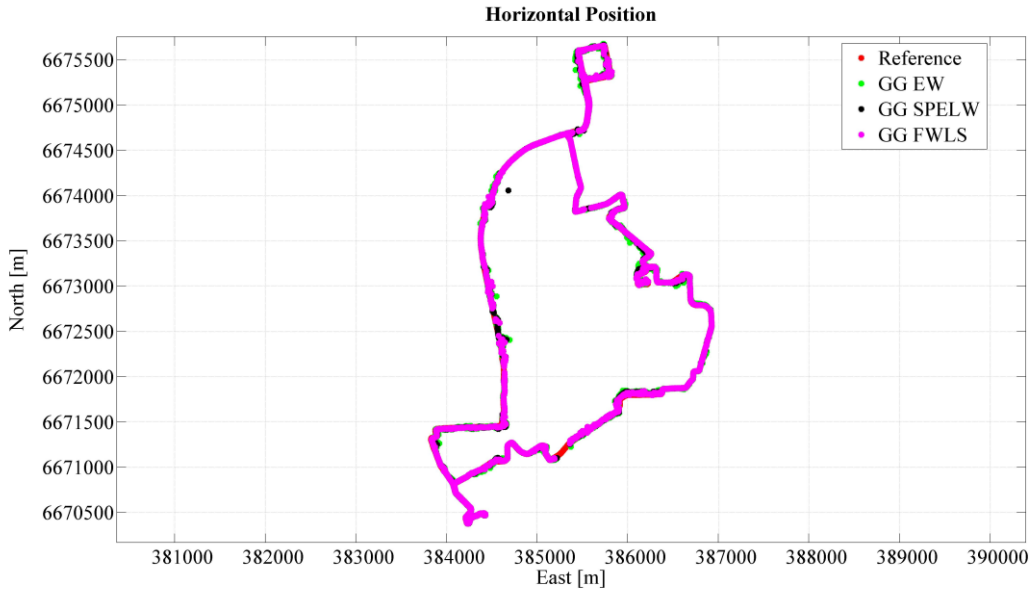

Figure 7.30 Horizontal positions obtained using Equal Weigths, the SPELW method, and the Fuzzy Logic process for the GPS/GLONASS configuration

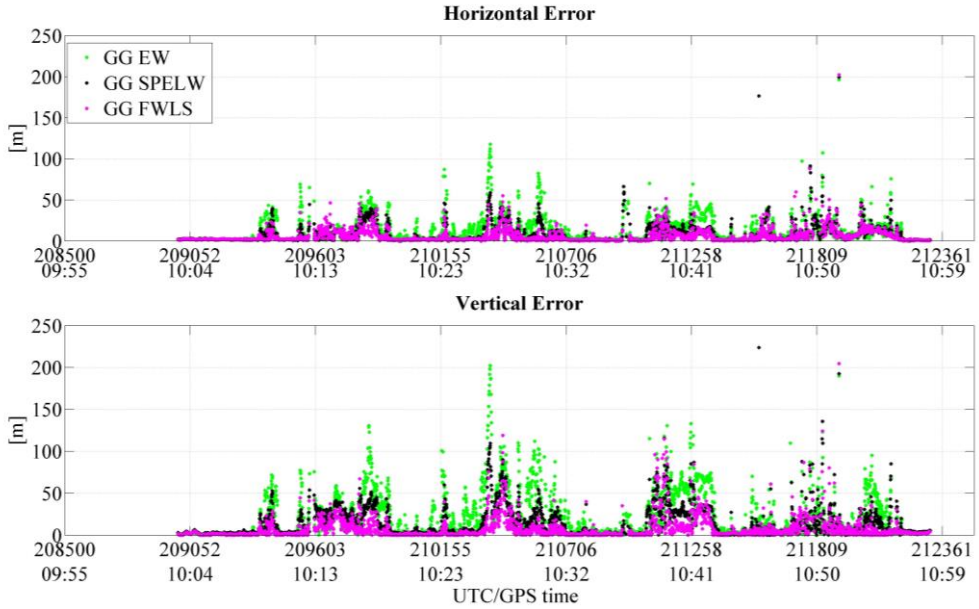

Figure 7.31 Horizontal and vertical errors of position obtained using Equal Weigths, the SPELW method, and the Fuzzy Logic process for the GPS/GLONASS configuration

The best performance is provided by the GG FWLS configuration that is almost coincident with the true path, while black (GG SPELW) and green (GG EW) points are sometimes far from the reference. This is also evident in Figure 7.31, where FWLS has the best behavior in the vertical domain except around 10:27 and at the end of the vehicular test where it has the highest value both for horizontal and vertical domains. These values are obtained after

the outages or when the number of available satellites is very low, as it can be noted comparing it to the Figure 7.26. Furthermore, as shown in Figure 7.29, on horizontal and vertical channels, FWLS and SPELW configurations have similar performance at the beginning of the test when the car is in an open-sky area, then during the test FWLS has a better behavior relative to the other configurations.

Also during this vehicular data collection, there are blunders that degrade the accuracy of the navigation solution, even if the scenario is lightly degraded; so the application of the FDE is necessary.

To verify the repeatability of the results obtained in the static tests and to investigate the performance of the FWLS also in a kinematic test, the weighting schemes with the best performance (SPELW and FWLS) are used in the Subset algorithm. The analysis is performed for both GPS only and multi-constellation cases and only the reliable epochs, according to the Subset algorithm, are taken into account.

Table 7.12 shows the results for GPS only case comparing the basic configuration with respect to GPS Sub/SPELW and GPS Sub/FWLS configurations. Furthermore, in the table the solution and reliability availability parameters are also presented for the analysis of the RAIM performance.

Table 7.12 Summury results for Horizontal (H) and Vertical (Up) component of the position obtained using only GPS and applying the Subset algorithm for the kinematic test

	H Mean Error [m]	**Up Mean Error [m]**	**H RMS [m]**	**Up RMS [m]**	**H Max Error [m]**	**Up Max Error [m]**	**S.A. [%]**	**R.A. [%]**
GPS EW	11.11	17.69	19.05	36.53	151.40	294.30	86.71	N.A.
GPS Sub/SPELW	3.91	4.34	6.68	10.90	50.60	100.45	N.A.	55.53
GPS Sub/FWLS	3.03	2.70	5.34	6.72	56.39	111.87	N.A.	56.44

The Table 7.12 shows the enhancement obtained using the Subset algorithm compared to the case without the application of any RAIM. In fact, all the statistical parameters are reduced by several meters order for both vertical and horizontal components. Also for the vehicular test, the best configuration is the one obtained using the fuzzy system to weight the PR measurements in the WLS estimation and to compute the test statistic of the Subset algorithm. An improvement of decimeter order can be noted for the horizontal RMS and

mean error using the FWLS with respect to SPELW method, while the vertical RMS and mean error decreases by 4.2 m and of 1.6 m. Furthermore, the FWLS also provides a better performance in terms of reliability availability (56.4%) with respect to the GPS Sub/SPELW (55.5%).

These results are confirmed by the next two figures. In Figure 7.32 the green points are relative to the horizontal position solutions, obtained assigning equal weights to all GPS PR without the application of the RAIM algorithm, the black ones to GPS Sub/SPELW and the magenta ones to the GPS Sub/FWLS configurations. The horizontal and vertical errors as function of the time for the three considered configurations are shown in Figure 7.33 using the same color convention. The qualitative analysis show that GPS Sub/FWLS and GPS Sub/SPELW configurations have mainly the same behavior on the horizontal plane: in fact, they are coinciding with the reference solution trajectory. However, in some epochs the enhancement provided by FWLS is evident principally on the vertical plane. This is shown in Figure 7.33 where the GPS Sub/SPELW configuration has higher error than the FWLS around 10:27 and 10:41 am.

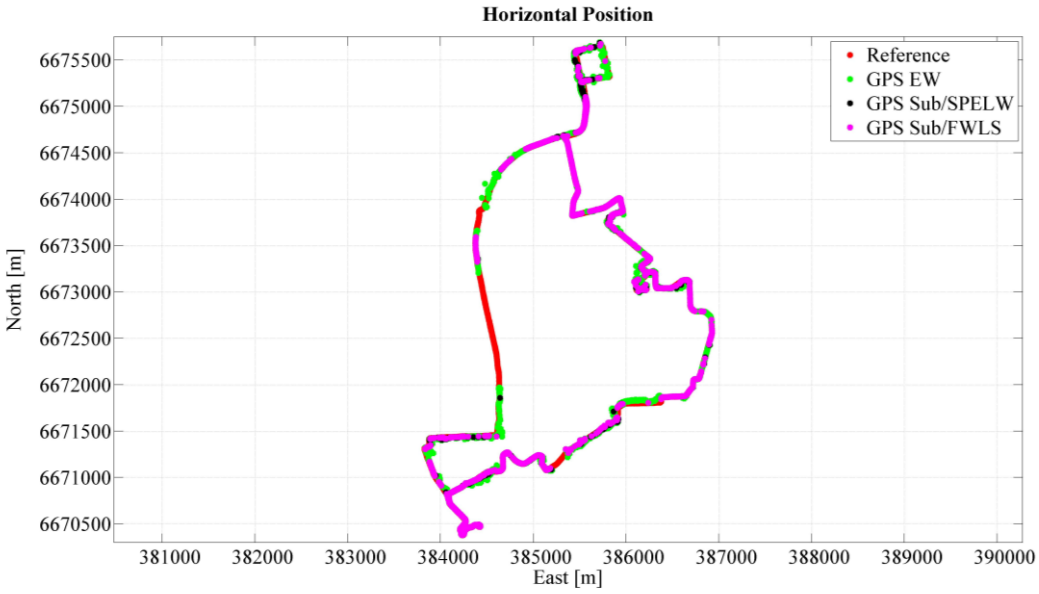

Figure 7.32 Horizontal position solutions for the tree considered configurations: the basic obtained assigning equal weights to GPS observations and without the use of Subset algorithm (GPS EW), and the solutions computed using the SPELW method (GPS Sub/SPELW) and the fuzzy system (GPS Sub/FWLS) in the Subset algorithm - for the configurations obtained using the RAIM, only reliable epochs are considered

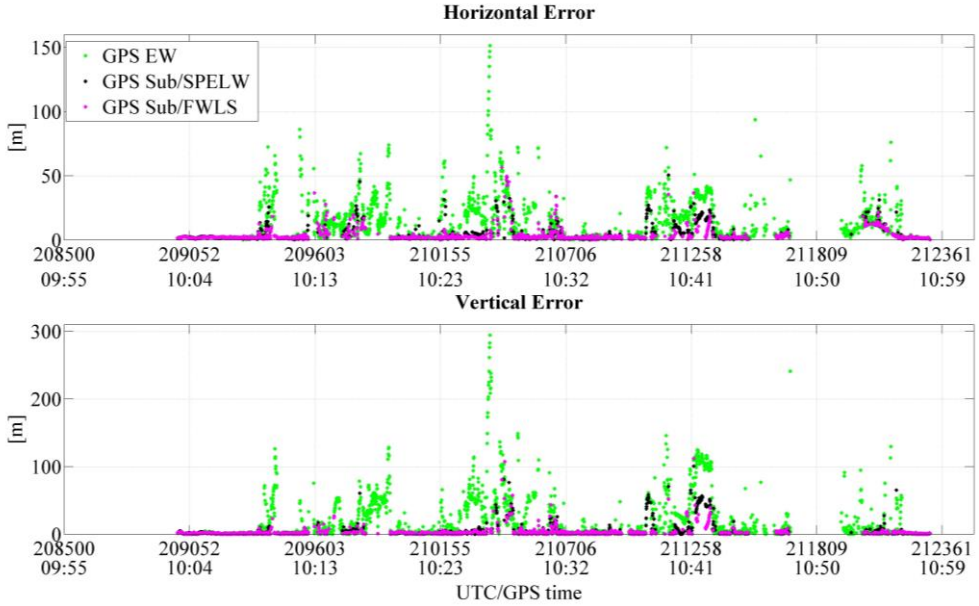

Figure 7.33 Horizontal and vertical errors during the vehicular test: comparison between the baseline (GPS EW), the configurations obtained applying the Subset algorithm using the SPELW method (GPS Sub/SPELW) and fuzzy weights (GPS Sub/FWLS)

For the multi-constellation case, Table 7.13 summarizes the statistical parameters for the accuracy and reliability analysis.

Table 7.13 Statistical paramenter of error analysys for Horizontal (H) and Vertical (Up) component of the position obtained using the multi-constellation (GPS/GLONASS) approach and applying the Subset algorithm

	H Mean Error [m]	**Up Mean Error [m]**	**H RMS [m]**	**Up RMS [m]**	**H Max Error [m]**	**Up Max Error [m]**	**S.A. [%]**	**R.A. [%]**
GG EW	12.38	21.58	27.24	37.30	1042.30	737.64	97.89	N.A.
GG Sub/SPELW	4.87	7.32	8.48	13.93	54.00	171.19	N.A.	76.80
GG Sub/FWLS	3.86	4.48	6.78	12.41	56.76	161.04	N.A.	75.83

Also for this case, the RAIM/FDE algorithm enhances the accuracy of the navigation solution, reducing considerably all the performance indicators. In the table, the configuration that provides the best performance is the GG Sub/FWLS: an enhancement of few meters is

evident for horizontal and vertical mean error and RMS using the FWLS respect to SPELW method. In fact, vertical mean error increases from around 4.5 m for GG Sub/FWLS configuration to 7.3 m for the GG Sub/SPELW, while a decrease of around 1.5 meter for vertical and horizontal RMS is obtained using the fuzzy logic. Furthermore, the use of SPELW method in the computation of the W matrix slightly increases the reliability availability (of about 2%).

The investigation of the performance of the three considered configurations is carried in the Figure 7.34 and the Figure 7.35. The green points are relative to the horizontal and vertical position errors, obtained assigning equal weights to all GNSS PR without the application of the RAIM algorithm, the magenta and the black ones to, respectively, GG Sub/FWLS and GG Sub/SPELW configurations (for the configurations using the Subset algorithm, only the reliable epochs are considered).

The performance of the two weighting methods in the horizontal and vertical domains are compared with the baseline configuration. The use of RAIM/FDE algorithm and fuzzy logic in the W matrix improves the performance with respect to the other configurations. On the horizontal domain, magenta and black routes have similar performance during the test; however GG Sub/FWLS configuration shows a better agreement with the reference solution with respect to the other considered configurations, confirming the results obtained in the previous cases.

The vertical and horizontal errors for the two configurations with different W matrices (Figure 7.35) are lower than the basic configuration with an improvement for the GG Sub/FWLS. The same behavior of FWLS obtained for the GPS only case (shown in Figure 7.33) can also be noted for the multi-constellation situation. These results confirm the enhancement obtained with the fuzzy system, which represents a valid approach to modify the stochastic model of both GPS and GLONASS observations and improve the efficiency of the RAIM/FDE algorithm.

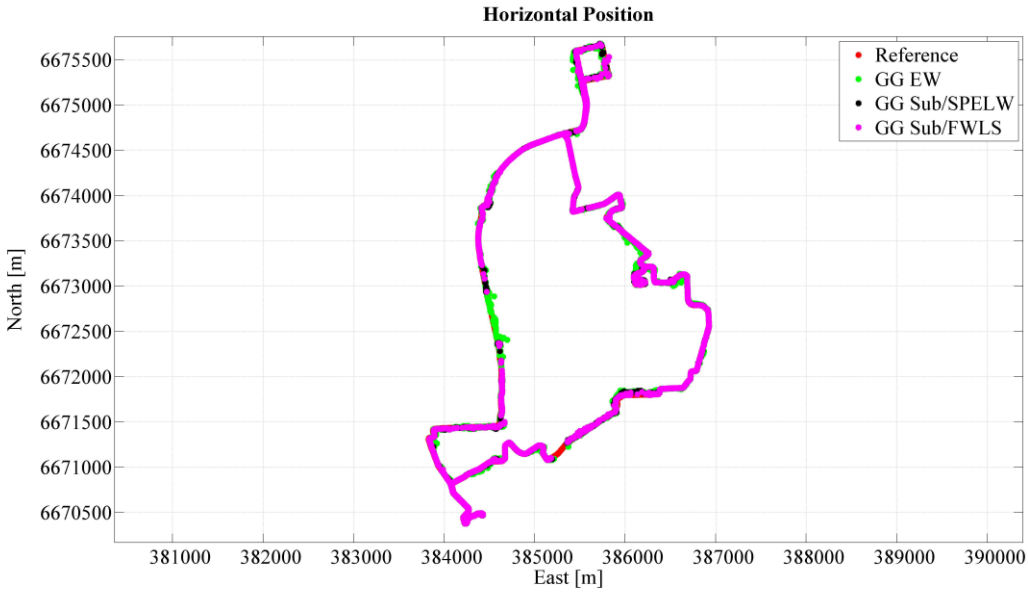

Figure 7.34 Horizontal position solutions for the tree considered multi-GNSS configurations: the basic approach obtained assigning equal weights to GNSS observations and without the use of Subset algorithm (GG EW), and the ones computed using the SPELW method (GG Sub/SPELW) and the fuzzy system (GG Sub/FWLS) in the Subset algorithm. For the configurations obtained using the RAIM, only reliable epochs are considered

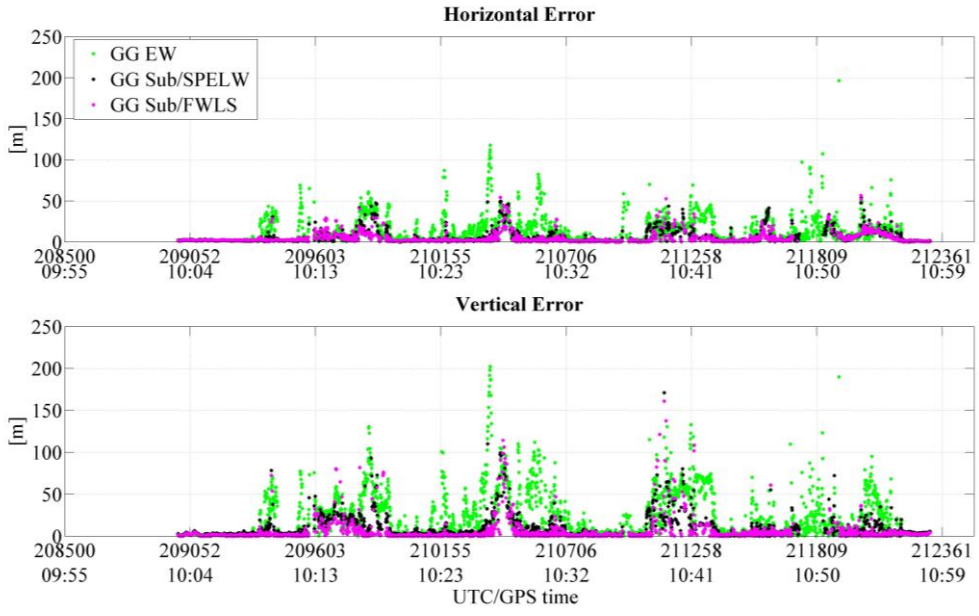

Figure 7.35 Horizontal and vertical positioning errors for the considered multi-GNSS configurations: the basic approachobtained assigning equal weights to GNSS observations and without the use of Subset algorithm (GG EW), and the ones computed using the SPELW method (GG Sub/SPELW) and the fuzzy system (GG Sub/FWLS) in the Subset algorithm. For the configurations obtained using the RAIM, only reliable epochs are considered

8. Conclusions

In signal-degraded environments, such as in urban canyons, city centers or mountains area, GNSS navigation faces critical performance challenges due to the presence of gross errors compromising the solution computation and reliability. The satellite navigation carried out in this operational environment has attracted significant interest in the last years, mainly in view of LBS developed for urban applications. In these scenarios, the gross errors strongly affect the measurements, decreasing the accuracy of the navigation solution and therefore integrity monitoring becomes an important task for the applications conducted in these situations. In this thesis, different types of signal environments potentially encountered by a typical road user were analyzed.

Several methods can be used to reduce the undesired effects introduced from the urban environment and to enhance the accuracy of the navigation solution.

Due to the recent improvements of the existing GNSSs, such as GPS and GLONASS, and the rapid development of new GNSSs, such as Galileo and BeiDou, multiple constellations are available to enhance navigation performance and safety. With the growing number of satellite constellations, the task of the GNSS navigation is to deal with the differences among systems but, on the other hand, higher levels of integrity and satellite visibility can be expected. In this dissertation, the multi-constellation benefits are analyzed, considering the GPS/GLONASS multi-constellation solution.

Furthermore, reliability and quality monitoring cannot always be applied in urban canyon scenarios due to the lower redundancy but when the number of available measurements is high, the RAIM algorithm can be used for fault detection and exclusion, enhancing the performance of the PVT algorithm in terms of navigation reliability, accuracy and integrity. This thesis studied the RAIM/FDE algorithm used in urban scenarios and is focused on the possibility to improve the performance of the quality improvement technique. Firstly, reliability theory, in terms of reliability testing and statistical reliability conditions of a navigation system, was discussed. Since the classical RAIM algorithms were developed mainly for the safety-critical aviation applications, they have to be modified in order to spread their use for urban applications potentially affected by multiple measurement errors. In these RAIM techniques, measurement errors are assumed normally distributed, but this assumption is not true in degraded signal environments. Indeed, if only a single blunder influences the measurements set, fault identification methods work properly while if there are two or more outliers in the measurements set, it is more difficult to detect them. In order

to improve the performance of classic RAIM to work properly when multiple outliers occurs or when they are difficult to detect due to their small magnitude, alternative approaches should be used. In fact, as previously described, in such situations, the exclusion of observations affected by signal distortion aids to reduce the effect of the bias, but it can compromise the strength of the solution. If the effect of the blunder is not so influential, it is better to reduce only the degree of its impact on the navigation solution. Weighting GNSS observations, through a suitable quality measure for each signal, represents a possible way to moderate the effect of the large errors.

In this research, in order to identify or mitigate unmodelled signal distortion effects, and improve the performance of the considered FDE methods, a quality assessment procedure was introduced. In detail, an alternative methodology, using fuzzy logic to set the measurements weighting matrix in Weighted Least Squares (WLS) estimation, has been proposed to improve the positioning accuracy with GNSS-based measurements. A purposely designed fuzzy controller allows computing the weights to be assigned to PR measurements, integrating in an implicitly nonlinear fashion two indicators of the signal quality: elevation angle and SNR. This fuzzy quality index was also used in the computation of the test statistic used in the FDE (Subset Observation Testing) algorithm.

To test the method, two data collections in static mode and a vehicular test were gathered in a typical signal-degraded situation. They have been processed using the Single Point Positioning (SPP) algorithm and the WLS estimation strategy, where several methods to compute the weighting coefficients have been compared: function of elevation angle ($1/\sin^2(el)$), SNR (indicated as SPW methods), a suitable combination of these two parameters (defined as SPELW method) and the proposed Fuzzy Weighting (FWLS). After these comparisons, the Subset algorithm is applied in order to remove the blunders in the measurements set as an RAIM/FDE approach and to analyze its performance thanks to the different weighting schemes. Furthermore, the performance of multi-constellation GPS/GLONASS and stand-alone GPS, using real life data collected through several tests in urban environments, were evaluated applying the considered weighting strategies in the WLS estimation and in the FDE algorithm. Additionally, pros and cons of using HS GNSS receivers were considered since the data were collected through two HS receivers. The accuracy analysis of the proposed methods was conducted in the position domain.

Results from all the data collections have shown that all considered weighting schemes perform better than the basic configuration (equal weights to all measurements) and that the weighting schemes integrating both quality indicators (elevation angle and SNR) perform

better than the ones based on a single quality indicator ($1/\sin^2(el)$ or SNR). Elevation dependent weighting method seems to be more effective than the SPW when only a single quality index is considered.

The application of the SPELW and FWLS methods in the weight matrix computation demonstrates evident benefits in terms of all analyzed figures of merit for both horizontal and vertical components. Specifically, FWLS allows a significant enhancement of the solution accuracy with respect to SPELW. FWLS seems hence to provide an effective tool for weighting GNSS measurements, especially when satellite navigation is performed in an urban canyon.

Furthermore, as it is already known, the application of RAIM algorithm improves the accuracy of navigation solution and the use of FWLS in the test statistic computation provides a more accurate position solution than the SPELW method. In conclusion, the best configuration for an urban canyon scenario is performed applying the FDE method to remove the blunders and using the FWLS scheme to weight GNSS measurements and to compute the decision variables of the applied FDE algorithm.

In the next paragraph, a more detailed summary about the obtained results is provided, comparing the best performing configurations during the several data collections.

8.1. Main Results

In this section, the main results obtained in the several tests are compared, considering the operational and environmental differences.

Three data collections are performed and analyzed in this dissertation: two static tests described in Section 7.1 and a vehicular one analyzed in Section 7.2.

The static tests were carried out in Centro Direzionale of Naples (Italy), which is a typical signal-degraded scenario due to the presence of the skyscrapers making the GNSS visibility conditions moderately difficult and leading to multipath effects compromising the navigation accuracy. Indeed, the static test 1 is characterized by solution availability of 99.8% for both GPS only and GPS/GLONASS configurations, while static test 2 has a solution availability of circa 99% for both configurations (GPS and GPS/GLONASS).

The data of the kinematic test were collected using a vehicle in downtown Helsinki (Finland) that is a lightly degraded signal scenario, where the GNSS visibility conditions are challenging due to the presence of medium high buildings and total GNSS outages caused

by the tunnels during the route. In this case, the solution availability is reduced with respect to the static tests: for GPS only it is equal to 86.7% while it increases by 10% for the GPS/GLONASS configuration.

The results obtained are recapped in this paragraph showing the improvements (in percentage) due to the FWLS and SPELW methods with respect to the basic configurations (GPS EW or GG EW). Horizontal and vertical RMS and mean errors are used as figures of merit. The improvements, in terms of errors, are summarized for the GPS only case in Table 8.1 and the multi-constellation configuration in Table 8.2 in order to conduct a performance comparison between the two weighting methods in the WLS estimation and in the RAIM technique.

In Table 8.1, SPELW and FWLS methods show evident improvements with respect to the basic configuration for all the figures of merit. In particular, for the static test 1, the use of the considered weighting methods in the WLS estimation improves the navigation accuracy more than 50% for GPS SPELW and 70% for GPS FWLS relatively to the baseline. The same behavior can be noted for the other data sets collected presenting error improvements higher for the GPS FWLS configuration than the GPS SPELW. However, the best configuration is obtained using the FWLS in the decisional variable computation for the RAIM algorithm. In fact, in the static test 1 the horizontal and vertical mean errors improve by 86% and 89%, respectively, while horizontal and vertical RMS improvements are equal to 81% and 78%, respectively, for the GPS Sub/FWLS configuration with respect to the GPS EW. These values are higher than the ones obtained for the GPS Sub/SPELW.

In static test 2, the horizontal and vertical mean errors are decreased with respect to the GPS EW configuration, with improvements of circa 36% and 32% thanks to the GPS FWLS configuration, while the improvements are equal to 31% and 28% for horizontal and vertical RMS. Also for the static test 2, the highest values of improvements are obtained for the GPS Sub/FWLS configuration for all the figures of merit on vertical and horizontal channels.

The best performance of FWLS can also be noted in the vehicular test: the horizontal and vertical mean errors are enhanced by 73% and 85%, respectively, while the improvements on horizontal and vertical RMS are equal to 72% and 82%, respectively, thanks to the GPS Sub/FWLS configuration with respect to GPS EW.

The values of horizontal and vertical RMS and mean errors for the four considered configurations and the performed data collections are shown in Figure 8.1. It can be noted that the FWLS scheme used in the WLS estimation shows the best performance for all the figures of merit, mainly in the static test 1 and the vehicular test. In static test 2, GPS FWLS

and GPS SPELW configurations have similar values of KPIs. However, for all the data collections, GPS Sub/FWLS provides the most evident improvements with respect to the other configurations.

Table 8.1 Horizontal (H) and Vertical (Up) RMS and mean error improvement (%) obtained by applying FWLS and SPELW methods with respect to the basic configuration (GPS EW) and using only GPS PR

Data Collection	Configuration	H Mean Error Improve [%]	Up Mean Error Improve [%]	H RMS Improve [%]	Up RMS Improve [%]
static test 1	**GPS SPELW**	58.59	54.79	54.86	51.46
	GPS FWLS	77.20	78.50	75.01	75.79
	GPS Sub/SPELW	84.73	88.76	80.63	76.36
	GPS Sub/FWLS	85.76	89.37	80.83	78.28
static test 2	**GPS SPELW**	26.38	19.83	25.81	18.88
	GPS FWLS	35.95	31.72	30.73	27.68
	GPS Sub/SPELW	50.36	52.06	42.26	35.82
	GPS Sub/FWLS	65.13	72.33	56.08	61.70
vehicular test	**GPS SPELW**	35.19	48.95	37.01	48.89
	GPS FWLS	48.24	64.39	46.30	58.42
	GPS Sub/SPELW	64.81	75.47	64.93	70.16
	GPS Sub/FWLS	72.73	84.74	71.97	81.60

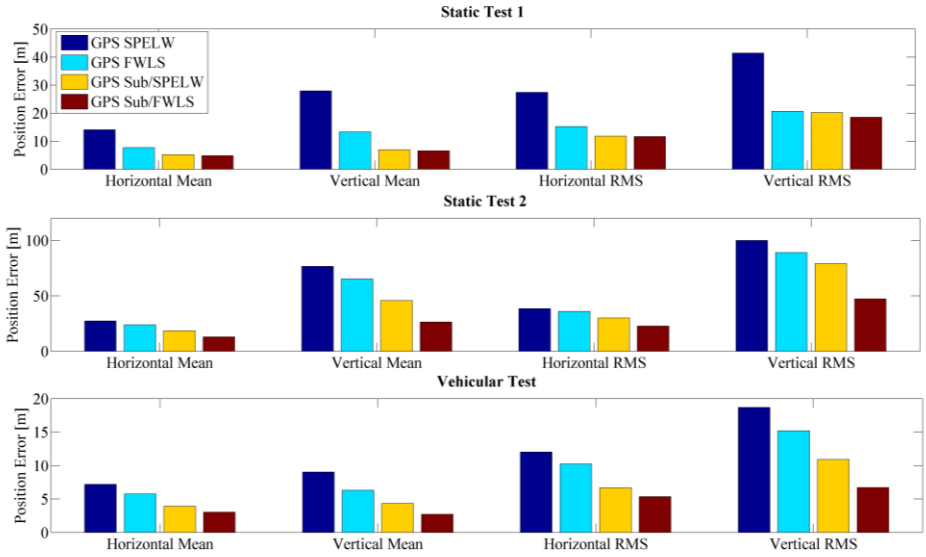

Figure 8.1 RMS and Mean position errors for the four configurations using only GPS PR in the several data collections carried out

For the multi-constellation case, the error improvements with respect to the baseline configuration regarding the best configurations are summarized in Table 8.2, using horizontal and vertical RMS and mean errors as figures of merit.

In the static test 1, the use of fuzzy logic and SPELW methods in the WLS technique lead to an error enhancement of circa 60% on the horizontal component and of around 50% on the vertical one for the GG SPELW configuration, and more than 75% for the GG FWLS in terms of all KPIs. The same improvement can be noted for the other data collections, presenting the highest values for the GG FWLS configuration.

The best setup is obtained applying the FWLS in the performed RAIM algorithm. In fact, in the static test 1, the horizontal and vertical mean errors improve by 88% and 80%, respectively, while horizontal and vertical RMS improvements are equal to 80% and 83%, respectively, for the GG Sub/FWLS configuration compared to GG EW. The error improvements of GG Sub/SPELW configuration are lower than the ones of GG Sub/FWLS.

In static test 2, the horizontal and vertical mean errors are enhanced with respect to GG EW configuration of circa 60% thanks to the GG FWLS configuration, while its error improvements are equal to 65% and 57% for horizontal and vertical RMS. Also for the static test 2, the highest values of error improvements can be highlighted for the GG Sub/FWLS configuration.

The enhancements thanks to the use of FWLS in the RAIM application can also be seen in the vehicular test where they are equal to 68% and 78% for the horizontal and vertical mean errors, respectively, while the enhancements on horizontal and vertical RMS are equal to 75% and 66%, respectively. The obtained errors are lower than the ones obtained with GG Sub/SPELW.

Table 8.2 Horizontal (H) and Vertical (Up) RMS and mean error improvement (%) obtained by applying FWLS and SPELW methods with respect to the basic configuration (GG EW) for the multi-constellation case

Data Collection	Configuration	H Mean Error Improve [%]	Up Mean Error Improve [%]	H RMS Improve [%]	Up RMS Improve [%]
static test 1	**GG SPELW**	61.29	55.34	64.15	57.65
	GG FWLS	77.81	79.01	76.64	76.82
	GG Sub/SPELW	84.31	88.98	74.91	78.62
	GG Sub/FWLS	88.24	91.38	80.38	83.51
static test 2	**GG SPELW**	43.08	40.56	52.56	41.81
	GG FWLS	61.56	60.32	65.12	57.21
	GG Sub/SPELW	59.46	71.59	54.53	57.56
	GG Sub/FWLS	62.85	73.00	59.25	60.93
vehicular test	**GG SPELW**	36.11	39.30	50.59	42.31
	GG FWLS	54.20	67.52	64.17	61.80
	GG Sub/SPELW	60.66	66.08	68.87	62.65
	GG Sub/FWLS	68.82	79.24	75.11	66.73

The results in Table 8.2 are confirmed by the Figure 8.2 where the values of horizontal and vertical RMS and mean errors for the four considered configurations are illustrated. The GG Sub/FWLS configuration has the lowest KPI values for vertical and horizontal components and this improvement is more evident in static test 1 and vehicular test, as noted in the GPS only case. This fact suggests that the use of FWLS is advantageous for both GPS and GLONASS measurements, leading to improvements in the multi-constellation case as well.

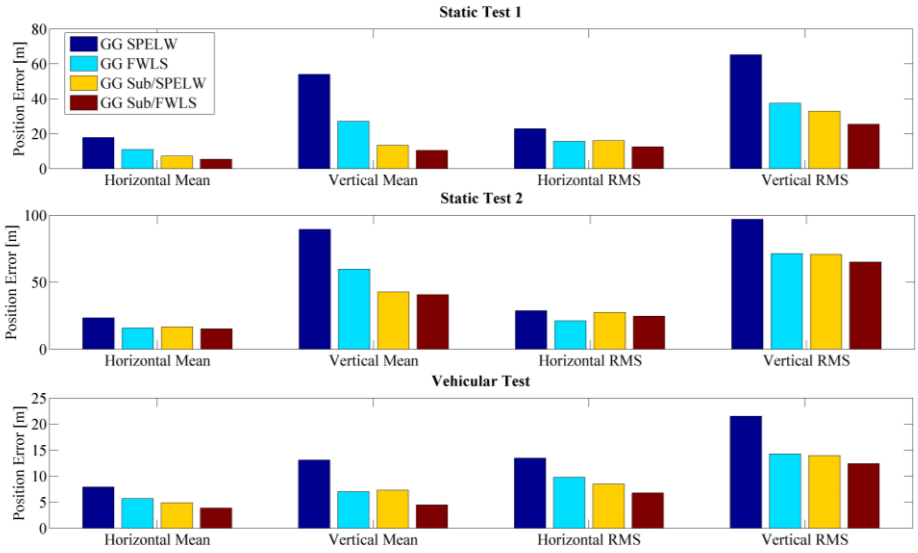

Figure 8.2 RMS and Mean position errors for the four configurations using GPS and GLONASS PRs in the several data collections carried out

Furthermore, in the static test 2 the enhancement due to the multi-constellation use can also be noted in terms of accuracy, availability and continuity. Indeed, comparing GPS FWLS and GG FWLS configurations for the static test 2, it is possible to see that all KPIs are reduced thanks to the inclusion of GLONASS measurements. The statistical parameters and error improvements obtained using the GG constellation with respect to GPS only and using the same weighting matrix are summarized in Table 8.3. Horizontal and vertical mean errors are improved by 34% and 8% due to the use of the combined GNSSs, while the enhancements of horizontal and vertical RMS errors are equal to 41% and 20%, respectively, for the GG FWLS configuration with respect to the GPS FWLS.

In order to have a clear comparison, the scatter plots for the GPS only and GPS/GLONASS constellations are shown in Figure 8.3. In detail, the blue points are relative to the horizontal position solutions for GPS FWLS configuration, the red markers for GG FWLS and the yellow one is the reference point for the static test 2. The figure shows that the cloud relative to GG FWLS configuration is smaller and more concentrated around the reference solution with respect to the blue results cloud, which contains also isolated points due to the presence of blunders. Indeed, the horizontal maximum error for GG FWLS is reduced by circa 77% with respect to the GPS FWLS. This fact confirms that in some situations it is possible to enhance the accuracy of the navigation solution using the combination of several GNSSs and without the application of a quality check algorithm.

Table 8.3 Summary results and the error improvements obtained using the multi-constellation approach with respect to the GPS only configuration and the same weighting matrix for the static test 2

Configuration	H Mean Error[m]	Up Mean Error[m]	H RMS [m]	Up RMS[m]	H Max Error[m]	Up Max Error[m]
GPS FWLS	23.82	65.2	35.93	89.08	454.53	836.31
GG FWLS	15.75	59.7	21.07	71.28	105.11	294.55
Error Improvements[%]	33.88	8.44	41.36	19.98	76.88	64.78

Figure 8.3 Horizontal positions obtained using GPS FWLS configuration (blue markers) and GG FWLS one (red markers) with respect to the reference solution of the point 2 (yellow point) located in Centro Direzionale of Naples (Italy)

8.2. Future Suggestions

The findings of this thesis show that the multi-constellation is beneficial for performance improvement mainly in signal degraded scenarios; for this reason, a future step should be the use of ranging measurements from more than two GNSS (for example a multi-constellation composed of four GNSS, GPS/GLONASS/Galileo/BeiDou). In this way, it will be possible to verify the effectiveness of the FWLS method, applied to weight measurements from other GNSSs. Furthermore, it could also be possible to analyze the benefit of FWLS for velocity computation.

In order to improve the FWLS performance, a future development should be the integration of other input LVs in the fuzzy controller, considering for examples the features of the operational scenarios. The idea is to find a parameter representing the characteristic of the scenario in order to evaluate how the scenario is degraded using proper linguistic terms (lightly, medium, heavily): this information could be fuzzified and integrated with the signal

quality parameters. In this way, the GNSS weights would be also dependent on the operational environment.

Since in this research only the Subset testing is used as FDE algorithm, a future development could be the use of the FWLS also in other FDE techniques, commonly used in GNSS navigation.

Furthermore, the fuzzy logic could be used in the hypothesis testing that is the basis of the RAIM algorithm. For example, the simple comparison between the decision variable and the threshold (as described in 5.3.1) can be overcome with the use of the fuzzy theory; moreover, other information could be used to improve the detection capability of classic RAIM in order to work properly when multiple outliers occurs, as it happens in signal degraded scenario.

References

Ackermann S., Angrisano A., Del Pizzo S., Gaglione S., Gioia C., Troisi S. (2014) Digital surface models for GNSS mission planning in critical environments. Journal of Surveying Engineering, Volume 140, Issue 2, doi: 10.1061/(ASCE)SU.1943-5428.0000119

Angrisano A. (2010) GNSS/Integration Methods, PhD Thesis, Dipartimento di Scienze Applicate, Parthenope University of Naples.

Angrisano A., Gaglione S., Del Core G., Gioia C. (2013a) GNSS reliability testing in signal-degraded scenario. International Journal of Navigation and Observation. doi:10.1155/2013/870365

Angrisano A., Gaglione S., Gioia C., Massaro M,. Troisi S. (2013b) Benefit of the NeQuick Galileo version in GNSS single-point positioning, International Journal of Navigation and Observation art. no. 302947

Atkinson A.C., and Riani, M. (1997) Bivariate boxplots, multiple outliers, multivariate transformations and discriminant analysis: the 1997 Hunter lecture. Environmetrics, 8(6), 583-602.

Bai Y., Wang D. (2006) Fundamentals of Fuzzy Logic Control – Fuzzy Sets, Fuzzy Rules and Defuzzifications. In: Advanced Fuzzy Logic Technologies in Industrial Applications. Springer

Bandemer H.Y. & Näther W. (1992) Fuzzy Data Analysis. Kluwer Academic Press, Dordretch, Netherlands

Barnes B.J., Ackroyd N. and Cross P.A. (1998) Stochastic modelling for very high precision real-time kinematic GPS in an engineering environment. In Proceedings of FIG XXI International Conference, Brighton, U.K., 21-25 July, 1998, Commission 6, pp 61-76

BDS-ICD (2012) BeiDou Navigation Satellite System (BDS) Signal In Space Interface Control Document (SIS ICD), Open Service Signal B1I, version 1.0, December, China Satellite Navigation Office

Berkan R.C., Trubatch S.L. (1997) Fuzzy Systems Design Principles –Building Fuzzy IF-THEN Rule Bases. IEEE Press, New York

Bhatta, B. (2011) Global Navigation Satellite Systems. CRC Press, Boca Raton.

Blanch, J., T. Walter, P. Enge, S. Wallner, F. Amarillo Fernandez, R. Dellago, R. Ioannides, B. Pervan, I.F. Hernandez, B. Belabbas, A. Spletter, and M. Rippl (2011) A Proposal for Multi-constellation Advanced RAIM for Vertical Guidance, Proceedings of the 24th International Technical Meeting of The Satellite Division of the Institute of Navigation, 20-23 September, Portland, OR, pp. 2665-2680

Brown R. G., (1992) A baseline GPS RAIM scheme and a note on the equivalence of three RAIM methods. Navigation, 39(3), 301-316.

Brown R.G. and G. Y. Chin, (1997) GPS RAIM: calculation of threshold and protection radius using chi-square methods-a geometric approach, Global Positioning System: Institute of Navigation, vol. 5, pp. 155–179, 1997.

Brown, A.K., (1998) Receiver autonomous integrity monitoring using a 24-satellite gps constellation, Navigation, Journal of The Institute of Navigation, V:2133, 1998. Red Book of RAIM.

Brunner F. K., Hartinger H., and L. Troyer (1999), GPS signal diffraction modelling: The stochastic SIGMA-Δ model, J. Geod., 73, 259–267, 1999

Cai C., and Gao Y. (2009) A combined GPS/GLONASS navigation algorithm for use with limited satellite visibility. Journal of Navigation, 62(04), 671-685.

Conley R., Cosentino R., Hegarty C. J., Kaplan E. D., Leva J. L., de Haag M. U., and Van Dyke K., (2006) Performance of stand-alone GPS. Understanding GPS: Principles and Applications (Elliott D. Kaplan and Christopher J. Hegarty, eds.), Artech House.

DoD Positioning Navigation and Timing Executive Committee, (2008) Gps standard positioning service performance standard. Technical report, DoD Positioning Navigation and Timing Executive Committee, September 2008.

ESA (2013) Galileo and GPS 'Synchronise Watches': New Time Offset Helps Working Together, 3 May, European Space Agency, http://www.esa.int/Our_Activities/Navigation/Galileo_and_GPS_synchronise_watches_new_time_offset_helps_working_ together, last accessed 24 May 2013

Eueler H. J., and Goad C. C., (1991) On optimal filtering of GPS dual frequency observations without using orbit information. Bulletin Geodesique, 65(2), 130-143.

European Union. European gnss (Galileo) open service signal in space interface control document. OS SIS IC 1.1, European Union, September 2010.

Gao Y. (1993) Reliability assurance for GPS integrity test, ION GPS-93, Salt Lake City, Utah, September 22-24, 567-574.

Ge, M., H. Zhang, X . Jia, S. Song, and J. Wickert (2012) What Is Achievable with the Current Compass Constellation?, GPS World, 1 November, http://www.gpsworld.com/what-is-achievable-with-the-current-compass-constellation

Gioia C., J. Fortuny-Guasch, F. Pisoni, (2014) Estimation of the GPS to Galileo Time Offset and its validation on a mass market receiver, 7th ESA Workshop on GNSS Signals and Signal Processing, December 2014.

Godha, S. (2006), Performance Evaluation of Low Cost MEMS-Based IMU Integrated With GPS for Land Vehicle Navigation Application, MSc Thesis, Department of Geomatics Engineering, University of Calgary, Canada, UCGE Report No. 20239

Gps.gov. (2016) Welcome to GPS.gov. [online] Available at: http://www.gps.gov [Accessed September 2016].

GPS World (2016) Galileo Service Interruption Planned for System Upgrade. [online] Available at: http://gpsworld.com/galileo-service-interruption-planned-for-system-upgrade/ [Accessed September 2016].

Groves, P.D. (2013), Principles of GNSS, Inertial, and Multisensor Integrated Navigation Systems, Second Edition. Artech House, April 2013.

Gsc-europa.eu, (2016) European GNSS Service Centre |. [online] Available at: https://www.gsc-europa.eu/ [Accessed September 2016].

Han S. (1997) Quality control issues relating to instantaneous ambiguity resolution for real-time GPS kinematic positioning. Journal of Geodesy, 71(7): 351-361

He L., Ge M., Wang J., Wickert J., and Schuh, H. (2013) Experimental study on the precise orbit determination of the BeiDou navigation satellite system. Sensors, 13(3), 2911-2928.

Hein G. W., Pielmeier J., Zink T., and Eissfeller B., (1997) GPS and GLONASS RAIM availability analysis over Europe. In Proceedings of the 10th International Technical Meeting of the Satellite Division of The Institute of Navigation (ION GPS 1997), pp. 465-474.

Hess J. (1996) Fuzzy logic and medical device technology. Medical Device Technology, 7(1): 19-22

Hewitson S., Wang J., and Lee H. K., (2004) Impact of dynamic information on GNSS receiver integrity monitoring. In Proc. International Symposium on GNSS/GPS, pp. 6-8.

Hewitson, S. and J. Wang (2006a) GNSS Receiver Autonomous Integrity Monitoring (RAIM) Performance Analysis. GPS Solutions, vol. 10, issue 3, pp. 155-170

Hewitson S., and Wang, J. (2006b) GNSS receiver autonomous integrity monitoring (RAIM) for multiple outliers. European Journal of Navigation, 4(4), 47-57.

Hoffmann-Wellenhof B., H. Lichtenegger, and J. Collins (1992) Global Positioning System: Theory and Practice. Springer, 1992.

Hopfield H. (1971) Tropospheric Effects on Electromagnetically Measured Range, Prediction from Surface Water Data, Radio Science, Vol. 6, No. 3, March 1971, pp. 356–367.

ICD-GLONASS (2008) Global Navigation Satellite System GLONASS Interface Control Document, version 5.1, Moscow.

ICAO SARPS, Annex 10 (2010): International Standards and Recommended Practices: Aeronautical Telecommunications, Volume 1, International Civil Aviation Organisation, 2004.

Innac A., Bhuiyan M.Z.H., Söderholm S., Kuusniemi H., Gaglione S., (2016) Reliability testing for multiple GNSS measurement outlier detection. In: Proceedings of European Navigation Conference (ENC) 2016, 30th May-2nd June 2016, IEEE Xplore, doi: 10.1109/EURONAV.2016.7530540

Inside GNSS (2013) ESA Adds System Time Offset to Galileo Navigation Message, Inside GNSS, issue May/June, published online http://www.insidegnss.com/node/3560

Jones, W. H. (1987). Navstar global positioning system: progress report. IEEE Aerospace and Electronic Systems Magazine, 2(3), 9-12.

Kaplan E.D. (2005) Understanding GPS: Principles and Applications. Second Edition. Artech House, November 2005

Kaplan, E.D. and Leva, J.L. (2006) Fundamentals of Satellite Navigation, Kaplan, E.D. ed., Understanding GPS: Principles and Applications (second edition), Chapter 2, Artech House Mobile Communications Series.

Kaufmann A. and Gupta M.M., (1985), Introduction to Fuzzy Arithmetic, Van Nostrand Reinhold Publications, New York, NY, USA.

Keller, S.F., Gnägi, H.R. (2001) Modelling Fuzy Geospatial Phenomena Using Application Pattern and Standards. In: Carosio A., Kutterer H. (eds) Proc: First International Symposium on Robust Statistics and Fuzzy Techniques in Geodesy and GIS, IAG SSG 4.190, Zürich, pp 151-158.

Klobuchar J.A. (1996), Ionospheric Effects on GPS, B. W. Parkinson and J. J. Spilker, Jr., eds., Global Positioning System: Theory And Applications, volume 1, chapter 12. American Institute of Aeronautics and Astronautics, Inc., Washington D.C., USA

Koch K. R., (2013) Parameter estimation and hypothesis testing in linear models. Springer Science & Business Media.

Kuang, S. (1996). Geodetic network analysis and optimal design: concepts and applications. Ann Arbor PressInc.

Kutterer H. (2001a) An imprecise search space for GPS phase ambiguity parameters. In First International Symposium on Robust Statistics and Fuzzy Techniques in Geodesy and GIS. ETH Zurich Institute of Geodesy and Photogrammetry, Bericht (Vol. 295, pp. 215-220).

Kutterer H. (2001b) Uncertainty assessment in geodetic data analysis. In First International Symposium on Robust Statistics and Fuzzy Techniques in Geodesy and GIS, Institute of Geodesy and Photogrammetry ETH Zurich, Bericht (No. 295, pp. 7-12).

Kuusniemi H. (2005) User-Level Reliability and Quality Monitoring in Satellite-Based Personal Navigation. PhD thesis, Tampere University of Technology, Finland, 2005. Publication 544.

Langley L.B. (1998) Propagation of the GPS signals, in GPS for Geodesy, A. Kleusberg and P. J. G. Teunissen, Eds., Springer, Berlin, Germany, 1998.

Langley, R. B. (1997). GPS receiver system noise. GPS world, 8(6), 40-45.

Lee Y. C., (1986,). Analysis of range and position comparison methods as a means to provide GPS integrity in the user receiver. In Proceedings of the 42nd Annual Meeting of the Institute

of Navigation, pp. 1-4.

Lee Y. C., (2001) Investigation of extending receiver autonomous integrity monitoring (RAIM) to combined use of Galileo and modernized GPS. In Proceedings of the 17th International Technical Meeting of the Satellite Division of The Institute of Navigation (ION GNSS 2004), pp. 1691-1698.

Lee Y.C. and T. Cashin (2010) Advanced RAIM Based on Inter-Constellation Comparisons to Detect Consistent Faults for LPV-200, Proceedings of the 23rd International Technical Meeting of The Satellite Division of the Institute of Navigation, 21-24 September, Portland, OR, pp. 272-284

Leick A., Rapoport L., Tatarnikov D (2015) GPS Satellite Surveying. John Wiley & Sons, Inc., New York, N.Y., 4th ed.

Leinen S. (2001) Fuzzy-Logic Based GPS On-The-Fly Ambiguity Search. In: Carosio A., Kutterer H. (eds) Proc: First International Symposium on Robust Statistics and Fuzzy Techniques in Geodesy and GIS, IAG SSG 4.190, Zürich, pp 209-214.

Lin C.J., Chen Y.Y., Chang, F.R., (1996) Fuzzy Processing on GPS Data to Improve Position Accuracy. IEEE Symposium on Soft Computing Intelligent Systems and Information Processing, pp. 557- 562

Liu H., Zheng G., Wang H., and Feng, C. (2010). Research on integrity monitoring for integrated GNSS/SINS system. Paper presented at the 2010 IEEE International Conference on Information and Automation, ICIA 2010, 1990-1995. doi:10.1109/ICINFA.2010.5512033

Moaiied M. M. and Mosavi M (2016). Increasing accuracy of combined GPS and GLONASS positioning using fuzzy kalman filter. Iranian Journal of Electrical and Electronic Engineering, 12(1), 21-28.

Navcen.uscg.gov. (2016) U.S. Coast Guard Navigation Center. [online] Available at: http://www.navcen.uscg.gov/ [Accessed September 2016].

Navstar GPS Directorate, (2012) Global positioning systems directorate systems engineering & integration interface specifcation is-gps-200. Technical report, Navstar GPS Directorate, September 2012.

New.glonass-iac.ru (2016) Information and Analysis Center for Positioning, Navigation and Timing [online] Available at: http://new.glonass-iac.ru [Accessed September 2016].

Ochieng W.Y., Sheridan K.F., Sauer K., Han X., Cross P.A., Lannelongue S., Ammour N., Petit K. (2002) An assessment of the RAIM performance of a combined Galileo/GPS navigation system using the marginally detectable errors (MDE) algorithm. GPS Solutions 5(3):42–51

O'Keefe, K., G. Lachapelle, A. Di Fazio, and D. Bettinelli (2011) Receiver Autonomous Integrity Monitoring in Urban Vehicle Navigation: The Five Satellite Case, Journal of Global Positioning Systems, vol. 10, no. 2, pp. 157-164

Özlüdemir M.T., (2004) The Stochastic Modeling of GPS Observations, Turkish Journal of Engineering and Environmental Sciences, 28(4): 223-231

Parsons J. D., (2000) The Mobile Radio Propagation Channel vol. 2nd West Sussex. UK: John Wiley & Sons, Ltd.

Parkinson B., J. Spilker Jr., P. Axelrad, and P. Enge (1996). Global Positioning System: Theory And Applications, volume I. American Institute of Aeronautics and Astronautics, Washington D.C., USA, 1996

Petovello, M. (2003) Real-time Integration of a Tactical-Grade IMU and GPS for High-Accuracy Positioning and Navigation. PhD thesis, Department of Geomatics Engineering, University of Calgary, Calgary, 2003. UCGE Report No. 20173

Petovello M., Pullen S., Syrjarinne J., and Wirola L., (2008) Quantifying the performance of navigation systems and standards for assisted-GNSS. Inside GNSS, 20-24.

Petovello M., (2009) Estimation for Navigation, ENGO 699.18 - Lecture Notes, Department of Geomatics Engineering, University of Calgary, Canada

Realini E, Reguzzoni M (2013) GoGPS: Open source software for enhancing the accuracy of low-cost receivers by single-frequency relative kinematic positioning. Measurement Science and Technology, 24(11). doi:10.1088/0957-0233/24/11/115010

Romay M.M., Alarcón A., J.G., Villares, I. J. and Monseco E. H. (2001) An integrated GNSS concept, Galileo & GPS, benefits in terms of Accuracy, Integrity, Availability and Continuit. ION GPS 2001, Salt Lake City, UT, 11-14 September, 2114-2125.

Ross T. J., (2009) Fuzzy logic with engineering applications. John Wiley & Sons.

Rostovsky N.S., Smirnov D.S., Tupchienko V.A. (2016) The model of decision-making of high-tech company on the formation of the optimal portfolio. Evaluation of projects under uncertainty using fuzzy logic. Applied Mathematical Sciences, 10(1-4): 59-69

Ryan S., and Lachapelle G., (1999) Augmentation of DGNSS with dynamic constraints for marine navigation. Proc. ION GPS 1999, 1303-1314.

Ryan S. and Lachapelle G. (2000) Impact of GPS/Galileo Integration on Marine Navigation. In: IAIN World Congress/ ION Annual Meeting, pp 721–731

Sairo H. (2006) Error Detection in Personal Satellite Navigation, Doctoral Thesis, Tampere University of Technology, 2006.

Sang J., and Kubik K. (1997). Probabilistic approach to derivation of geometrical criteria for evaluating GPS RAIM detection availability. Paper presented at the Proceedings of the National Technical Meeting, Institute of Navigation, 511-517.

Salvatori, P., Neri, A., Stallo, C., Palma, V., Coluccia, A., Rispoli, F. (2014) Augmentation and integrity monitoring network and EGNOS performance comparison for train positioning. In: 2014 Proceedings of the 22nd European Signal Processing Conference (EUSIPCO); 2014. p. 186–90.

Sastamoinen J., (1993) Contribution to the theory of atmospheric refraction, part II refraction

correction in satellite geodesy. Bulletin Geodesique, 107, 13-34.

Satellite-navigation.eu (2016) Satellite Navigation [online] Available at: http://www.satellite-navigation.eu/ [Accessed September 2016].

Satirapod C. (2004) A review of stochastic models used in static GPS positioning technique, 25th ACRS & 1th ASC, November 22-26 2004, Thailand

Schwieger V. (2008) High-Sensitivity GPS-an availability, reliability and accuracy test. In: Proceedings on FIG Working Week, Stockholm, pp 14-19.

Sentman O. L. (1987). Navy Navigation Satellite System (Transit). IEEE Aerospace and Electronic Systems Magazine, 2(7), 25-26.

Shyllon E.A. (2001) Techniques for Modelling Uncertainties Inherent in Geomatics Data: Fuzzy Systems Approach. In: Carosio A., Kutterer H. (eds) Proc: First International Sympsosium on Robust Statistics and Fuzzy Techiniques in Geodesy and GIS, IAG SSG 4.190, Zürich, pp 139-143.

Shytermeja, E., Garcia-Pena, A., and Julien, O. (2014). Proposed architecture for integrity monitoring of a GNSS/MEMS system with a fisheye camera in urban environment. Paper presented at the Proceedings of 2014 International Conference on Localization and GNSS, ICL-GNSS 2014, doi:10.1109/ICL-GNSS.2014.6934179

Spilker, J. J., Jr. (1997), Digital Communications by Satellite, Englewood Cliffs, NJ: Prentice-Hall, 1977.

Sükeová, L., Santos M.C., Langley R.B., Leandro R.F., Nnani O., and Nievinski F. (2007) GPS L2C signal quality analysis. In: Proceedings of the ION 63rd Annual Meeting, pp. 23-25.

Syed S., and Cannon E. (2005) Map-aided GPS navigation: Linking vehicles and maps to support location-based services. GPS World, 16(11): 39-44

Tanka K. and Niimura T. (1996) An Introduction to Fuzzy Logic for Practical Applications, Springer-Verlag Publications, New York, NY, USA

The Mathworks, Inc., (2005) Fuzzy Logic Toolbox, for Use with MATLAB®, User's Guide, Version 2, The Mathworks, Natick, MA.

Van Diggelen, F. S. T. (2009). A-GPS: Assisted GPS, GNSS, and SBAS. Artech House.

Wang J. (1998) Stochastic assessment of the GPS measurements for precise positioning, Proc. GPS ION 1998, Institute of Navigation, Nashville, Tennessee, September 15-18, pp 81-89

Walter T., and Enge P. (1995). Weighted RAIM for precision approach. Paper presented at the Proceedings of ION GPS, 2, 1995-2004.

Węzka K., Herrera-Pinzon I. and Galas R. (2016) Reliability monitoring of GNSS observables under the influence of ionospheric disturbances. In: Proceedings of the IEEE/ION Position, Location and Navigation Symposium, PLANS 2016, pp 431-441. doi:10.1109/PLANS.2016.7479731

Wieser A. (2002) Robust and fuzzy techniques for parameter estimation and quality assessment in GPS. Doctoral thesis, Graz University of Technology, Shaker Verlag, Aachen, Germany

Wieser, A., and Brunner, F. K. (2002). SIGMA-F: variances of GPS observations determined by a Fuzzy system. In Vistas for Geodesy in the New Millennium (pp. 365-370). Springer Berlin Heidelberg.

Wieser A., Gaggl M., and Hartinger H. (2005) Improved positioning accuracy with high-sensitivity GNSS receivers and SNR aided integrity monitoring of pseudo-range observations. Paper presented at the Proceedings of the 18th International Technical Meeting of the Satellite Division of the Institute of Navigation, ION GNSS 2005, 1545-1554.

Winit R., (2013) Four-constellation GNSS reliability and the estimation of inter-system time-offsets for improved performance in challenging signal environments. Doctoral dissertation, University of Calgary.

Zadeh L.A. (1965) Fuzzy Sets. Information And Control, 8(3): 338-353

Zadeh L. (1995) Preface to Mathwork.s User Guide to Fuzzy Logic Toolbox. Mathwork Inc., Release 9, version 2, January, Natick, MA, USA

Zadeh L., Lotfi A. (1996) Fuzzy sets, fuzzy logic, and fuzzy systems: selected papers by Lotfi A Zadeh. Vol. 6. World Scientific, 1996

Zhao, Q., J. Guo, M. Li, L. Qu, Z. Hu, C. Shi, and J. Liu, (2013) Initial Results of Precise Orbit and Clock Determination for COMPASS Navigation Satellite System, Journal of Geodesy, vol. 87, issue 5, pp 475-486